The Journal of The Royal Astronomical Society of Canada

Journal

Le Journal de la Société royale d'astronomie du Canada

PROMOTING ASTRONOMY IN CANADA

April/avril 2026
Volume/volume 120
Number/numéro 2 [837]

Inside this issue:

The Great Orion Nebula

Great Images

By Trudy Almon

Trudy Almon writes "The conjunction of the Moon and Mars was on the 6th but due to clouds in the forecast I took some photos the night before." Waning gibbous Moon at 87% on 2020 September 5, ~ 11:48 p.m. Imaged with a Canon T4i EF 75–300 mm ƒ/4–5.6 III USM ISO 100, ƒ/5.6 for 1/200 sec; shot at 300 mm from Fairfield, New Brunswick.

(Editor's Note: All the images in this issue are submissions to the Astroimaging Certificate Program by RASC members achieving the requisite astrophotographs in the categories Wide Field, Solar System, and Deep Sky)

Journal

April / avril 2026 | Vol. 120, No. 2 | Whole Number 837

Royal Astronomical Society of Canada

Société Royale d'Astronomie du Canada

contents / table des matières

Research Articles / Articles de recherche

Feature Articles / Articles de fond

Pen & Pixel / Stylo et pixel

Columns / Rubriques

Departments / Départements

Great Images / Superbes images

The Great Orion nebula acquired by Erich Krause with a ZWO1600-MM Pro, Esprit 80, Apex 0.65× reducer, on a Celestron CGEM mount. He writes "The image consists of 5×240s SII, 5×240s OIII, 15×240s Hα acquired through SGP (SequenceGenerator Pro). I was testing backfocus with a newly acquired Apex 0.65× reducer (thus the corner stars are a pinch out) but I liked the image so much I kept the data. I was very surprised to see the amount of dust and detail with my gear now working at ƒ/3.25. The image was taken at Wilson Coulee Observatory (Calgary Centre) in January 2020 and processed using PixInsight (SHO- green removed) with final touch up in Photoshop (including the star spikes I added for flavour)."

Journal

The *Journal* is a bi-monthly publication of The Royal Astronomical Society of Canada and is devoted to the advancement of astronomy and allied sciences. It contains articles on Canadian astronomers and current activities of the RASC and its Centres, research and review papers by professional and amateur astronomers, and articles of a historical, biographical, or educational nature of general interest to the astronomical community. All contributions are welcome, but the editors reserve the right to edit material prior to publication. Research papers are reviewed prior to publication, and professional astronomers with institutional affiliations are asked to pay publication charges of $100 per page. Such charges are waived for RASC members who do not have access to professional funds as well as for solicited articles. Manuscripts and other submitted material may be in English or French, and should be sent to the Editor-in-Chief.

The *Journal* of The Royal Astronomical Society of Canada is published at an annual subscription rate of $125 (plus Canadian tax), $140 USD for US subscriptions, $150 USD for International subscriptions. Membership, which includes the publications (for personal use), is open to anyone interested in astronomy. Applications for subscriptions to the ***Journal*** or membership in the RASC and information on how to acquire back issues of the ***Journal*** can be obtained from:

The Royal Astronomical Society of Canada
203-489 College St
Toronto ON M6G 1A5

nationaloffice@rasc.ca
www.rasc.ca
Tel: 416-924-7973
Fax: 416-924-2911

Canadian Publications Mail Registration No. 09818
Canada Post: Send address changes to 203–489 College St, Toronto ON M6G 1A5

Canada Post Publication Agreement No. 40069313

Funded by the Government of Canada | Financé par le gouvernement du Canada | Canada

FSC Mixed Sources
Product group from well-managed forests and other controlled sources
www.fsc.org Cert no. SW-COC-005174
© 1996 Forest Stewardship Council

President's Corner

Astronomy: Big, Fulfilling, Timeless

Brendon Roy (Thunder Bay), President
novationheart@hotmail.com

The days are getting longer here in the Northern Hemisphere, bringing good news to farmers, swimmers, and to anyone who is not fond of the cold. The increasing amount of daylight is one of those astronomical events that often goes unnoticed, yet it deserves our full appreciation.

One of the key ideas I try to share with people who are learning about astronomy for the first time is a simple but powerful perspective: Earth—our home—is a member of the family of planets within the Solar System. Many of the features we associate with Earth are, in fact, a direct result of being part of this planetary family.

One such feature, frequently discussed in the latter part of winter, is the length of the day. Most people, when referring to this, mean the increasing number of hours of sunlight rather than the actual time it takes Earth to rotate once on its axis. This provides an opportunity to introduce an important concept: if Earth did not have a companion, the length of our day would be vastly different—and likely much shorter.

The Moon, orbiting Earth, has played a significant role in shaping our planet's rotation. Over billions of years, tidal interactions and the conservation of energy have gradually slowed Earth's spin from a period as short as ten hours to the nearly twenty-four-hour day we now enjoy. A consequence of this process (tidal braking) is that the Moon is slowly drifting away from us. Both bodies have had an impact on each other over the course of billions of years, this being just one example of many.

A second important consequence of having a large Moon is the stability it provides to Earth's axis of rotation. This stability is essential for life, helping to keep our seasons predictable and allowing the stars to remain reliable guides so we may set our direction upon them.

Although not a feature of either world, ambitious explorers are now preparing to journey from one to the other.

The Artemis II mission will be the first crewed mission to the Moon in my lifetime and the first crewed mission to travel beyond low-Earth-orbit since the Apollo era. I am eager for the opportunities this will create: the revitalization of the

conversation about humanity's future in space, and the inspiration of a new generation of dreamers.

This dream is only possible because of turbulent times in the Solar System's youth and an unlikely collision that set an unknowable chain of events in motion. And it is sustained by curious minds—like yours—who find their way into organizations such as the RASC to learn more about our place in the Universe and how we came to be.

Like Earth and the Moon, we are connected companions, influencing one another in ways we may not always perceive, while collectively setting in motion our boundless curiosity.

Astronomy: big, fulfilling, timeless… there is nothing I would rather be doing.

Brendon Roy
President ✶

News Notes / En manchettes

Compiled by Jay Anderson FRASC

Milky Way magnetic fields in detail

Magnetic fields leave fingerprints on light. One of these effects is the gradual rotation of the angle of polarization of the beam as it passes through an interstellar medium of plasma and dust. This process is called Faraday rotation, which occurs whenever electromagnetic radiation passes through a magnetic field.

For astronomers, the process starts with polarized light—light whose electric field vibrates in a specific direction. Most likely, you have encountered linearly polarized light when you put on your sunglasses on a bright summer day. The glasses pass only one orientation of light, blocking others and reducing the intensity of the Sun's glare. In the Milky Way, light first becomes polarized by a number of processes: synchrotron radiation, passage through dust grains aligned in a magnetic field, ionized gases around supernovae and black holes, and so on. Once generated, however, the initial angle of polarization is modified along the way as it passes through intervening interstellar plasmas and magnetically aligned dust grains. The change in polarization angle is known as Faraday rotation.

If we can measure polarization and trace it back to the originating source, we can reconstruct the magnetic fields encountered at the source and along the way. To do so requires measurements at several frequencies, since Faraday rotation is influenced by the frequency of the electromagnetic wave, as well as by the composition of the interstellar (or intergalactic) medium and the distance travelled.

Recently, a UBC Okanagan-led research project has given a group of international scientists their clearest view yet of the Milky Way's magnetic field, revealing that it is far more complex than previously believed. A team led by Dr. Alex Hill, Assistant Professor in the Irving K. Barber Faculty of Science at UBCO, and working at the Dominion Radio Astrophysical Observatory (DRAO), near Penticton, used data from the DRAO 15-metre radio telescope to complete the first broadband map of Faraday rotation, allowing the team to decipher magnetic fields across the sky in fine detail.

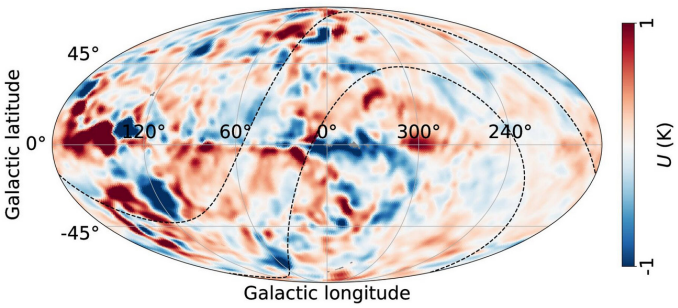

This research is part of a larger initiative called the Global Magneto-Ionic Medium Survey (GMIMS), initiated by Dr. Tom Landecker, an astronomer at DRAO and adjunct professor at both UBCO and the University of Calgary. The observations, known as DRAO GMIMS of the Northern Sky (DRAGONS) and led by former UBCO postdoctoral researcher Dr. Anna Ordog, captured polarized radio emissions across a wide range of frequencies, allowing astronomers to see magnetic structures that were previously invisible.

"With our new dataset, we can look at the polarized emissions from within the galaxy itself, and we see that the magnetic field has a lot of structure to it," Dr. Ordog explains. "DRAGONS is the first to show this level of complexity on such large spatial scales and across the entire northern sky."

The work builds on a theoretical insight first proposed in 1966, which showed that polarized radio waves observed at many frequencies could enable measurements of the three-dimensional structure of the Milky Way's magnetic field. At the time, the technology needed to observe this effect across wide frequency ranges did not exist. Modern broadband telescopes, including the DRAO 15-m telescope, have made this research possible.

The project was the first scientific use of the 15-m telescope, which DRAO originally built as a prototype antenna for the Square Kilometre Array (SKA)—a large radio telescope network currently under construction in Southern Africa and Western Australia. Dr. Ordog led the setup for the DRAGONS project, supported by five students from UBCO and the University of Calgary, along with the expertise of DRAO engineers and technologists.

Figure 1 — Map of the Stokes U parameter, which quantifies the amount of linear polarization at a specific orientation. Image: Anna Ordog et al. 2026 ApJS 282 53 DOI 10.3847/1538-4365/ae2471

"The 15m is the ideal instrument for this all-sky survey of large-scale magnetized structures—it can scan rapidly, effectively 'painting' a map of the polarized sky in just six months," she says. "Having the 15m so close to UBCO allowed students to contribute to hands-on testing in preparation for the survey."

UBCO students analyzed "first light" signals from the instrument, developed algorithms to identify human-made radio interference and assessed the survey data quality. The study, published in *The Astrophysical Journal Supplement Series*, tracks how polarized radio waves twist as they travel through the galaxy, revealing the strength, structure, and direction of magnetic fields along the line of sight. This survey shows that more than half the sky contains complex magnetic structures rather than simple, uniform fields.

Dr. Landecker says the biggest surprise for the researchers was just how much of the sky is what is known as "Faraday complex."

"With our new dataset, we can look at the polarized emission from within the galaxy itself, and we can see that the magnetic field has much more structure to it than we could detect with earlier observation methods," says Dr. Landecker, who is also the leader of a larger effort to map magnetic fields in three dimensions and an astronomer emeritus at DRAO.

"DRAGONS is like a compass, telling us how matter and magnetic fields in the galaxy are organized and how the magnetic field interacts with bubbles created by supernova explosions, spiral arms, and other parts of the galaxy in ways that have never been possible before."

Magnetic fields shape how stars are formed and how galaxies evolve, explains Dr. Hill. "For decades, we could only measure the Milky Way's magnetic field in a very averaged, simplified way," says Dr. Hill. "But its magnetic field is an important piece of the puzzle when it comes to understanding how the Universe and everything in it operates and came into being."

Already, the DRAGONS data have been used in a study of the mysterious large-scale reversal in the galactic magnetic field. This latest study was led by University of Calgary doctoral student Rebecca Booth and published in an accompanying paper in *The Astrophysical Journal*. This is a good example of how the dataset will provide opportunities for continued research in this field, says Dr. Ordog.

"DRAGONS is part of a new generation of radio surveys that allow scientists to map the Milky Way's three-dimensional magnetic field structure in the space between the stars," she adds. "It is an important Canadian contribution to the global astronomical community."

Compiled in part with material provided by the University of British Columbia (Patty Wellborn).

Chillin' on the newest Earth-like planet

Scientists continue to mine data gathered by NASA's *Kepler Space Telescope*, retired in 2018, and continue to turn up surprises. A new paper reveals the latest: a possible rocky planet slightly larger than Earth orbiting a 10.1-magnitude, orange K3.5V, Sun-like star about 146 light-years away. The candidate planet, HD 137010 b, might be remarkably similar to Earth, but it has one potentially big difference: It could be colder than perpetually frozen Mars.

An international science team was led by astrophysics Ph.D. student Alexander Venner of the University of Southern Queensland, Toowoomba, Australia, now a postdoctoral researcher at the Max Planck Institute for Astronomy, Heidelberg, Germany; the group included other astronomers from Harvard University and the University of Oxford.

A single transit implies that the orbital period of the planet—listed as a "candidate" pending further confirmation—is likely to be similar to Earth's, around one year. Planet HD 137010 b also might fall just within the outer edge of its star's "habitable zone," the orbital distance that could allow liquid water to form on the planet's surface under a suitable atmosphere.

This could turn out to be the first exoplanet with Earth-like properties that, from our vantage point, crosses the face of a Sun-like star that is near enough and bright enough for meaningful follow-up observations.

Now the bad news. The amount of heat and light such a planet would receive from its star is less than a third of what Earth receives from our star. Although of a stellar type similar to our Sun, the star, HD 137010, is about 550 °C cooler and dimmer. That could mean a planetary surface temperature no higher than –68 °C. By comparison, the average surface temperature on Mars runs about –65 °C.

Figure 2— Artist's concept of exoplanet candidate HD 137010 b, dubbed a "cold Earth" because it's a possible rocky planet slightly larger than Earth, orbiting a Sun-like star about 146 light-years away. Credit: NASA/JPL-Caltech/Keith Miller (Caltech/IPAC)

Planet HD 137010 b also will need follow-up observations to be promoted from "candidate" to "confirmed." Exoplanet scientists use a variety of techniques to identify planets, and this discovery comes from a single "transit"—only one instance of the planet crossing its star's face in a kind of miniature eclipse—detected during Kepler's second mission, known as K2.

Even with just one transit, the study's authors were able to estimate the candidate planet's orbital period. They tracked the time it took for the planet to move across the star's face—in this case 10 hours—then compared it to orbital models of the system itself. Still, though the precision of that single detection is much higher than most transits captured by space-based telescopes, astronomers need to see these transits repeat regularly in order to confirm that they are caused by a real planet.

In an interview with ABC Southern Queensland, UniSQ professor Jonti Horner agreed with the findings of the research, but stressed caution around the term "potentially habitable."

"If you were observing the Solar System from another star, you'd see three planets here that we'd consider to be potentially habitable—Venus, Earth, Mars—and only one of them is actually habitable," Dr. Horner said. But he also added that this was a "tantalising sneak peek of what there is still to discover."

Capturing more transits is going to be tricky. The planet's orbital distance, so similar to Earth's, means such transits happen far less often than for planets in tighter orbits around their stars; it's a big reason why exoplanets with Earth-like orbits are so hard to detect in the first place. With luck, confirmation could come from further observation by the successor to Kepler/K2, NASA's TESS (the *Transiting Exoplanet Survey Satellite*), the still-functioning workhorse for planetary detection, or from the European Space Agency's *CHEOPS* (CHaracterizing ExOPlanets Satellite). Otherwise, gathering further data on planet HD 137010 b might have to wait for the next generation of space telescopes.

Despite the possibility of a frigid climate, HD 137010 b also could turn out to be a temperate or even a watery world, say the authors of the paper. It would just need an atmosphere richer in carbon dioxide than our own. The science team, based on modelling of the planet's possible atmospheres, gives it a 40-percent chance of falling within the "conservative" habitable zone around the star, and a 51% chance of falling within the broader "optimistic" habitable zone. On the other hand, the authors of the study say the planet has about a 50–50 chance of falling beyond the habitable zone entirely.

Compiled with material provided by the University of Southern Queensland, ABC Southern Queensland, and NASA.

Europa wears an icy shell of considerable depth

Data from NASA's *Juno* mission has provided new insights into the thickness and subsurface structure of the icy shell encasing Jupiter's moon Europa. Using the spacecraft's Microwave Radiometer (MWR), mission scientists determined that the shell averages about 29 kilometres thick in the region observed during a *Juno* 2022 flyby of Europa. The *Juno* measurement is the first to discriminate between thin and thick shell models that have previously suggested the ice shell is anywhere from less than half a mile to tens of miles thick.

Slightly smaller than Earth's Moon, Europa is one of the Solar System's highest-priority science targets for investigating habitability. Evidence suggests that the ingredients for life may exist in the saltwater ocean that lies beneath its ice shell. Uncovering a variety of characteristics of the ice shell, including its thickness, provides crucial pieces of the puzzle for understanding the moon's internal workings and the potential for the existence of a habitable environment.

On 2022 September 29, *Juno* came within about 360 kilometres of Europa's frozen surface. During the flyby, MWR collected data on about half the moon's surface, peering beneath the ice to measure its temperatures at various depths.

"The 18-mile estimate relates to the cold, rigid, conductive outer-layer of a pure water ice shell," said Steve Levin, *Juno*

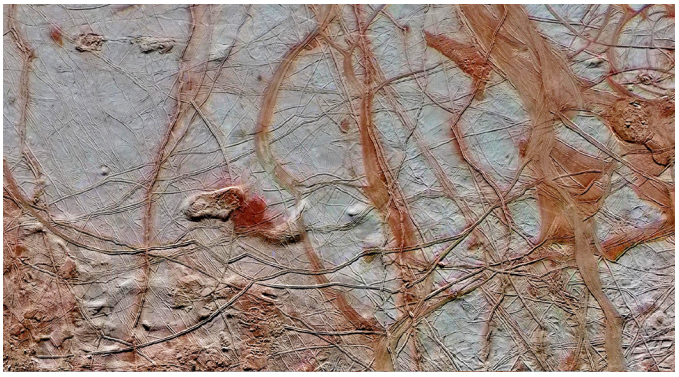

Figure 3 — An image showing a 350 by 750-kilometre swath across the surface of Jupiter's tantalizing moon Europa. Smooth ice plains, long fractures, and jumbled blocks of chaos terrain are thought to hide a deep ocean of salty liquid water beneath. Though the ice-covered alien ocean world is outside the Solar System's habitable zone, new studies show the potential chemistry driving its oxygen and hydrogen production, a key indicator of the energy available for life, could produce amounts comparable in scale to planet Earth. Image: NASA

project scientist and co-investigator from NASA's Jet Propulsion Laboratory in Southern California, which manages the mission.

"If an inner, slightly warmer convective layer also exists, which is possible, the total ice shell thickness would be even greater. If the ice shell contains a modest amount of dissolved salt, as suggested by some models, then our estimate of the shell thickness would be reduced by about 3 miles [5 km]."

The thick shell, as suggested by the MWR data, implies a longer route that oxygen and nutrients would have to travel to connect Europa's surface with its subsurface ocean. Understanding this process may be relevant to future studies of Europa's habitability.

Although the MWR instrument was designed to investigate Jupiter's atmosphere below the cloud tops, the novel instrument has proven valuable for studying the gas giant's icy and volcanic moons as well.

The MWR data also provides new insights into the makeup of the ice just below Europa's surface. The instrument revealed the presence of "scatterers"—irregularities in the near-surface ice such as cracks, pores, and voids that scatter the instrument's microwaves reflecting off the ice (similar to how visible light is scattered in ice cubes). These scatterers are estimated to be no bigger than a few inches in diameter and appear to extend to depths of only hundreds of feet below Europa's surface.

The small size and shallow depth of these features, as modelled in the study, suggest they are unlikely to be a significant pathway for oxygen and nutrients to travel from Europa's surface to its salty ocean.

"How thick the ice shell is and the existence of cracks or pores within the ice shell are part of the complex puzzle for understanding Europa's potential habitability," said Scott Bolton, principal investigator of *Juno* from the Southwest Research Institute in San Antonio.

"They provide critical context for NASA's *Europa Clipper* and the ESA (European Space Agency) *Juice* (JUpiter ICy moons Explorer) spacecraft—both of which are on their way to the Jovian system."

Europa Clipper will arrive there in 2030, while *Juice* will arrive the year after.

Rethinking the habitable zone

Astronomers have long searched for life within a rather narrow ring around a star, the "habitable zone," where a planet should be neither too hot nor too cold for liquid water. A new study argues that this ring is too strict: on tidally locked worlds that keep one face in daylight and the other in permanent night, heat may still circulate enough for liquid water to persist on the dark side, even when the planet orbits closer to cool M- and K-dwarf stars than conservative climate models allow.

The study also points outward: liquid water could exist far beyond the classical outer edge, hidden beneath ice as subglacial or intraglacial lakes, meaning the number of worlds worth checking for water, and potentially life-friendly conditions, may be much larger than the traditional map suggests.

For years, astronomers have relied on a simple rule of thumb when searching for life beyond Earth: look for planets in the "habitable zone," the narrow range around a star where liquid water can exist on a planet's surface. In our own Solar System, that zone lies roughly between the orbits of Earth and Mars.

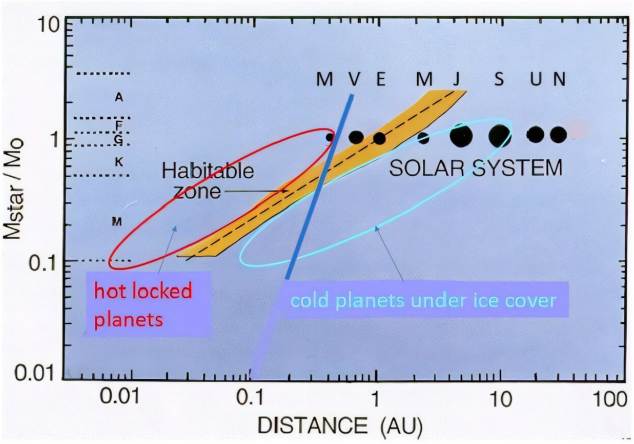

Figure 4 – Traditional and Extended Habitable Zones: The traditional habitable zone is shown by the diagonal orange stripe. Its distance from the host star (horizontal axis, in astronomical units) increases with luminosity, which in turn increases with the mass of the star and the stellar type (M, K, G, etc.) shown on the vertical axis. The ellipses represent the extensions of the habitable zone presented in the research. Credit: Amri Wandel

But many of the planets now being discovered do not fit neatly into this framework, orbiting stars quite different than our Sun, at distances closer than the inner edge of the habitable zone or farther out.

In a study published in *The Astrophysical Journal*, astrophysicist Prof. Amri Wandel from the Hebrew University asks what happens when scientists break the assumptions built into traditional habitability models. The focus is on tidally locked exoplanets, worlds that always face their star with the same hemisphere. These planets experience permanent daylight on one side and permanent night on the other, a configuration often considered to challenge surface liquid water and life.

Wandel's analysis suggests otherwise.

Using an analytical climate model that tracks temperature across the surface of such planets, the study shows that worlds orbiting M- and K-dwarf stars could sustain liquid water on their night side, even when they orbit significantly closer to their star than classical habitable-zone models allow. Heat transported from the day side can keep parts of the night side above freezing, expanding the range of environments where water may persist.

This extended definition of the habitable zone may help explain recent observations by the *James Webb Space Telescope*, which detected water vapour and other volatile gases in the atmospheres of warm, close-in Super-Earths orbiting M-dwarf stars—planets previously thought to lie outside the safe range for surface water.

The study also looks in the opposite direction, beyond the outer edge of the habitable zone. Even on cold planets far from their stars, liquid water could exist beneath thick ice layers, in the form of intraglacial lakes or subglacial melting, further widening the habitable zone and enhancing the number of worlds that may support water-based environments by a large factor.

By revisiting the assumptions behind the habitable zone and recalculating its boundaries, this research reframes where astronomers might look for conditions suitable for life, suggesting that potential habitats may exist on planets once ruled out. ✶

Composed with material provided by the Hebrew University of Jerusalem

Research Article / Articles de recherche

Gravity: A First Principles Derivation Connecting the Fundamental Constants G, c, and h

by Mauricio Vélez-Domínguez
mauriciovelez@post.harvard.edu

Abstract

Originating from a conceptual thought experiment rooted in fundamental physical principles, the proposed framework reinterprets gravity as an effect arising from local modulations in the intrinsic oscillatory energy of space. Rather than being a fundamental force or the result of spacetime curvature, gravity emerges from gradients in energy frequencies caused by the presence of matter. The resulting equation incorporates all three fundamental constants: the gravitational constant G, the speed of light c, and Planck's constant h.

I. Introduction

Newton's Law of Universal Gravitation states that two objects attract each other with a force that is directly proportional to the product of their masses and becomes weaker as the square of the distance between them increases (Newton, 1687)[1]:

$$F = G\frac{Mm}{r^2} \quad (1)$$

Where (G) represents the universal constant of gravitational (Freedman & Kaufmann III)[2].

Newton's framework implies that gravitation acts instantaneously across space, conflicting with Einstein's postulate that no information can travel faster than the speed of light (Einstein, 1920)[3]. To solve this, Einstein's general theory of relativity redefined gravity as the curvature of spacetime caused by the presence of matter and energy (Einstein, 1916)[4].

Although enormously successful in its predictive power, Einstein's geometric model works well on a cosmic scale, but it fails to account for phenomena at the atomic level, where quantum mechanics better describes the behavior of matter. This incompatibility suggests the two theories cannot both be entirely correct (Rovelli, 2014)[5].

The proposed gravitational model finds inspiration in James Clerk Maxwell's "A Dynamical Theory of the Electromagnetic Field". Maxwell elicits that gravitation is "traceable to the action of a surrounding medium (and that) every part of this medium possesses, when undisturbed, an enormous intrinsic energy, and that the presence of dense bodies influences the medium so as to diminish this energy wherever there is a resultant attraction". Maxwell finishes his note on gravitation adding, "As I am unable to understand in what way a medium can possess such properties, I cannot go any further in this direction in searching for the cause of gravitation" (Maxwell, 1864)[6].

In response to Maxwell's unresolved question and further developing notions presented in Vélez Domínguez (2024)[7], this paper reframes gravity as gradients in frequencies of the intrinsic energy of space caused by the presence of matter.

II. Methods

"We are to admit no more causes of natural things than such as are both true and sufficient to explain their appearance." (Newton, 1687)[8]

This inquiry is built upon two guiding principles: the first is to develop a conceptual framework that arises directly from first principles. The second is to describe gravitational dynamics through the most minimal and simplest possible mathematical formulations.

Let's imagine a sphere of empty space of volume (V) undisturbed by the presence of matter. Let us insert an object of mass (M) into the hypothetical sphere. The presence of the object in the sphere reduces the volume of empty space enclosed within the sphere. The change in volume by virtue of the presence of the object is expressed mathematically as:

$$\Delta V = V - V_0 \tag{2}$$

Where (V_0) is the volume of empty space remaining after the object (M) is introduced.

Based on Heisenberg's Uncertainty Principle, a volume of space "cannot be completely empty because it would mean that all the fields, such as the gravitational and the electromagnetic field, would have to be exactly zero" (Hawkings, 2017)[9]. Any given volume of empty space therefore has a certain amount of energy, and the amount of energy present in the vacuum is proportional to the volume of empty space (Bothwell, 2021)[10].

As per Maxwell's analysis, the presence of the dense body diminishes the volume of empty space, causing a proportional decrease in the total amount of intrinsic energy associated within said volume of space:

$$\Delta V = \Delta E \tag{3}$$

According to Planck's fundamental relationship between energy and frequency, a particle's energy (E) is proportional to the frequency of the particle (f), scaled by Planck's constant h (Planck, 1901)[11]:

$$E = hf \tag{4}$$

It can therefore be deduced that a change in energy (ΔE) implies a proportional change in frequency (Δf), as expressed in the equation:

$$\Delta E = h\Delta f \tag{5}$$

However, this local decrease in energy within the sphere does not imply that energy is being destroyed. The model suggests that the presence of the object in the imaginary sphere causes a proportional outflow of energy. The possible existence of this hypothetical gravitational energy flow can be demonstrated through the effect it produces in the motion of objects orbiting around the imaginary sphere. Any deviations in the object's expected path could indicate the presence of this energy flow Please refer to Appendix A for a calculation of the variation of Mercury's orbit based on this model, resulting in 43 arc seconds per century, in line with general relativity (Einstein, 1915)[12].

Hence, when the object of mass (M) is inserted into the imaginary sphere, it reduces the amount of energy of space in proportion to the object's energy (E_m):

$$E - E_0 = E_m \tag{6}$$

Where (E) is the energy of empty space inside the sphere undisturbed by the presence of matter, and (E_0) is the energy of empty space remaining after the object of mass (M) is introduced.

One of the most relevant features of this approach is its covariance with general relativity, which ensures consistency across different reference frames. Both models work because curvature and volume are covariant properties of the geometry of space, (Kaku, 2004)[13]. Gravity can therefore be quantified by measuring the curvature that objects cause in the geometry of spacetime, as per general relativity, or by measuring the change that objects cause in the energy content of a given volume of space. As a result, energy produces the gravity in both frameworks. Hence, through their own geometry, curvature and volume both express how much gravitational field there is (Rovelli, 2014)[14].

III. Results and Discussion

A. Deriving Gravitation from First Principles.

Consider now a point particle of mass (m), located at a distance (r) from the centre of the sphere, falling with velocity (v) toward the mass (M). We know that at its root, the force between (M) and (m) can be expressed as a gradient (rate of change) of energy with respect to the change in position (Carroll, 2022)[15]:

$$F_g = \frac{E - E_0}{\Delta r} = \frac{\Delta E_m}{\Delta r} \tag{7}$$

Furthermore, if only gravitation is acting on the point-mass particle, its total mechanical energy is the sum of the particle's kinetic and potential energy. By virtue of the Law of Conservation of Energy, the body's energy remains constant during the trajectory and can be expressed as:

$$E_m = K + U = \frac{1}{2}mv^2 - \frac{GMm}{r} \tag{8}$$

Where (E_m) is the total mechanical energy of the particle, (K) is the kinetic energy ($1/2mv^2$); (U) the potential energy ($-GMm/r$); (v) is the velocity of the point mass particle of mass (m), and (r) the distance between (M) and (m) (Ohanian & Markert, 2007)[16]. Substituting ΔE_m in equation 7 yields:

$$F = \frac{\Delta E_m}{\Delta r} = \frac{\Delta\left(\frac{1}{2}mv^2 - \frac{GMm}{r}\right)}{\Delta r} \quad (9)$$

However, this paper hypothesizes that the force acting on (m) emerges from frequency shifts in the energy of the gravitational field as the point-mass particle moves toward (M). Therefore, the gravitational force is not only proportional to the energy gradient as per equation 9, but it is also proportional to the frequency shift. Expressed mathematically, it is the product of the energy gradient and the corresponding shift in frequency:

$$F = \frac{\Delta\left(\frac{1}{2}mv^2 - \frac{GMm}{r}\right)}{\Delta r} \cdot \left(\frac{f_0 - f}{f_0}\right) \quad (10)$$

Here, (F) is the gravitational force that emerges from the change in energy and frequency caused by the presence of the object of mass (M) inside the imaginary sphere; (f) is the frequency of the intrinsic energy of space unperturbed by the presence of matter inside the sphere; (f_0) is the frequency of the intrinsic energy of space in the presence of object (M); and ($f_0 - f)/f_0$ the frequency shift, acting as the modulating factor that scales the relationship and determines how changes in energy relate proportionally to gravitational force.

B. Derivation in Weak Field Limit

Let's now explore the dynamics of the point-mass particle as it falls towards (M). When the particle is farthest away from the object (M), where the gravitational field is weakest, the force it experiences is at its minimum and its frequency at its maximum. At this point, the kinetic energy ($1/2mv^2/r$) is zero, and the potential energy reaches its maximum value. Substituting ($1/2mv^2/r$) by 0 in equation 10 yields:

$$F_g = -\frac{\frac{GMm}{r}}{r} \cdot \left(\frac{f_0 - f}{f_0}\right) \quad (11)$$

Solving,

$$F_g = -G\frac{Mm}{r^2} \cdot \left(\frac{f_0 - f}{f_0}\right) \quad (12)$$

Where GMm/r^2 is Newton's Universal Law of Gravitation. In this extreme weak field limit scenario, there is no frequency shift when the distance between objects (M) and (m) is very large ($r \to \infty$), both masses are in the same gravitational potential ($f_0 = f$), or when (M) is zero (M=0), no frequency shift occurs and there is no gravitational force.

Moreover, if instead of a point mass particle we have a photon of light, we can replace the particle's energy (E_m) in equation 10 with *hf* as per Planck's energy equivalence principle (equation 4), resulting in:

$$F_g = \frac{hf}{r} \cdot \left(\frac{f_0 - f}{f_0}\right) \quad (13)$$

On the other hand, based on Einstein's energy equation,

$$E = mc^2 \quad (14)$$

in which (E) is the rest energy associated with the mass (m) of a particle, and (c) is the speed of light (Einstein, 1905)[17], we can equate the energy equations from quantum mechanics and general relativity according to de Broglie, (1925)[18] and Penrose (2010)[19]:

$$fh = mc^2 \quad (15)$$

Replacing (fh) in equation 13 by (mc^2) from equation 15 yields:

$$F_g = \frac{mc^2}{r} \cdot \left(\frac{f_0 - f}{f_0}\right) \quad (16)$$

Setting equation 13 equal to Newton's Universal Law of Gravitation:

$$\frac{hf}{r} \cdot \left(\frac{f_0 - f}{f_0}\right) = G\frac{Mm}{r^2} \quad (17)$$

Solving for frequency shift ($f_0 - f)/f_0$:

$$\left(\frac{f_0 - f}{f_0}\right) = G\frac{Mm}{hfr} \quad (18)$$

Likewise, we can set equation 16 equal to Newton's equation:

$$\frac{mc^2}{r} \cdot \left(\frac{f_0 - f}{f_0}\right) = G\frac{Mm}{r^2} \quad (19)$$

Solving for frequency shift ($f_0 - f)/f_0$ yields:

$$\left(\frac{f_0 - f}{f_0}\right) = \frac{GM}{c^2 r} \quad (20)$$

Here, GM/c^2r is a dimensionless ratio that emerges naturally in the context of this gravitational model. Although derived independently of general relativity, the result is consistent with Einstein's gravitational redshift equation (Einstein, 1920)[20], describing the displacement of spectral lines towards the red in weak gravitational fields (Misner, Thorne and Wheeler, 1970 and 1971)[21].

This relationship is significant because gravitational fields affect the vibrational frequency of atoms, which refers to the rate at which atoms oscillate. It therefore defines a mechanism by which atoms can act as tools to measure changes in the gravitational force, in line with this paper's hypothesis proposed that gravity arises from gradients in frequency and energy. The relationship is captured in a general frequency gradient gravitational force equation expressed as:

$$F_g = \frac{\Delta E_m}{\Delta r} \cdot \left(\frac{f_0 - f}{f_0}\right) \quad (21)$$

C. Strong Field Limit Dynamics

When the particle is closest to the object (M), where the gravitational field is strongest, the force it experiences is at its maximum and the frequency of oscillation at its minimum. At this point—representing the strong-field limit—the potential energy (–GMm/r) is zero, and the kinetic energy reaches the

maximum value. Substituting (–GMm/r) by 0 in equation 10 yields:

$$F_g = \frac{1}{2}\frac{mv^2}{r} \cdot \left(\frac{f_0 - f}{f_0}\right) \quad (22)$$

We can calculate frequency shift in this scenario by setting equation 22 equal to Newton's Universal Law of Gravitation (equation 1):

$$\frac{1}{2}\frac{mv^2}{r} \cdot \left(\frac{f_0 - f}{f_0}\right) = G\frac{Mm}{r^2} \quad (23)$$

It can be easily demonstrated that solving for frequency shift $(f_0 - f)/f_0$ yields:

$$\left(\frac{f_0 - f}{f_0}\right) = \frac{2GM}{v^2 r} \quad (24)$$

Stating that the frequency shift experienced by the point-mass particle (m) in a strong gravitational field is proportional to two times (G) multiplied by the mass of the object (M) in the imaginary sphere, and inversely proportional to the square of the particle's velocity, multiplied by the distance between (M) and (m).

Let's now imagine that the point-mass particle is a photon travelling at the speed of light (c). Substituting velocity (v) by (c) in equation 24 yields:

$$\left(\frac{f_0 - f}{f_0}\right) = \frac{2GM}{c^2 r} \quad (25)$$

Let's also imagine a scenario in which the gravitational field of (M) is so strong, that the frequency of the photon is attenuated down to zero, as per the expression:

$$\left(\frac{f_0 - f}{f_0}\right) = \frac{f_0 - 0}{f_0} = \frac{f_0}{f_0} = 1 \quad (26)$$

Where (f) is the starting frequency and (f_0) the final frequency. By substituting the frequency shift $(f_0 - f)/f_0$ by 1 in equation 25 yields:

$$1 = \frac{2GM}{c^2 r} \quad (27)$$

And solving for r:

$$\mathrm{r} = \frac{2GM}{c^2} \quad (28)$$

Where (r) denotes the critical radius at which the frequency of a light wave is reduced to zero by an intense gravitational field.

Equation 28 ($r=2GM/c^2$) as derived through the gravitational frequency framework, precisely matches Schwarzschild's Radius (Schwarzschild, 1916)[22]. In Schwarzschild's solution to Einstein's field equations, $2GM/c^2$ represents the critical radius such that, if an object's entire mass were to be compressed within a sphere of said radius, the resulting gravitational field would be so intense that no form of radiation, including light, could escape—thereby forming a black hole (Kilmister, 1971)[23].

Furthermore, solving for the mass of object (M) yields:

$$\mathrm{M} = \frac{c^2 r}{2G} \quad (29)$$

Where (M) represents the minimum mass that must be enclosed within a radius (r) for the gravitational field to reduce the frequency of a light wave to zero.

Similarly, equation 29 ($M=c^2r/2G$), also derived without invoking general relativity, represents the mass required for radius (r) to be a black hole in Schwarzschild's solution (Schwarzschild, 1916)[24].

D. Expressing Gravitation with the Fundamental Constants G, c and h.

We have derived the gravitational equations and their corresponding frequency shift expressions from first principles. We will now show that they are all contained within a single, compact expression—one intrinsically present in Newton's law of gravitation, though not immediately apparent. Since gravity travels at the speed of light (Einstein, 1916),[25] like the proposed gravitational flow in the thought experiment, Newton's Universal Law of Gravitation can be rephrased as:

$$F = G\frac{Mm}{c^2 t^2} \quad (30)$$

Where (c) is the speed of light and (t) is the time that it takes gravity to travel between objects (M) and (m). Here, Newton's distance (r^2) in denominator is expressed as the square of the product of velocity (v) and time (t), given that the average velocity is defined as the change in distance divided by the change in time (Pask, 2019)[26],

$$\Delta v = \frac{\Delta r}{\Delta t} \text{ or } r = v \cdot t \quad (31)$$

Substituting velocity (v) by the speed of light (c), the distance (r^2) becomes c^2t^2. Furthermore, based on the energy equivalence between quantum mechanics and general relativity as per equation 15 ($fh=mc^2$), solving for mass yields:

$$m = \frac{hf}{c^2} \quad (32)$$

Replacing the mass of the point mass particle (m) in equation 30 with hf/c^2 from equation 32 above, and solving, yields:

$$F = G\frac{Mhf}{c^4 t^2} \quad (33)$$

The presence of the three universal constants (G), (h) and (c) in the same equation suggests a domain where gravity, quantum mechanics and relativity intersect (Rovelli, 2014)[27].

Furthermore, since distance (r^2) can be expressed as (c^2t^2), as seen in equation 30, we can factor the denominator and obtain:

$$c^4 t^2 = c^2 \cdot c^2 t^2 = c^2 r^2 \quad (34)$$

We can therefore rephrase equation 33 as:

$$\boldsymbol{F} = G\frac{Mhf}{c^2r^2} \text{ or } \mathrm{F} = \frac{hf}{r}\cdot\frac{GM}{c^2r} \quad (35)$$

Resulting in an expression that is consistent with the proposed notion that gravity emerges from gradients in frequency and energy, as per equation 21:

$$F_g = \frac{\Delta E}{\Delta r}\cdot\left(\frac{f_0 - f}{f_0}\right) \quad (21)$$

Here, the energy gradient can be expressed as fh/r, or mc^2/r or $1/2mv^2/r$, as per equations 13, 16 and 22.

Furthermore, equation 33 can be rephrased as:

$$F = \frac{hG}{c}\cdot\frac{Mf}{c^3t^2} \quad (36)$$

A dimensional analysis of the factor $\hbar G/c$ results in units of volume multiplied by units of acceleration ($m^3 \cdot m/s^2$), pointing to the possibility that this expression represents the product of a minimum volume of space (m^3) scaled by acceleration (m/s^2).

Drawing from Einstein's insight that $E=mc^2$ and his framing of gravity as a universal interaction between all forms of energy (Hartle, 2003)[28], $\hbar G/c$ can be interpreted as being analogous to Newton's Second Law of Motion, suggesting that hG/c may refer to the minimal action required to induce an *alteration* in the state of motion of the gravitational field within the minimum volumetric structure of space.

Support for this interpretation is rooted in the fact that the constant relationship hG/c (1.475×10^{-52} m^4/s^2) appears as a building block in the structure of Planck-scale geometry or Planck units. For example, Gh/c^3 provides a means to calculate the fundamental geometrical quantity at the Planck scale, representing the smallest physically meaningful unit of spatial dimension in physics, Planck's length (Planck, 1899)[29]:

Planck's length:

$$\text{Planck's length: } l_p = \sqrt{\frac{hG}{2\pi c^3}} \quad (37)$$

Confirmation of the model's alignment with theoretical and observational data in the strong field limit can be found in Appendixes A. Further support in the weak field limit is offered in Appendixes B and C. The data used in the calculations is provided for purposes pertaining verification or replication of the results.

IV. Conclusions

The theoretical structure of gravity proposed in this paper suggests that the phenomenon of gravitation has its roots in energy-frequency gradients within a universal undulatory field, where the steepness of the slope determines the strength of gravitation. Objects therefore "roll down" the gradient, from high frequency regions, where time flows faster and entropy is lower, toward low frequency regions, where time flows slower and entropy is higher. Matter coalesces in low frequency nodes by virtue of the presence of matter, instead following the curvature of spacetime.

A conceptual parallel with cymatics offers potential theoretical and experimental support for this assertion (Velez Domínguez, 2024)[30]. Cymatics explores how particles on a surface form geometric patterns under the influence of sound and vibration at specific frequencies (Jenny, 2001)[31]. This phenomenon, discovered by Ernst Chladni (Chladni, 1809)[32], shows how matter coalesces in areas of minimal or very low vibration, demonstrating how frequencies may act as the driving force behind the organization of matter.

Moreover, the simultaneous presence of the Gravitational constant (G), Planck's constant (h), and the speed of light (c), through the factor Gh/c, suggests that quantum phenomena may significantly influence gravitational interactions, potentially providing a pathway toward bridging gravity with the other fundamental forces. Further work is required to assess the validity of this formulation and implications and consistency with established theories must be critically examined. ✶

Acknowledgments

I want to thank the authors referenced throughout the paper for making their knowledge accessible to everyone. I express my gratitude to Tania Vélez, Joaquín Illiceto, Karim Salem, Fernando Guzmán, Freddy Jiménez, Arthur Maury, Julian Sancton, Jorge Enrique Abello, Pedro Conrado, Victor De La Hoz, and the students in the IEA José Celestino Mutis class of 2028, for constructive discussions. To Tatiana Pérez, and to my mother, Lucía Domínguez, for their support. Finally, I dedicate this journey to my daughters, Martina and Olivia, who inspire my every day. The author used OpenAI's GPT-3 language model to help polish and condense parts of the text. The author takes full responsibility and accountability for the content and declares that is it entirely his original creation and work.

Appendix A: Calculating The Motion Of Mercury's Perihelion And The Gravitational Deflection Of Light.

The gravitational framework based on frequency shift, as proposed in this paper, finds further proof in the fact that it can predict the motion of Mercury's perihelion and the angle by which light is deflected by a gravitational field, without invoking the mathematical machinery of general relativity, nor attributing gravity to the curvature of spacetime. Both results are in complete accordance with general relativity, yielding the additional 43 arc seconds per century of orbit rotation for Mercury (Einstein, 1916)[33], and 1.75 arcseconds for the deflection of light by the Sun (Einstein, 1916)[34]. A full derivation of the angle of Mercury's precession is available upon request to the

author, yielding the equation:

$$\Delta\emptyset = \left(\frac{f_0 - f}{f_0}\right) \cdot \frac{6\pi}{(1-e^2)} \quad (38)$$

Which can also be expressed by substituting $(f_0 - f)/f_0$ by GM/c^2r:

$$\Delta\emptyset = \frac{GM}{c^2 r} \cdot \frac{6\pi}{(1-e^2)} \quad (39)$$

Here, $\Delta\emptyset$ is the angle by which the perihelion shifts, (e) is the eccentricity of Mercury's orbit; and the term 6π emerges as a drag factor caused by the hypothetical gravitational flow, derived by normalizing to unity the variables for viscosity (n), radius (r) and velocity (V) in Stokes Law (Stokes, 1851)[35]:

$$F_{drag} = 6\pi nrV \quad (40)$$

Furthermore, as demonstrated in equation 25, the gravitational frequency shift in strong field limits was calculated to be $2GM/c^2r$, which is twice the factor obtained by Soldner (1801)[36] in his derivation of the angle of deflection of light. It follows that the resulting equation for the deflection of light by a gravitational field yields a result that is in line with Einstein's derivation (Einstein 1916)[37]:

$$\Delta\emptyset = 4\left(\frac{f_0 - f}{f_0}\right) \; or \; \Delta\emptyset = \frac{4GM}{c^2 r} \quad (41)$$

Appendix B: Verification of $F_g = mc^2/r \cdot (f_0 - f)/f_0$

Frequency of spectral line of Cesium in Earth = 9.1926317700×10^9 Hz NIST (2022)[38]

Frequency of spectral line of Cesium in the Sun: $f_0 = f/ (GM/c^2r+1) = 9.1926316792 \times 10^9$ Hz

Gravitational constant G: 6.67×10^{-11} N·m^2 /kg^2 NIST (2022)[39]

Sun's Mass (M): 1.9890E+30 kg Bishop (2024)[40]

Earth's Mass (m): 5.9722×10^{24} Bishop (2024)[41]

Speed of light (c) = 2.9979×10^8 m/sec NIST (2022)[42]

Orbital Distance (r):1.495×10^{11} m Bishop (2024)[43]

$GM/c^2r = 9.8797398382 \times 10^{-9}$ Hz

$\nabla f = (f_0 - f)/f_0 = -9.8797398382 \times 10^{-9}$ Hz

Substituting in the values for the equation $\mathbf{F_g = mc^2/r \cdot (f_0 - f)/f_0}$, we obtain:

$F = ((5.972 \times 10^{22}) \times (2.9979 \times 10^8)^2 \times (-9.879739832 \times 10^{-9})) / 1.4950 \times 10^{11}$

Which amounts to $-3.54707822 \times 10^{22}$ N (The negative sign indicates gravity is a repulsive force in this frequency based framework). The benchmark gravitation using Newton's Law is GMm/r^2, which yields: $3.54707819 \times 10^{22}$ N

Appendix C: Verification of $F_g = fh/r \cdot (f_0 - f)/f_0$ and $F = GMfh/c^4t^2$

Plank's constant (h): 6.63×10^{-34} kg·m^2/s NIST (2022)[44]

Earth's mass frequency ($f = mc^2/h$): 8.1002431×10^{74} Hz

Orbital Distance (r):1.495×10^{11} m Bishop (2024)[45]

$\nabla f = (f_0 - f)/f_0 = -9.8797398382 \times 10^{-9}$ Hz

Substituting in the values for the variables for $\mathbf{F_g = fh/r \cdot (f_0 - f)/f_0}$, we obtain:

$F = (6.63 \times 10^{-34} \times 8.1002431 \times 10^{74}$ Hz) / 1.495×10^{11}m

Resulting in $-3.54707822 \times 10^{22}$N

And substituting the variables in equation $F_g = GMfh/c^4t^2$ yields:

Time ($t = r/c$): 4.99×10^2 sec

$F = GMfh/c^4t^2 = 3.5471 \times 10^{22}$ N

References

1 Newton, Isaac (1687), *The Mathematical Principles of Natural Philosophy*. Translated into English by Andrew Motte (1846), Published by Daniel Adee, 45 Liberty Street, New York, Book III, Proposition VII. Theorem VII P.397, https://archive.org/details/newtonspmathema00newtrich/page/n7/mode/2up.

2 Freedman, Roger and Kaufmann, William III (2008), *Universe*, W.H. Freeman and Company, 8th Edition, P. 84.

3 Einstein, Albert (1920), introduced by Nigel Clader (1920), *Relativity: The Special and The General Theory*, Penguin Classics, p. 36.

4 Einstein, Albert (1916), The Foundation of the General Theory of Relativity, translated from "Die Grundlage der allgemeinen Relativitätstheorie", Annalen der Physik, 49,

5 Rovelli, Carlo (2014), *Reality is not What it Seems: The Journey to Quantum Gravity*, Riverhead Books 2017, An imprint of Penguin Random House LLC, p. 147.

6 Maxwell, James Clerk(1864), A Dynamical Theory of the Electromagnetic Field, Rough Draft Printing (2013), pp. 38–39.

7 Vélez-Dominguez, Mauricio (2024), Redshift Variation Asymptotics: Signatures of cosmic deceleration of time in an oscillating and non-expanding universe, *JRASC*, Volume 118, Number 4, August 2024, p. 164

8 Newton, Isaac (1687), The Mathematical Principles of Natural Philosophy. Translated into English by Andrew Motte (1846), Published by Daniel Adee, 45 Liberty Street, New York, Book III, Rule 1, p. 384,

9 Hawking, Stephen (2017). A Brief History of Time, Bantham Books Trade Paperback Edition, p. 109

10 Bothwell, Mathew (2021). The Invisible Univere, Why There's More to Reality Than Meets the Eye, One World Publications, p. 271.

11 Planck, Max (1901), On the Law of Distribution of Energy in the Normal Spectrum, Annalen der Physik, Vol.4, p. 553 ff

12 Einstein, Albert (1915). Explanation of the Perihelion Motion of Mercury from General Relativity Theory, Königlich PreuBishe Akademie der Wissenschaften, P 831–839. Albert Einstein (1920), introduced by Nigel Clader (1920), *Relativity: The Special and The General Theory*, Penguin Classics, p. 115

13 Kaku, Michio (2004), Einstein's Cosmos: How Albert Einstein's Vision Transformed Our Understanding of Space and Time, Atlas Books and W.W. Norton & Company, p. 102.

14 Rovelli, Carlo (2014), *Reality is not What it Seems: The Journey to Quantum Gravity*, Riverhead Books 2017, An imprint of Penguin Random House LLC, p. 163.

15 Carroll, Sean (2022). The Biggest Ideas in the Univere: Space, Time and Motion, Dutton, An imprint of Penguin Random House LLC, p. 65

16 Ohanian, Hans C. and Markert, John T. (2007). *Physics for Engineer and Scientists Third Edition*, W.W. Norton & Company, p. 290

17 Einstein, Albert (1905). Trägheit eines Körpers von seinem Energieinhalt abhängig?, in *Annalen der Physik*. 18:639, p. 3.

18 de Broglie, Louis (1925), Recherches Sur La Theorie Des Quanta, Annales de Physique - 10e Série - Tomè III, p. 33

19 Penrose, Roger (2010). Cycles of Time: An Extraordinary New View of the Universe. The Bodley Head, p. 93.

20 Einstein, Albert (1920), introduced by Nigel Clader (1920), *Relativity: The Special and The General Theory*, Penguin Classics, p. 120.

21 Misner, Charles W., Thorne, Kip S., and Wheeler, John Archibald (1970 and 1971). Gravitation, W.H. Freeman and Company, p. 187

22 Schwarzschild, K (1916), (translation and foreword by S.Antoci and A.Loinger) On the gravitational field of a mass point according to Einstein's theory, arXiv:physics/9905030, Sitzungsber.Preuss.Akad. Wiss.Berlin (Math.Phys.) (1916) pp. 189–196. A contemporary derivation of Schwarzschild's original equations can be found in https://en.wikipedia.org/wiki/Derivation_of_the_Schwarzschild_solution?utm_source

23 Kilmister, Clive (1971). The Nature of the Universe, Thames and Hudson Ltd London, p. 173.

24 Schwarzschild, K. (1916), (translation and foreword by S.Antoci and A.Loinger) On the gravitational field of a mass point according to Einstein's theory, arXiv:physics/9905030, Sitzungsber.Preuss.Akad. Wiss.Berlin (Math.Phys.) 1916 (1916) pp. 189–196. A contemporary derivation of Schwarzschild's original equations can be found in https://en.wikipedia.org/wiki/Derivation_of_the_Schwarzschild_solution?utm_source

25 Einstein, Albert (1916). *Näherungsweise Integration der Feldgleichungen der Gravitation*, Sitzungsberichte der Preußischen Akademie der Wissenschaften (Berlin), p. 688 https://articles.adsabs.harvard.edu/pdf/1916SPAW.....688E. An English translation https://einsteinpapers.press.princeton.edu/vol6-trans/213, The Collected Papers of Albert Einstein, einsteinpapers.press.princeton.edu. The Hebrew University of Jerusalem and Princeton University Press, Volume 6: The Berlin Years: Writings, 1914–1917 (English translation supplement) p. 201

26 Pask, Colin (2019), *Magnificent Principia: Exploring Isaac Newton's Masterpiece*, Prometheus Books, p. 114.

27 Rovelli, Carlo (2014), *Reality is not What it Seems: The Journey to Quantum Gravity*, Riverhead Books 2017, An imprint of Penguin Random House LLC, p. 153.

28 Hartle, J.B. (2003). *Gravity: An introduction to Einstein's General Relativity*. San Francisco: Addison-Wesley. p. 4

29 Planck, Max (1899). *Ueber irreversible StrahlungsvorgiXnge; Sitzungsberichte der Königlich Preußischen Akademie der Wissenschaften zu Berlin* (Proceedings of the Royal Prussian Academy of Sciences), p. 122

30 Vélez-Dominguez, Mauricio (2024), Redshift Variation Asymptotics: Signatures of cosmic deceleration of time in an oscillating and non-expanding universe, *JRASC, Volume 118, Number 4*, August 2024, p. 177

31 Jenny, Hans (2001). *Cymatics: A Study of Wave Phenomena & Vibration*, MACROmedia Publishing; 3rd edition (July 1, 2001), ISBN-10 1888138076, https://ia803402.us.archive.org/11/items/hans-jenny-cymatics/Hans%20Jenny%20-%20Cymatics.pdf. p. 97

32 Chladni, E.F.F (1809). Traité D'Acoustieque, Courcier. Treatise on Acoustics: The First Comprehensive English Translation of E.F.F. Chladni's Traité d'Acoustique, translated by Robert T. Beyer.ASA Press, Springer International Publishing Switzerland 2015, ISBN 978-3-319-20360-7 DOI 10.1007/978-3-319-20361-4, pp. 73–22

33 Einstein, Albert (1916), *The Foundation of the General Theory of Relativity*, translated from "Die Grundlage der allgemeinen Relativitätstheorie", Annalen der Physik, p. 163 http://eotvos.dm.unipi.it/documents/EinsteinPapers/Einstein1911English.pdf

34 Einstein, Albert (1916), *The Foundation of the General Theory of Relativity*, translated from "Die Grundlage der allgemeinen Relativitätstheorie", Annalen der Physik, p. 163 http://eotvos.dm.unipi.it/documents/EinsteinPapers/Einstein1911English.pdf

35 Stokes, George Gabriel (1851), On The Effect of the Internal Friction of Fluids on the Motion of Pendulums, *Transactions of the Cambridge Philosophical Society*, p. 38

36 Jaki, Stanley (1978). Johann Georg von Soldner and the Gravitational Bending of Light, with an English Translation of his Essay on It Published in 1801, *Foundations of Physics, Vol. 8, Nos. 11/12*. pp. 927–948

37 Einstein, Albert (1916), *The Foundation of the General Theory of Relativity*, translated from "Die Grundlage der allgemeinen Relativitätstheorie", Annalen der Physik, p. 163 http://eotvos.dm.unipi.it/documents/EinsteinPapers/Einstein1911English.pdf

38 Tiesinga, Eite, Mohr, Peter J., Newell, David B., and Taylor, Barry N. (2022), *2022 CODATA recommended values*, National Institute for Standards and Technology, https://physics.nist.gov/cgi-bin/cuu/Value?bg

39 Tiesinga, Eite, Mohr, Peter J., Newell, David B., and Taylor, Barry N. (2022), *2022 CODATA recommended values*, National Institute for Standards and Technology, https://physics.nist.gov/cgi-bin/cuu/Value?bg

40 Bishop, Roy (2024), The Royal Astronomical Society of Canada *Observer's Handbook*, p. 22.

41 Bishop, Roy (2024), The Royal Astronomical Society of *Canada Observer's Handbook*, p. 22.

42 Tiesinga, Eite, Mohr, Peter J., Newell, David B., and Taylor, Barry N. (2022), *2022 CODATA recommended values*, National Institute for Standards and Technology, https://physics.nist.gov/cgi-bin/cuu/Value?bg

43 Bishop, Roy (2024), The Royal Astronomical Society of Canada *Observer's Handbook*, p. 22.

44 Eite Tiesinga, Peter J. Mohr, David B. Newell, and Barry N. Taylor (2022), *2022 CODATA recommended values*, National Institute for Standards and Technology, https://physics.nist.gov/cgi-bin/cuu/Value?bg

45 Bishop, Roy (2024), The Royal Astronomical Society of Canada *Observer's Handbook*, p. 22.

The June 2026 *Journal* deadline for submissions is 2026 April 1.

See the published schedule at rasc.ca/sites/default/files/jrascschedule2026.pdf

Photometric Characterization of Newly Discovered Potentially Hazardous Asteroid 2025 FA22

by Arushi Nath, Masason Scholar;
Founder MonitorMyPlanet.com

Abstract

Potentially Hazardous Asteroid (PHA) 2025 FA22 made a close approach to Earth on 2025 September 18 (UTC) at a distance of approximately two lunar distances. Time-resolved CCD photometry of the asteroid was obtained during its close Earth approach in September 2025. Observations spanning six nights were used to determine the asteroid's synodic rotation period, lightcurve amplitude, and broadband colour indices. A well-defined rotation period of 13.075 ± 0.002 h was derived from R-band photometry, with a peak-to-peak lightcurve amplitude of 0.62 mag, implying a significantly elongated shape and a minimum equatorial axis ratio of a/b ≳ 1.77. Multi-filter BVRI photometry yields moderately red colours consistent with an S-complex taxonomic classification, although broadband colour degeneracy prevents a unique assignment. These observations demonstrate that citizen scientists can provide meaningful physical characterization of near-Earth asteroids.

1. Introduction

Asteroid 2025 FA22 was discovered by the Pan-STARRS 2 survey on 2025 March 29. Initial orbit determinations indicated a small but non-zero probability of Earth impact during a possible return in 2089, briefly placing the object at Torino Scale level 1 (Jet Propulsion Laboratory ECHO, 2025). Subsequent astrometric follow-up rapidly refined the orbit, reducing the impact probability to effectively zero and removing the object from planetary risk lists by early May 2025.

The asteroid made a close approach to Earth on September 18, 2025 (UTC), passing at a distance of approximately 0.005 au (two lunar distances) from the Earth. Based on its absolute magnitude and an assumed range of geometric albedos typical of near-Earth asteroids, its diameter was estimated to lie between approximately 130 m and 290 m. (European Space Agency, 2025). With a minimum orbit intersection distance (MOID) of approximately 0.00173 au, 2025 FA22 satisfies the criterion for classification as a potentially hazardous asteroid (PHA).

Owing to its size, close-approach geometry, and early impact-risk assessment, the International Asteroid Warning Network (IAWN) selected 2025 FA22 as the target of an international planetary-defense exercise aimed at testing coordinated optical recovery and physical characterization of a simulated impactor (International Asteroid Warning Network, 2025). The author contributed time-resolved photometric observations to this campaign.

2. Observations

Observations were conducted remotely by the author using a 0.305-m *f*/6 Ritchey–Chrétien telescope at her Monitor-MyPlanet Observatory (Minor Planet Centre code R60), located in Nerpio, Spain. The telescope was equipped with a thermoelectrically cooled CCD camera operating at a resolution of 6248 × 4176 pixels, corresponding to a pixel scale of 0.848 arcsec pixel^{-1}. Standard Johnson-Cousins B, V, R, and I broadband filters were used.

Time-series CCD photometry was obtained on six nights between 2025 September 19 and 26, for a total on-sky integration time of approximately 35 hours (Table 1). The dataset comprises just over 3000 individual exposures, with observations conducted predominantly in the R band. Multi-filter BVRI observations were obtained on one night (2025 September 22).

Over the observing interval, the mean phase angle decreased from approximately 60° to 25°. As the asteroid's rotation period was unknown at the time of observation, coverage over multiple nights was required to ensure adequate rotational phase sampling and to mitigate period aliasing in subsequent lightcurve analysis.

Date (UT) (all 2025)	Time (UT)	Duration	Images	Exposure Time (s)	Filters Used	Mean Phase Angle (deg)
Sep 19	02:57 - 04:24	1h27m	779	4	R	60.2
Sep 21	22:07 - 04:59	6h52m	872	20-25	R	32.3
Sep 22	21:39 - 04:59	7h20m	538	40	R, V, B, I	30.0
Sep 23	21:19 - 03:03	5h44m	457	40	R	28.4
Sep 25	21:48 - 04:50	7h02m	183	120	R	26.0
Sep 26	20:58 - 04:50	7h52m	190	120	R	25.0

Table 1 — Observing log for asteroid 2025 FA22.

2.1 Specialized Photometry Techniques for a Fast-Moving Near-Earth Asteroid

During close Earth approaches, near-Earth asteroids can exhibit rapid apparent sky-plane motion, complicating time-series photometry through image trailing, frequent repointing, and changes in the available comparison-star field. These challenges necessitated specialized observing strategies for 2025 FA22.

During the observation night of its closest approach (early hours of 2025 September 19), the asteroid exhibited an apparent angular motion of approximately 3 arcsec s^{-1}. Exposure times were dynamically adjusted to limit image trailing. At the highest apparent rates, exposures were reduced to 4 s, limiting trailing to ≤12 arcsec. As the apparent motion decreased over subsequent nights, exposure times were progressively increased to as long as 120s to improve the signal-to-noise ratio.

All observations were conducted in sidereal tracking mode with short exposures in rapid succession. To maximize uninterrupted temporal coverage within a single pointing, the asteroid was intentionally positioned near an edge of the detector rather than at the field centre. This strategy enabled longer continuous observing sequences using a stable ensemble of comparison stars before the target exited the field of view (Figure 1). Because the comparison-star ensemble changed between pointings, photometric reductions were performed independently for each field and for each observing night.

3. Data Reduction and Photometry

Raw CCD images were calibrated using standard bias subtraction, dark-current correction, and flat-field normalization. Aperture photometry of the target asteroid and field stars was performed using the Tycho Tracker software package. Differential photometry was performed using an ensemble of 5–8 non-variable comparison stars per field to correct for variations in transparency and atmospheric extinction.

Candidate comparison stars were visually inspected to identify variability, saturation, or contamination from nearby sources, and unstable stars were excluded from the ensemble. Instrumental magnitudes were placed on a consistent relative scale through nightly zero-point normalization.

Photometric uncertainties were computed by Tycho Tracker from the signal-to-noise ratio of each aperture measurement, accounting for source photon noise, sky background, and detector read noise. These uncertainties represent internal statistical errors. All observation times were recorded as mid-exposure Julian Dates and converted to heliocentric Julian dates (HJD).

4. Lightcurve Analysis

The R-band time-series photometry was analyzed using the period-search tools implemented in Tycho Tracker. The resulting period spectrum exhibits a well-defined dominant minimum near 13.1 h (Figure 2). The synodic rotation period was refined by fitting a fourth-order harmonic Fourier model to the phased lightcurve. This model order adequately reproduces the observed morphology without overfitting.

The best-fit rotation period is:

$P = 13.075 \pm 0.002$ h,

where the uncertainty represents the empirical period resolution associated with the dominant minimum in the period spectrum, given the six-night observational baseline (Figure 2).

The composite R-band lightcurve phased to this period displays a stable, double-peaked morphology characteristic of an elongated body undergoing principal-axis rotation. The peak-to-peak lightcurve amplitude is 0.62 mag (Figure 3).

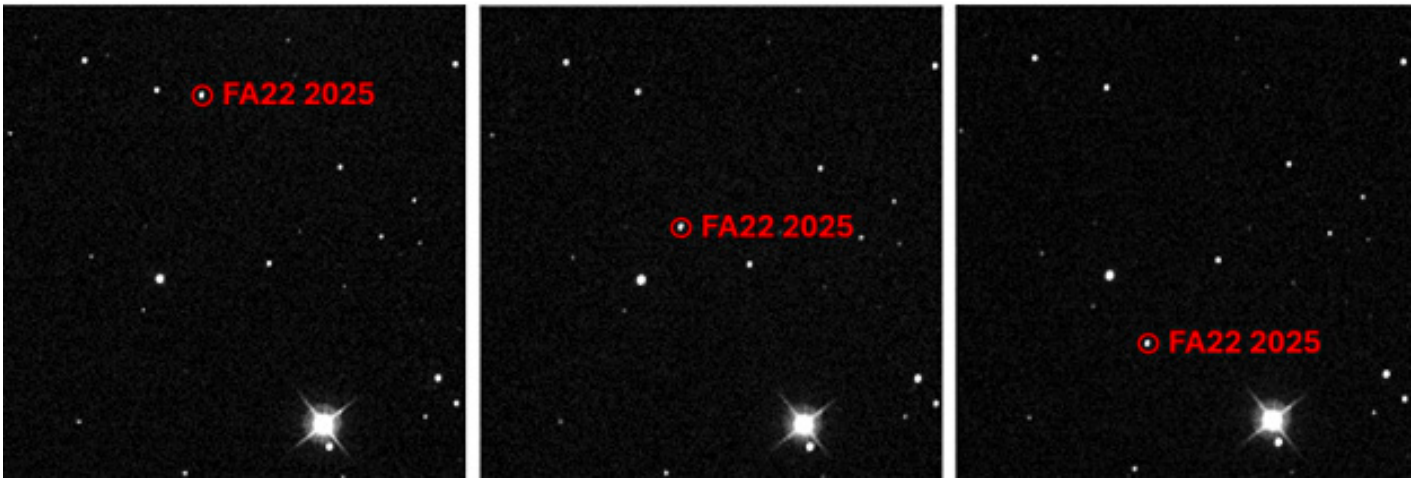

Figure 1 — Apparent sky-plane motion of asteroid 2025 FA22 relative to background stars over a 30-minute interval on 2025 September 21 (UTC), observed from MonitorMyPlanet Observatory (MPC R60).

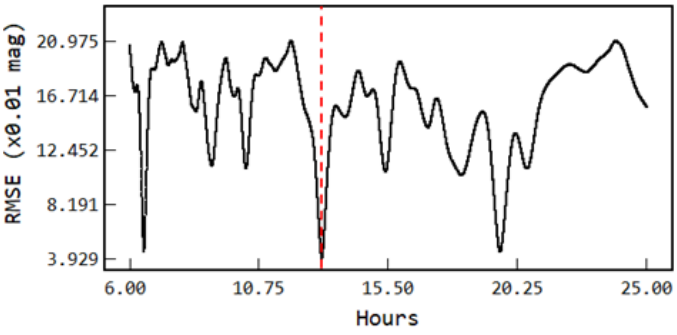

Figure 2 — Period spectrum derived from R-band photometry of asteroid 2025 FA22. The dominant minimum near 13.1 h indicates a well-constrained rotation period.

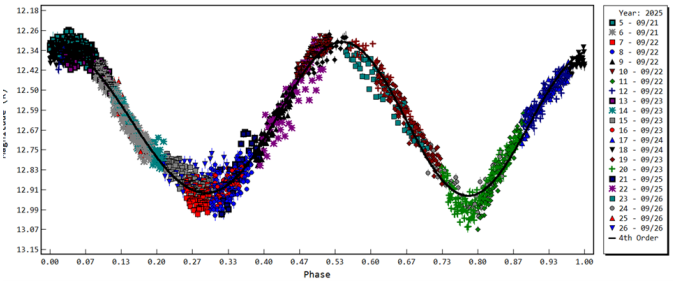

Figure 3 — Composite R-band lightcurve of asteroid 2025 FA22 phased to a rotation period of 13.075 h. The double-peaked morphology and 0.62-mag peak-to-peak amplitude are characteristic of an elongated body undergoing principal-axis rotation.

5. Phase-Angle Dependence and Absolute Magnitude

Reduced R-band magnitudes were computed to remove the effects of changing heliocentric and geocentric distances using (Bowell et al., 1989):

$$m(1,1,\alpha) = m_R - 5log_{10}(r\Delta),$$

where m_R is the observed R-band magnitude, r is the heliocentric distance in au, Δ is the geocentric distance in au, and α is the solar phase angle in degrees.

The phase-angle coverage of the observations (approximately 25°–60°) is insufficient to independently constrain the slope parameter G of the HG phase function (Figure 4). Therefore, a canonical value of G = 0.15 was adopted, and a conditional R-band absolute magnitude was derived using the HG phase law (Bowell et al., 1989):

$$H_R = m(1,1,\alpha) + 2.5\ log_{10}[(1-G)\,\Phi_1(\alpha) + G\,\Phi_2(\alpha)]$$

where Φ_1 and Φ_2 are the HG basis functions.

The resulting conditional R-band absolute magnitude is:

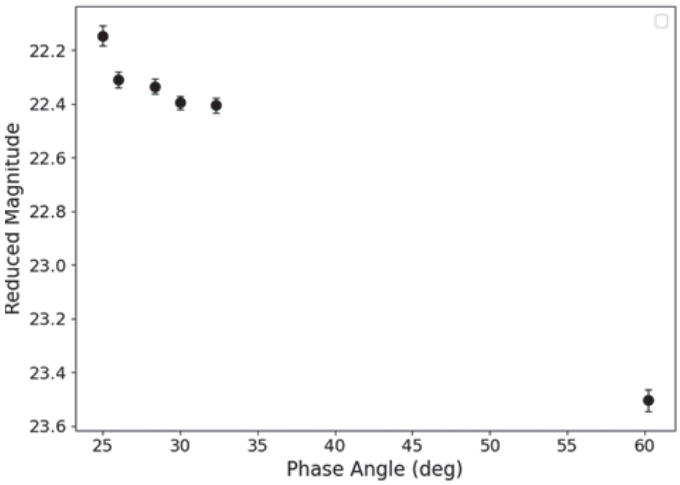

Figure 4 — Reduced R-band magnitude of asteroid 2025 FA22 as a function of solar phase angle.

H_R = is 21.052 ± 0.281.

The relatively large uncertainty reflects the substantial rotational brightness modulation, combined with limited phase-angle sampling, rather than photometric measurement error.

6. Shape Constraints

Assuming the asteroid can be approximated as a rotating triaxial ellipsoid viewed equator-on, and that surface albedo variations are negligible, the peak-to-peak lightcurve amplitude Δm is related to the equatorial axis ratio by (Binzel et al., 1989)

$$\frac{a}{b} \geq 10^{0.4\Delta m},$$

where a and b are the projected lengths of the asteroid's long and intermediate equatorial axes, respectively.

The inequality reflects the fact that most viewing geometries yield observed amplitudes smaller than the true equatorial amplitude. Applying this relation to the observed amplitude yields a lower-bound equatorial axis ratio of a/b ≥ 1.77.

7. Multi-filter Photometry and Colour Indices

Calibrated broadband measurements in the Johnson–Cousins B, V, R, and I filters were obtained on 2025 September 22 (UTC). As the asteroid exhibited a smooth brightness variation over the observing sequence, rotational effects were corrected by fitting an R-band lightcurve and interpolating magnitudes in the other filters to the corresponding rotational phase. The model fit employed inverse-variance weighting and was used to interpolate R-band magnitudes at the heliocentric Julian dates of the B, V, and I exposures.

Colour indices were computed from these rotation-corrected magnitudes, with uncertainties propagated in quadrature and weighted means derived from individual measurements.

B–R = 1.22 ± 0.02, V–R = 0.45 ± 0.02, and R–I = 0.36 ± 0.04, yielding derived colours of B–V = 0.77 ± 0.03 and V–I = 0.81 ± 0.05. When compared with solar colours, the asteroid is consistently redder than the Sun across all indices (Table 2).

Comparison with the broadband taxonomic complexes defined by Lin et al. (2018) places 2025 FA22 within the silicate S-cluster, in the region overlapping the S and Q complexes, consistent with a moderately red, silicate-dominated surface. Owing to the significant degeneracy among individual taxonomic classes in broadband colours, the taxonomic interpretation is restricted to the complex (cluster) level.

For visualization, the measured colour indices were converted to a V-normalized reflectance spectrum by subtracting solar colours and adopting the effective wavelengths of the BVRI filters (Holmberg et al. 2006). The resulting reflectance spectrum is shown in Figure 5.

Table 2 — Rotation-corrected Johnson–Cousins colour indices of asteroid 2025 FA22 compared to solar colours. Uncertainties in the difference (Δ) are propagated from both measurements.

Colour Indices	Value (mag)	Solar Colour (mag)	Δ (Asteroid – Sun)
B - R	1.22 ± 0.02	1.00 ± 0.02	0.22 ± 0.03
V – R	0.45 ± 0.02	0.35 ± 0.01	0.10 ± 0.02
R – I	0.36 ± 0.04	0.33 ± 0.01	0.03 ± 0.04
B – V (derived)	0.77 ± 0.03	0.64 ± 0.02	0.13 ± 0.04
V - I (derived)	0.81 ± 0.05	0.69 ± 0.01	0.12 ± 0.05

8. Discussion

The derived synodic rotation period of 13.075 ± 0.002 h places asteroid 2025 FA22 among the slower-rotating near-Earth asteroids. This rotation rate is well above the ~2.2 h spin barrier for cohesionless rubble-pile bodies (Pravec & Harris 2000) and therefore does not impose constraints on the asteroid's internal cohesion or material strength. The stability of the phased lightcurve morphology over six observing nights further suggests a principal-axis rotation state, with no evidence for non-principal axis (tumbling) rotation.

The observed R-band lightcurve amplitude of 0.62 mag indicates a significantly elongated shape. Under the assumption of a triaxial ellipsoid viewed near the equatorial plane and negligible albedo variegation, the inferred minimum equatorial axis ratio of a/b ≥ 1.77 is consistent with elongations commonly observed among near-Earth asteroids (Warner et al. 2009).

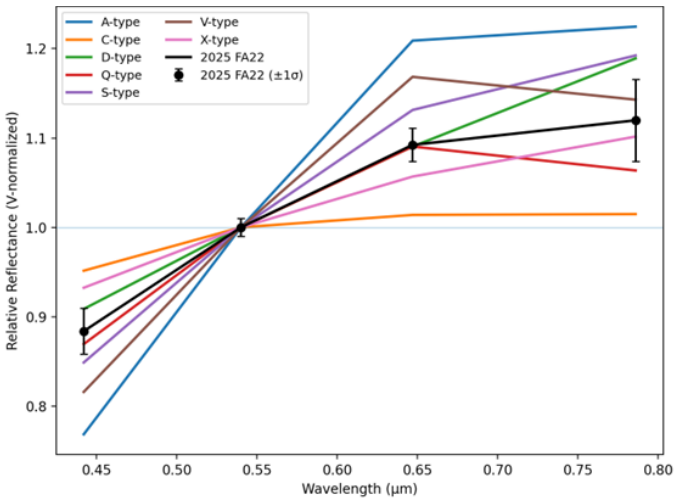

Figure 5 — V-normalized BVRI reflectance spectrum of asteroid 2025 FA22 derived from Johnson–Cousins colour indices (black symbols and connecting line), compared with the mean reflectance spectra of asteroid taxonomic complexes defined by Lin et al. (2018).

The broadband BVRI colour indices indicate a surface that is systematically redder than the Sun, consistent with a silicate-rich composition. When interpreted within the broadband photometric taxonomy framework of Lin et al. (2018), the colours place 2025 FA22 within the silicate S-cluster, specifically in the region overlapping the S and Q complexes. This location is consistent with moderately weathered ordinary-chondrite–like material, as commonly observed among near-Earth asteroids.

Definitive taxonomic classification would require spectroscopic observations, particularly in the near-infrared wavelengths.

8.1. Planetary Defence Context

Although 2025 FA22 does not pose a credible impact threat, it is representative of the class of near-Earth asteroids for which timely rotational and shape characterization is important in an impact-risk assessment. Knowledge of rotation state and shape can inform mitigation strategy selection. Elongated bodies may respond differently to kinetic impactors than more spheroidal objects, and rotation period influences both impact geometry and post-impact evolution. This study demonstrates that modest-aperture observatories, including independent and citizen-science facilities, can provide scientifically useful rotational constraints and physical characterization within coordinated planetary-defense frameworks.

9. Conclusions

Photometric observations of potentially hazardous asteroid 2025 FA22 obtained during its 2025 close approach yield a robust determination of its rotational properties and

broadband colours. The asteroid is a slow rotator with a synodic period of 13.075 ± 0.002 h, exhibits a large lightcurve amplitude of 0.62 mag, and has a minimum equatorial axis ratio of a/b ≥ 1.77. Broadband BVRI colour indices are most consistent with an S-complex classification, though degeneracies inherent to photometric taxonomy prevent a unique assignment. ✶

Acknowledgements

This work was carried out at the MonitorMyPlanet Observatory, Nerpio, Spain (MPC code R60), established with support from the Masason Foundation (Japan) and achieved first light in August 2025.

References

Binzel, R.P., et al. 1989, "Asteroid rotation rates: Distributions and statistics," in Asteroids II, ed. R. P. Binzel, T. Gehrels, & M. S. Matthews (Tucson: University of Arizona Press), 416

Bowell, E., et al. 1989, "Application of photometric models to asteroids," in Asteroids II, ed. R.P. Binzel, T. Gehrels, & M.S. Matthews (Tucson: University of Arizona Press), 524

European Space Agency (ESA) (2025, September 16). Close approach of asteroid 2025 FA22. ESA Space Safety. www.esa.int/ESA_Multimedia/Images/2025/09/Close_approach_of_asteroid_2025_FA22

International Asteroid Warning Network. (2025). 2025 FA22 IAWN campaign. IAWN. https://iawn.net/obscamp/2025FA22/

Jet Propulsion Laboratory (JPL) ECHO. (2025). Goldstone radar observations planning for asteroid 2025 FA22. NASA Jet Propulsion Laboratory. https://echo.jpl.nasa.gov/asteroids/2025fa22.2025.goldstone.planning.html

Holmberg, J., Flynn, C., & Portinari, L. (2006). The colours of the Sun. *MNRAS, 367(2)*, 449–453. https://doi.org/10.1111/j.1365-2966.2005.09832.x

Lin, C.-H., et al. (2018). Photometric survey and taxonomic identifications of 92 near-Earth asteroids. *Planetary and Space Science, 152*, 116–135. https://doi.org/10.1016/j.pss.2017.12.019

Parrott, D. (2025). Tycho Tracker: Photometry and astrometry software. https://www.tycho-tracker.com

Pravec, P., & Harris, A.W. (2000). Fast and slow rotation of asteroids. *Icarus, 148*, 12–20.

Warner, B. D., Harris, A. W., & Pravec, P. (2009). The asteroid lightcurve database. *Icarus, 202*, 134–146.

Feature Article / Articles de fond

The Major Lunar Standstill — a Real, Visual Representation

by Alister Ling and Luca Vanzella (both of Edmonton Centre)

Abstract

Mirroring the annual swing of the sunrise points from June solstice in the northeast to December solstice in the southeast and back, the monthly full Moons swing out to their lunistice and return, but in the opposite direction. In addition, as the Moon's orbit slowly regresses in an 18.6-year cycle, the span of moonrise points contracts and expands: the narrower minor standstill of 2015 and most recently the wider major standstill in March 2025. The composite image in a time slice form records this and related phenomena with an observer's perspective.

Article

Celebrating the northeastern and southeastern extremes of sunrise points (solstices) are familiar experiences to all casual skywatchers but the moonrise ones (lunistices) mostly go unnoticed except to attentive observers. During a Major Lunar Standstill, the extreme moonrise points are several degrees farther north and south than the sunrise ones. We wanted to capture these events photographically in a manner both educationally and visually compelling.

A complete graphical explanation of how the Moon's 5°17′ orbital inclination and regression of the nodes adds to or subtracts from the Earth's tilt affecting its rise points along the horizon is beyond the scope of this article.

Technically the standstill is a point in time on the dates of the extreme north and south lunar declinations, both occurring in March 2025, but similar to solstices, it is best appreciated in the context of a period of observation. Any consistent phase would reveal the pattern, but a full Moon is the most eye-catching and stands out best in very wide images.

The period from the June 2024 solstice to the June 2025 solstice nicely surrounds the standstill, so we planned to shoot 13 full moonrises and 13 sunrises during that interval. Inspired by an earlier project that created a vertical time slice of sunrises, we realized we could assemble a similar composite to show how the greatest northern and southern positions of the Moon extend beyond those of the Sun during a Major Lunar Standstill.

What Phenomena Can We See?

Apart from "the difference is night and day!" joke, there are a couple of obvious and several subtle effects to take note of.

Extremes: the whole point of the project was to showcase that the Moon's rise points over an annual cycle are notably

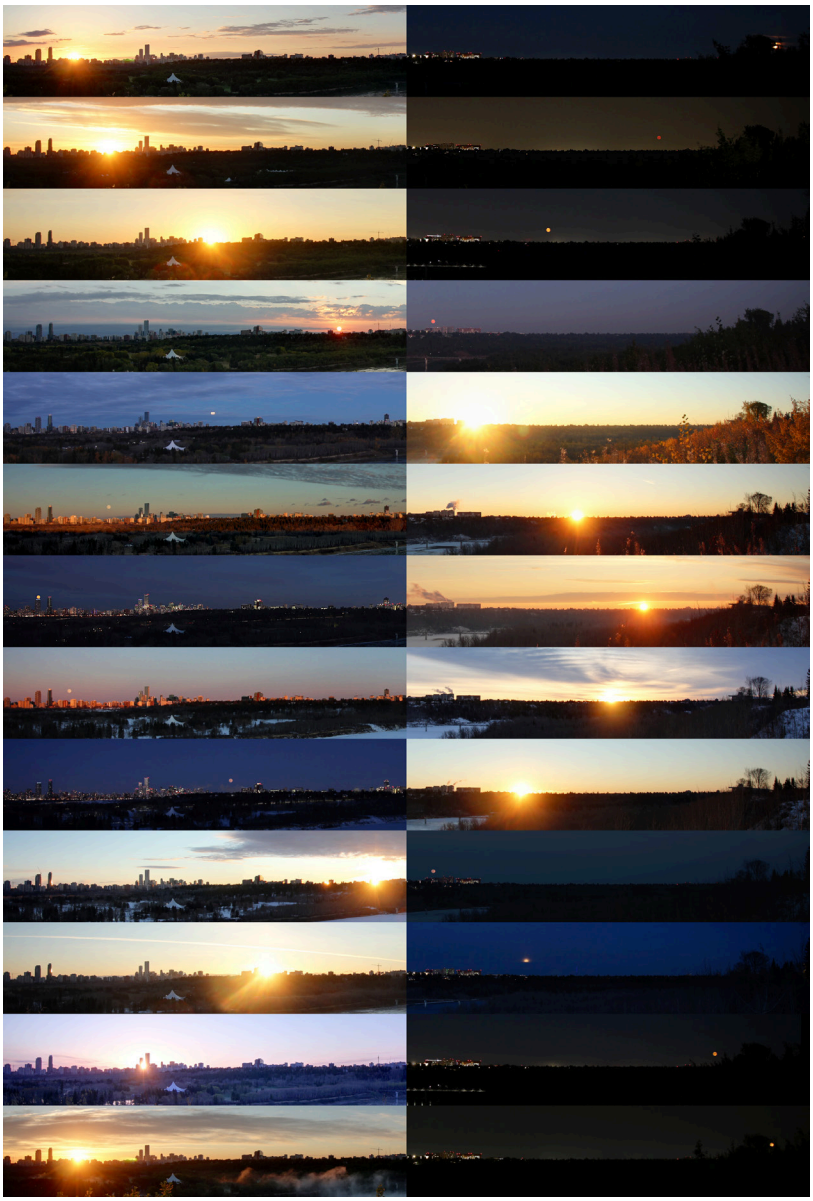

Figure 1 — A composite image illustrating the monthly swing of full moonrise points and the annual swing of sunrise points of the Major Lunar Standstill of 2024–25.

wider than the Sun's. That's just this year however. It takes a discerning eye, attentive mind, and decent record keeping to realize that the span expands and contracts in an 18+ year cycle Observers farther north would be more likely to say "wow, that Moon sure is low and south this summer" because it tracks closer to the horizon.

Opposites: the two curves are mirror images of each other. Many of us learn the expression "the full Moon rises at sunset and sets at sunrise." It is, of course, because the only way it can be full is if it is opposite the Sun from us. When you call attention to "where is the setting Sun in (northern) summer?" and answer "it is in the northwest," it becomes obvious that the rising full Moon has to be in the southeast. At the equinoxes when the Sun sets due west, the Moon rises due east, and in (northern) winter the Sun sets southwest, the full Moon must rise in the northeast.

Seasons: A time slice offers a lovely parade of changing elements. Summer grass grows, then leaves turn colour and quickly fall as snow arrives. Note the time lag of river ice.

Sky Light and Darkness: Hang on, if the Moon rises at sunset, why are the winter scenes in daylight and the summer ones very dark? At the major standstill, the full Moon is at its extreme northern declination in winter. For the same ecliptic longitude (or with hand-waving, Right Ascension), an object farther north than another must rise earlier. For the December 15th event, the Sun's declination was –23°19′ (its equivalent opposite then being +23°19′) whereas the full Moon was at +27°30′, more than 4 degrees farther north, rising about 30 minutes sooner than if it had been exactly opposite. That's why the sky is bright blue. A summer full Moon is more than 4° south of the point opposite the Sun, making it rise much later than sunset and consequently in a dark sky. Fun fact, due to Edmonton's northerly latitude and Daylight Saving Time pushing the clock forward, the June 2025 moonrise was so late it occurred after midnight.

There is an additional variation from average timing, in that the moment of full Moon may have been 12 hours earlier or later than its actual rise. That means it could be about 6° ahead or behind its opposition to the Sun, enough to skew the rise time before or after sunset to affect the light in the sky.

Tilt: Although the apparent tilt of the Moon's facial features has nothing to do with the standstill, it is remarkable once it is noticed. The Moon's north pole is almost perpendicular to the ecliptic. In the northern hemisphere the angle of the ecliptic is very shallow from June through October at full moonrise, making the face "upright" with "horizontal eyes," and steep from December through March, producing a considerably tilted face.

Transparency: We all know from looking at the blue sky and colourful sunsets and twilights that Earth's atmosphere can vary from clean and transparent to dirty and dull from day to day. Without delving into exceptions, on average the air is clearer in winter and early spring, then gets filled with pollen, switching over to wildfire smoke in summer and harvest dust in autumn. Is this recognizable in the time slice?

Moon and Sun Arcs Are Offset: If we had done this through computer graphics, a Moon rising due east would lie in the

centre of the diagram. Because we had to let it rise to 2.5° altitude to make sure it was not obscured by buildings or attenuated, the Moon azimuths are all displaced to the south, moreso when the ecliptic is shallow. In contrast the Sun's shifts are less because we could capture it as it crested the hills and buildings at a little more than 1° altitude.

Perigee and Apogee Moons: Much harder to notice is the modest change in apparent size of the Moon, and at the scale presented here, likely not visible without measuring pixel widths on the original images.

Planning the Project

On paper, we simply capture evening moonrises and the morning sunrises on the full Moon dates from the June 2024 solstice to the June 2025 solstice. However, years of shooting sunrises and moonrises in the Edmonton area had taught us two things:

One, it **is** possible to shoot 13 consecutive sunrises spaced about a month apart within a few days of desired dates. Alberta is a sunny province and clear skies at sunrise are common. Plus, the sunrise azimuth changes only slightly from day to day, even at the equinoxes, and in these panoramic images it's hardly noticeable.

Two, it is **not** possible to shoot 13 consecutive full moonrises because the probability of a clear sky precisely a few minutes after moonrise on the exact date of a full Moon is perhaps 50%. Since the moonrise azimuth changes significantly from day to day, even shooting one day on either side of the target date puts the Moon out of place (especially at the extremes).

The simplest option that avoided being clouded out, to use AI or computer graphics to generate it all left us with a "where's the fun in that?" Likewise, duplicating old foregrounds then copy-pasting in different Moons in the correct positions felt like cheating.

To maintain a high degree of authenticity, we came up with a plan to capture moonrises beforehand that could serve as proxies for the target moonrises that would be obscured by cloudy skies. Each proxy moonrise needed these attributes:

- Very similar moonrise azimuth (plus or minus 2°).
- Very similar moonrise time with respect to sunset (proxy for sky brightness).
- Very similar moonrise month (proxy for ground conditions).
- Very similar moon phase (full or plus or minus one day).

We examined the circumstances of every full or near full moonrise from January 2022 to May 2024 and selected those events that met the above attributes. This two and half year period is approximately the size of the lunistice period in which the extreme moonrise azimuths remain essentially the same (similar to solstice sunrise azimuths). We shot as many of these proxy moonrises as possible given our personal schedules and clear skies permitting.

Fun fact—we captured a total of 50 events: 24 proxy moonrises, 13 target moonrises, (5 had clear skies, 8 had cloudy skies), and 13 sunrises.

For all events we managed to obtain one or more usable proxies, except for one target rise where all we could muster was a proxy that met the month, sky brightness, and ground condition attributes but had no Moon. As it happened, that particular target was cloudy so we were forced to break our rule and use the moonless proxy with the Moon added from another event (with correct scale and position and with similar tilt).

Capturing the Images

Sunrise is a bright event compared to moonrise. Even though sky brightness at sunrise can vary considerably due to clouds or haze or smoke, it is easy to see the Sun close to 0.5° altitude in an image exposed for the foreground since the disk is blown out and the sunlight glow extends into the foreground below the horizon.

Shooting the 13 target sunrises on the same dates as the target moonrises, although more likely than shooting 13 target moonrises, was not guaranteed. Since the sunrise azimuths are essentially the same year after year, we decided to capture the sunrises from January to December 2022, with two in June 2022, as close as possible to the dates of the target moonrises. This would get half the required images out of the way in the first year of the project, leaving plenty of time to capture additional sunrises if we missed any in the first year. As expected, we were successful in capturing all 13 sunrises in consecutive months.

We shot the moonrise on all 13 target dates whether skies permitted or not since we wanted to be able to show target conditions in a "behind the scenes" epilogue of the eventual movie animating the standstill.

The atmosphere attenuates the light from all rising objects, moreso when loaded with particulates, haze, or fog droplets. For the Sun, this typically doesn't matter. It does for the Moon. Furthermore the surrounding sky may still be in sunlight at moonrise, effectively obscuring it. Generally, to clearly see the Moon in an image exposed for the foreground, the Moon has to be higher in altitude, especially if horizon buildings are in the way. We decided to shoot each rise when the Moon was at 2.5° altitude.

At first we considered using a fisheye lens for the project, but at that image scale, the Moon's size was only a few pixels

across, resulting in a featureless blob when enlarged to a decent display dimension. A 10-mm focal-length lens could still resolve the key maria, presenting us with its recognizable face should we produce a poster-sized print. Consequently the field of view was too small to cover the full range in azimuth, forcing us to shoot two image panels which we would later stitch into panoramas.

Our next challenge was tackling the large dynamic range between the foreground and the Moon (or Sun). Our marvelous eyes can handle it easily, but our camera sensors cannot. A properly exposed Moon leaves the ground black, but capturing detail on the dark terrain blows out the Moon. We shot a bracketed set (a range of exposures taken in rapid succession) then blended them into a result that is reasonably close to the natural scene. A key philosophy of ours: "this is how it would have looked had you been there in person."

For sunrises, each panel consisted of a 3×1EV bracket, for example 1/125, 1/250, 1/500 of a second. For moonrises, each panel consisted of a 6×2EV bracket (2, 1/2, 1/8, 1/30, 1/125, 1/500 second) to cover the enormous range of brightness from grass through sky to the sunlit Moon. For very dark moonrises, we could simplify by taking pre-rise images bracketed for sky and foreground lighting plus a second bracket exposed for the Moon and wispy clouds.

Processing the Images

The panorama brackets were stitched, fused and blended in Hugin. For the dark moonrises, the pre-rise brackets were stitched, fused, and blended in Hugin while keeping the Moon panels separate but receiving the identical remapping to the equirectangular projection; then the final panorama was composited in GIMP.

We also made cosmetic edits to the images. Since we used relatively old cameras, we erased hot and dead pixels resulting from the old sensors. In some of the dark moonrise images, we erased construction floodlights in the foreground since these were distracting or might be confused with the Moon itself.

The goal was to have 26 panoramas with virtually identical image frames. This would be important for the final composite image and for the movie animating the image.

For each session, no matter how careful we were, tiny shifts in camera placement and aim resulted in subtly different panorama frames, enough to be disturbing when lined up in our composite, especially at the seam. Every frame varied slightly in width, tilt, horizon skew, and projection distortion. Even if we had avoided the need for panoramas by using a fisheye lens, we couldn't prevent the mismatches at the centre due to the sensitivity of the inherent distortion on position and aim. People really find it jarring when horizontal and edge features don't line up.

One sunrise panorama was selected as the fixed, base image. All other panoramas were adjusted to match the base image with a four-step process in GIMP: scale, align, rotate, and a cage transform to rectify nonlinear distortions. In the end we could overlay them to a precision of a handful of pixels.

Assembling the Final Composite

The principal result of this project is a vertical time slice of 13 moonrise and 13 sunrise images from June 2024 to June 2025, to visually depict the change in moonrise/sunrise position over a year and to illustrate that the greatest northern and southern positions of the Moon extend beyond those of the Sun during a Major Lunar Standstill.

Since we captured both sunrises and moonrises, we also produced two other images: a vertical time slice of full moonrise positions over a year and a corresponding sunrise one.

The final assembly took place in GIMP by importing all moonrise and sunrise images into separate layers. These were aligned to the fixed, base sunrise image then cropped two different ways: narrow strips centred on the horizon for the final composite images, and larger rectangles that excluded edge artifacts for the movie.

A detailed explanation of how we assembled the images into three vertical timeslices (moonrise, sunrise, moonrise+sunrise) can be found here on Flickr: Major Lunar Standstill.

www.flickr.com/photos/53851348@N05/54585073867/

Animating the Final Image

We also made a movie that animates the Major Lunar Standstill by showing the sequence of moonrise and sunrise images and how they were cropped and stacked to make the vertical time slices. https://youtu.be/u1tkLRdaFNk

Conclusion

Had it been clear, you would have seen the Major Lunar Standstill similar to this. It might be argued that the final result is not "real" due to our use of proxies. True, but using cloudy panels hurt the educational value and acquiring a full set with clear skies, although theoretically possible, is practically speaking quite unlikely for sites in the mid-latitudes. Our image is one that observers can instantly relate to.

This project is a prime example of collaboration being critical for success. Collaborating covers photographer absences, spreads the workload, sparks ideas, and motivates slogging through a long-term project. ✶

We hope this story inspires observers and imagers to capture the Minor Lunar Standstill of 2033–34.

Pen & Pixel

Figure 1 — Tenho Tuomi snapped this image of the Super Moon rising over the farmyard taken from one mile away. Details: Tuomi farm, Lucky Lake, Saskatchewan, 2016 November 13 17:40 CST

Figure 2 — Scott Barrie writes "This image was shot from my rural backyard northwest of Milton, Ontario, on 35-mm film, using, I believe, Ektachrome E200. The camera was mounted on a hand-turned barn door tracker." Detail: Date: March 1999; Camera: Nikkormat Ftn; Lens: Nikkor 24-mm ƒ/2.8 Settings: Not recorded; Location: Rural Milton, Ontario

Continues on page 63

What's Up in the Sky?

April/May 2026

Compiled by James Edgar FRASC

April Skies

The Moon begins the month in full phase, and slightly south of Spica, the bright star in Virgo, The Maiden. On the 6th, Antares in Scorpius is occulted in the Southern Hemisphere; for northerners, the star is just half a degree away from the Moon. Apogee of 404,970 km is reached on the 7th. The Moon is at last quarter on the 10th. By the 15th, a gathering of planets join up with a very slender Luna in the early morning sky – first is Mercury, 5 degrees south; then comes Mars, 4 degrees south; and Saturn, 5 degrees south on the 16th. New Moon is on the 17th, almost at perigee of 361,630 km on the 19th. Then Venus, hugging the western evening horizon that day, is 5 degrees south of a very slender crescent Moon in Taurus, The Bull. Uranus is between the two. On the 22nd, Jupiter is 4 degrees south of the crescent Moon, and a day later our satellite is at first quarter, among the stars of the Beehive Cluster (M44). The 25th sees the second occultation of April, when Regulus, in Leo, gets hidden for viewers in southern Canada and most of the USA. Then Spica once again takes centre stage at the end of April, 1.8 degrees north of an almost-full Moon.

Mercury makes for a poor apparition for northern observers, hugging the morning horizon at dawn. On the 20th, a tight triple conjunction with Mars and Saturn will be worth watching. Also in the frame, distant Neptune needs optical magnification to make this a quadruple conjunction.

Venus is prominent in the west at sundown, rising higher throughout the month. The waxing crescent Moon passes by on the 18th. Venus, Uranus, and the Moon complete a dancing trio among the stars of Taurus; then the Moon exits, leaving the two planets together from the 21st to the 26th.

Mars is too close to the horizon for decent viewing, but the trio mentioned above might be worth the early morning rise – needs a clear horizon for observing the triple conjunction.

Jupiter is in Gemini, crossing the sky all through the night. The waxing crescent Moon pairs up on the 22nd.

Saturn is mentioned above – one of the three planets hugging the horizon at sunrise.

Uranus, in the western evening twilight among the stars of Taurus, is joined by the Moon and Venus on the 22nd.

Neptune suffers from the horizon-hugging ecliptic, just like Mars, Mercury, and Saturn. It's there, but you need a good binocular or telescope to see it.

The Lyrid meteors peak in the evening of the 22nd.

April 19 sees the cluster of planets hovering near the horizon. They might be seen, with difficulty.
Image: Courtesy of Starry Night Pro Plus

Continues on page 62

The Sky April/May 2026

Compiled by Nicole Jiang with cartography by Glenn LeDrew

Celestial Calendar (bold=impressive or rare)

April 2025

Apr. 1 full Moon at 10:12 p.m. EDT

Apr. 3 Spica 1.8° north of waning gibbous Moon

Apr. 6 Antares 0.6° north of waning gibbous Moon

Apr. 7 Moon at apogee (404,970 km)

Apr. 10 Moon at last quarter

Apr. 16 Saturn 5° south of waning crescent Moon

Apr. 17 new Moon (lunation 1278)

Apr. 19 Moon at perigee (361,630 km)

Apr. 19 Venus 5° south of waxing crescent Moon

Apr. 19 Moon in Pleiades (M45)

Apr. 22 Lyrid meteors peak at 3:15 p.m. EDT

Apr. 22 Jupiter 4° south of waxing crescent Moon

Apr. 24 Moon at first quarter

Apr. 24 Venus 0.8° north of Uranus

Apr. 24 Moon 1.0° north of Beehive (M44)

Apr. 26 Regulus 0.2° south of waxing gibbous Moon, occultation

Apr. 30 Spica 1.8° north of waxing gibbous Moon

May 2026

May 1 full Moon at 1:23 p.m. EDT

May 4 Antares 0.5° north of waning gibbous Moon

May 4 Moon at apogee (405,839 km)

May 6 Eta Aquariid meteors peak at 11:51 p.m. EDT

May 9 Double Shadows on Jupiter

May 9 Moon at last quarter

May 16 Double Shadows on Jupiter

May 16 new Moon (lunation 1279)

May 17 Moon at perigee (358,075 km) Large tides

May 19 *Venus 3° south of waxing crescent Moon

May 20 *Jupiter 3° south of waxing crescent Moon

May 21 Venus 0.8° north of Shoe Buckle (M35)

May 21 *Moon 0.8° north of Beehive (M44)

May 23 Double Shadows on Jupiter

May 23 Regulus 0.1° north of first quarter Moon

May 27 Spica 1.9° north of waxing gibbous Moon

May 30 Double Shadows on Jupiter

May 31 full Moon at 4:45 a.m. EDT (smallest in 2026)

May 31 Antares 0.4° north of waning gibbous Moon

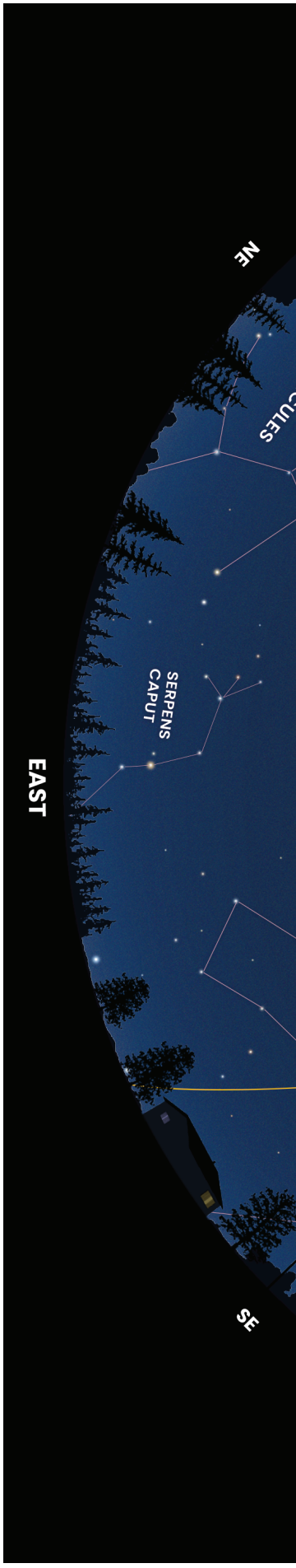

Planets at a Glance

	DATE	MAGNITUDE	DIAMETER (″)	CONSTELLATION	VISABILITY
Mercury	Apr. 1	—	8.0	Aquarius	—
	May 1	—	5.4	Pisces	—
Venus	Apr. 1	–3.9	10.6	Aries	Evening
	May 1	–3.9	11.6	Taurus	Evening
Mars	Apr. 1	—	4.1	Aquarius	—
	May 1	—	4.2	Pisces	—
Jupiter	Apr. 1	–2.2	38.9	Gemini	Evening
	May 1	–2.0	35.6	Gemini	Evening
Saturn	Apr. 1	—	15.9	Pisces	—
	May 1	—	16.1	Cetus	—
Uranus	Apr. 1	5.8	3.5	Taurus	Evening
	May 1	—	3.5	Taurus	—
Neptune	Apr. 1	—	2.2	Pisces	—
	May 1	—	2.2	Pisces	—

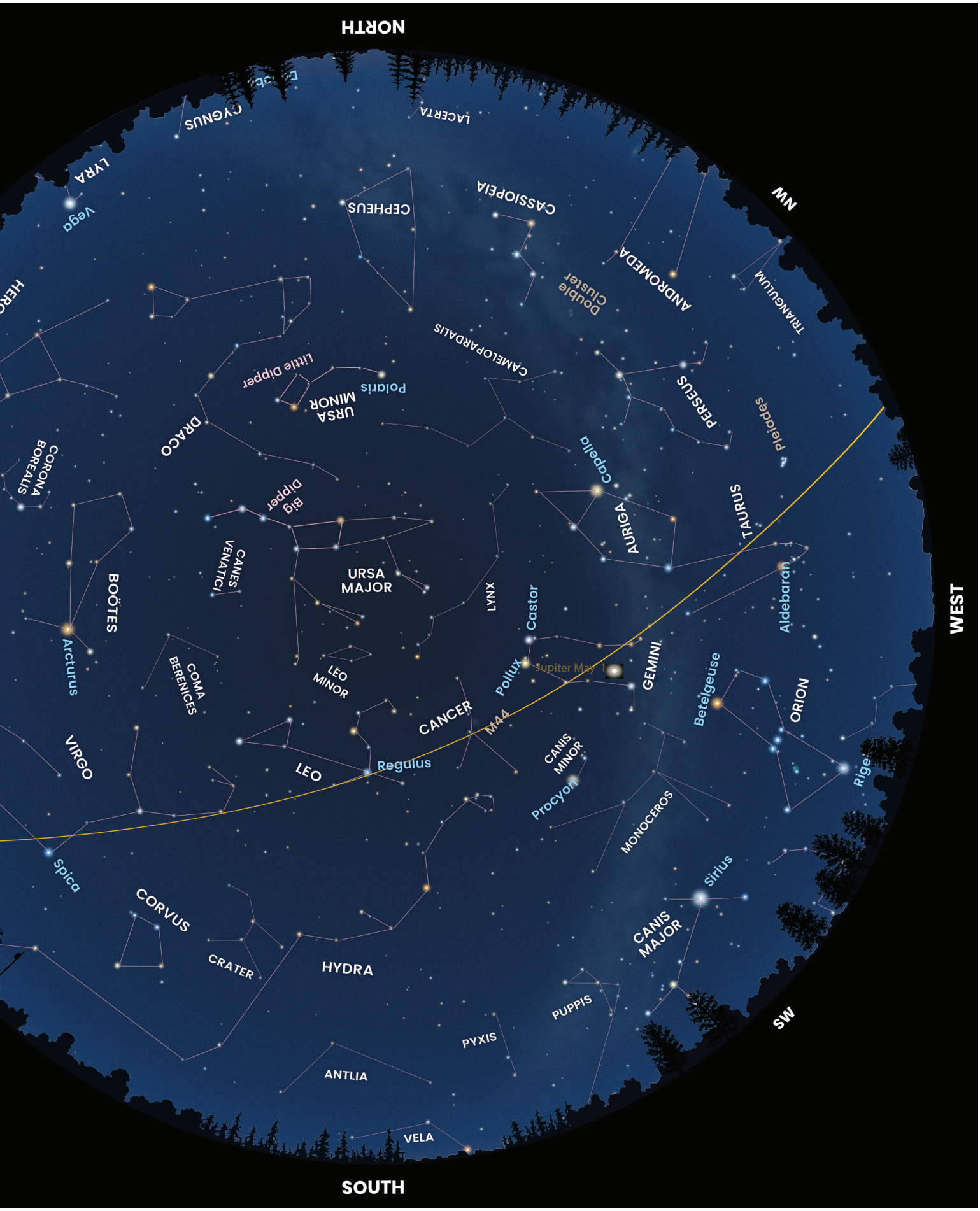
NORTH
WEST
SOUTH
NW
SW
CYGNUS
LACERTA
LYRA
Vega
CEPHEUS
CASSIOPEIA
ANDROMEDA
Double Cluster
TRIANGULUM
CAMELOPARDALIS
Little Dipper
Polaris
URSA MINOR
DRACO
PERSEUS
Pleiades
CORONA BOREALIS
Capella
AURIGA
TAURUS
Big Dipper
CANES VENATICI
URSA MAJOR
LYNX
Castor
Aldebaran
BOÖTES
Arcturus
COMA BERENICES
LEO MINOR
Pollux
Jupiter May 1
GEMINI
Betelgeuse
ORION
CANCER
M44
VIRGO
LEO
Regulus
CANIS MINOR
Procyon
Rigel
MONOCEROS
Spica
Sirius
CORVUS
CRATER
HYDRA
CANIS MAJOR
PUPPIS
PYXIS
ANTLIA
VELA

Continued from page 59

May Skies

The Moon is full as May begins. On the 3rd, Antares, the bright star in Scorpius, is a half-degree away from the Moon, an occultation in the Southern Hemisphere. Apogee occurs on the 4th, at a distance of 405,839 km. The Moon is at last quarter on the 9th. On the 14th, Mars is 5 degrees south of a slim-crescent Luna, just prior to new Moon on the 16th. Perigee occurs on the 17th, at a distance of 358,075 km. Large tides occur in coastal areas. The following evening sees Venus 3 degrees south of a slender crescent Moon, then Jupiter a couple of days later, on the 20th, is also 3 degrees south. The 21st finds the Moon among the stars of the Beehive Cluster (M44). The "M" refers to Charles Messier, a French astronomer in the 18th century. He hunted comets, but discovered numerous annoying comet-like objects that just confused his searches. He made a list for his friends, named The Messier Catalogue, with 106 objects. Four more have been added since by other observers. A spring challenge among astronomers is to see all 110 objects in one night of observing—a Messier Marathon. May 23 has another southern occultation, this time with Regulus, only 0.1 degrees away from the first-quarter Moon. On the 27th, Spica is 1.9 degrees north. Finally, the 31st is full Moon, the smallest in 2026, and Antares is once again occulted in the south, only 0.4 degrees away for northern viewers.

Mercury is too close to the Sun for viewing, but may be seen in the west during the last week of May.

Venus puts on a show in the western evening sky, remaining high among the stars of Taurus. It slowly rises along the ecliptic, almost catching up to Jupiter in Gemini by month-end.

Mars by the middle of May has risen away from the horizon in the morning sky, among the stars of Aries, The Ram.

Jupiter, high up after sunset, has double shadows from two of the Galilean moons on its disk four times in May: on the 8th, 16th, 23rd, and 30th. On the 20th, the waxing crescent Moon is 3 degrees north.

Saturn has pulled away from the April crowd, rising shortly after 3 a.m. The waning crescent Moon passes by on the 13th.

Uranus is too close to the Sun to be seen.

Neptune and the waning crescent Moon are a pair on the 13th, but you'll need a good telescope to see the very distant planet–it's *only* 30.5 astronomical units away from Earth, about 4.58 billion kilometres!

The **eta Aquariid meteor**s peak on the morning of May 6. ✶

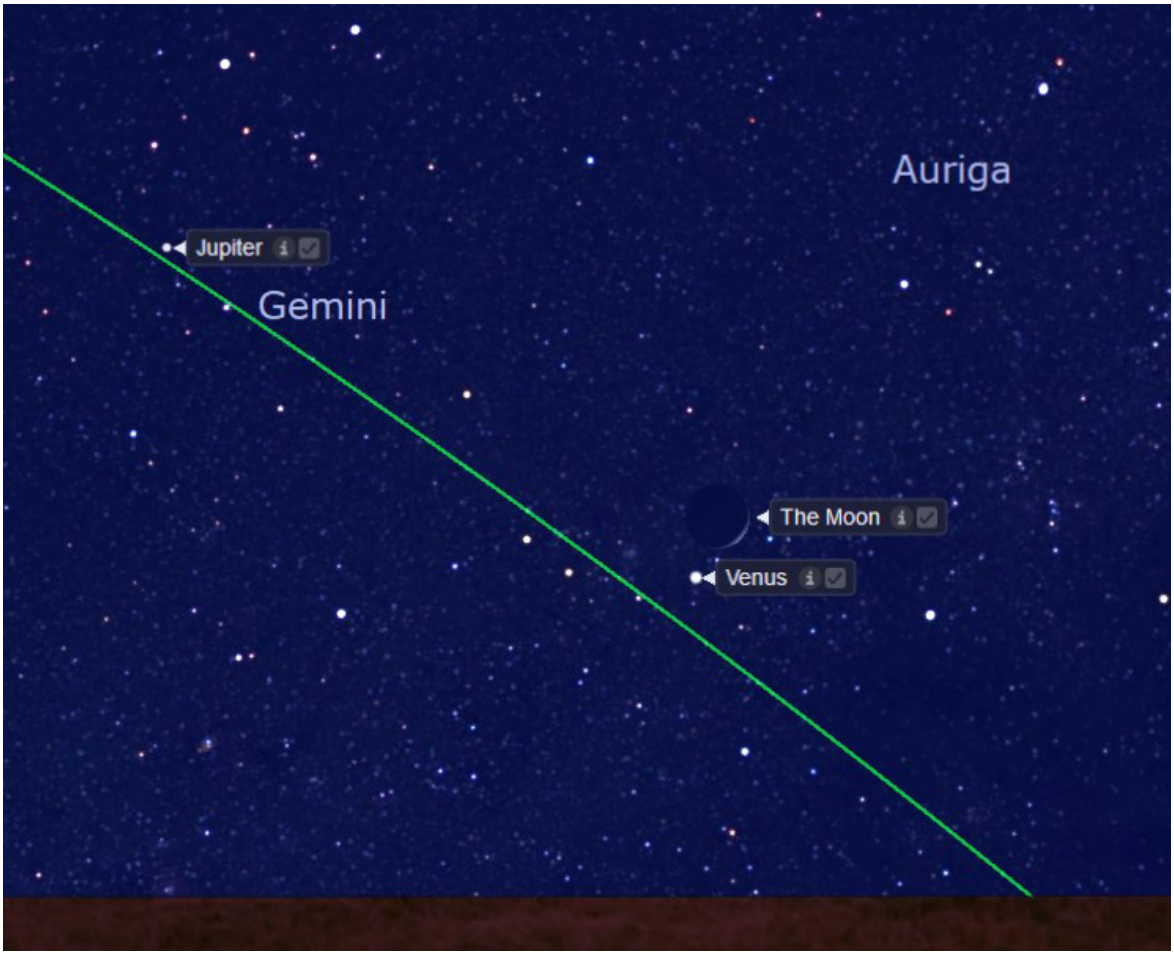

May 18 has Venus and the Moon north of the ecliptic in the stars of Taurus. Venus inches its way toward Jupiter by month-end.

Image: Courtesy of Starry Night Pro Plus

Continued from page 58

Figure 3 — Rick Stankiewicz says "While returning from a successful caribou hunt in northern Québec (west of James Bay) our drive south rewarded us with atmospheric phenomena associated with a cold upper atmosphere. We were treated to solar halos and various arcs and things, but the image selected here is a pair of sundogs. Technically known as perhelion, these mock Suns, when visible, will be 22 degrees on either side of the Sun. Typically, the Sun shines too brightly to image this phenomenon easily, but some interference by cloud cover can help, as in this image. The most difficult part of capturing this image was getting the driver of the vehicle to slow down." Details: 2011 November 26, in the La Grande-Quatre Region of Northern Québec. Canon 400D with Sigma lens at ISO 200, 1/640 sec., ƒ/16, 18 mm

Figure 4 — Tim Yaworski of Saskatoon Centre snapped this image. He writes "After a night of photographing Comet NEOWISE (C/2020 F3) from the Sleaford Observatory, I stopped on the Yellowhead Highway east of Saskatoon to capture this image. Hidden among the clouds (about 1/4 of the way in from the right) is the comet." Details: 2020 July 7 at approximately 04:14 CST. Fujifilm X -T10, Fujifilm 18–55 mm zoom lens at 35.8 mm, ƒ/5

Skyward

Pathetic Jupiter

by David Levy FRASC,
Kingston & Montréal Centres

Why would I want to write something insulting about Jupiter? After all, Jupiter is the first thing I looked at through a telescope. Only last month I wrote how, when I began searching for comets, I was looking for an activity that did not involve me dealing with other people. I had a few friends as a youngster. Now in my ripe age of 77, I have many good friends, of whom the current editor of *Desert Skies* is one of my closest. But I still enjoy, more than anything, the idyllic solitude of looking through my telescope, field after field of sky, for a new elusive comet. A related part of that same solitude is looking at the planet Jupiter, which I consider to be a faithful and lifelong friend.

Jupiter and I have been friends since I first looked at it, with Mom and Dad, on 1960 September 1. Since then, the planet has never failed to give me an emotional, pathetic look. And thus I introduce that word pathetic. Applied to a person, pathetic could mean a loser. I am pathetic. I do not want to see myself as a loser, but as someone who deals intensely in emotions. Applied to Jupiter, I do not intend for it to be considered a loser of a planet, but rather as a planet that yields always an emotional response in the observer.

Jupiter is pathetic, but not a loser, not insulting. I use the word as a derivative of *pathos*, an idea from Greco-Roman philosophy. The concept survived all the way into Shakespeare's *Julius Caesar*, where Brutus exemplifies the stoic, logical personality that is brought to fame at the very end, in Antony's celebrated obituary:

> This was the noblest Roman of them all.
> All the conspirators save only he,
> Did that they did in envy of great Caesar;
> He only, in a general honest thought
> And common good to all, made one of them.
> His life was gentle, and the elements
> So mix'd in him that Nature might stand up
> And say to all the world, "This was a man!"
> (*JC*.5.5.68-75.)

Pathos alludes to a person's emotions, and it ignites feelings related to those emotions. For my sense, Jupiter is pathetic because it fosters the emotions I felt when I first looked at it. That world is incredibly turbulent; a brief look at the *Voyager* images from decades ago shows us the roiling of the little clouds as they circle the Great Red Spot. More important to me, those of us who were alive in 1994 remember the profound effect that the daily addition of big black spots the size of Earth had on that weeping world, as though some cosmic force was pounding the daylights out of the Solar System's biggest planet.

Thaxted

According to NASA, my favourite government agency, there is a special musical allusion to this mighty comet's breakup and collision. It is called *Thaxted*, and on the occasion of NASA's last Shoemaker-Levy 9 press conference late in July, as a way of celebration, they played the *Thaxted* section of Gustav Holst's *The Planets*, from its Jupiter movement. Holst adapted it in 1921. He loved living in that small English town. In my opinion the *Thaxted* portion of *The Planets,* from near the centre of the Jupiter movement, is one of the most stunning pieces of music ever written, equivalent to Mozart's Jupiter symphony or Beethoven's Fifth.

The NASA presentation included many images of comet fragments, impacts, and people. Gustav Holst lived in Thaxted from 1917 to 1925. Holst wrote the piece as the middle section of the Jupiter movement of *The Planets*. He adapted *Thaxted* to fit the words of the hymn "I vow to thee, my country":

> I vow to thee, my country, all earthly things above,
> Entire and whole and perfect, the service of my love;
> The love that asks no questions, the love that stands
> the test,
> That lays upon the altar the dearest and the best;
> The love that never falters, the love that pays the price,
> The love that makes undaunted the final sacrifice.
>
> And there's another country, I've heard of long ago,
> Most dear to them that love her, most great to them
> that know;
> We may not count her armies, we may not see her King;
> Her fortress is a faithful heart, her pride is suffering;
> And soul by soul and silently her shining bounds
> increase,[11]
> And her ways are ways of gentleness, and all her paths
> are peace.

Before returning to pathetic Jupiter, one additional thought about Thaxted and its related hymn; its final line is from Proverbs 3:17. It belongs to a song, "Eitz Chayim," I sing at our synagogue every year on the Day of Atonement:

> "Her ways are ways of pleasantness,
> And all her paths are peace."

These words help connect the emotional pathos I feel toward Jupiter with the memorable black spots that graced that world. The dark, soot-like spots lasted for months and they dissipated only gradually. As much as my earlier observations of Jupiter

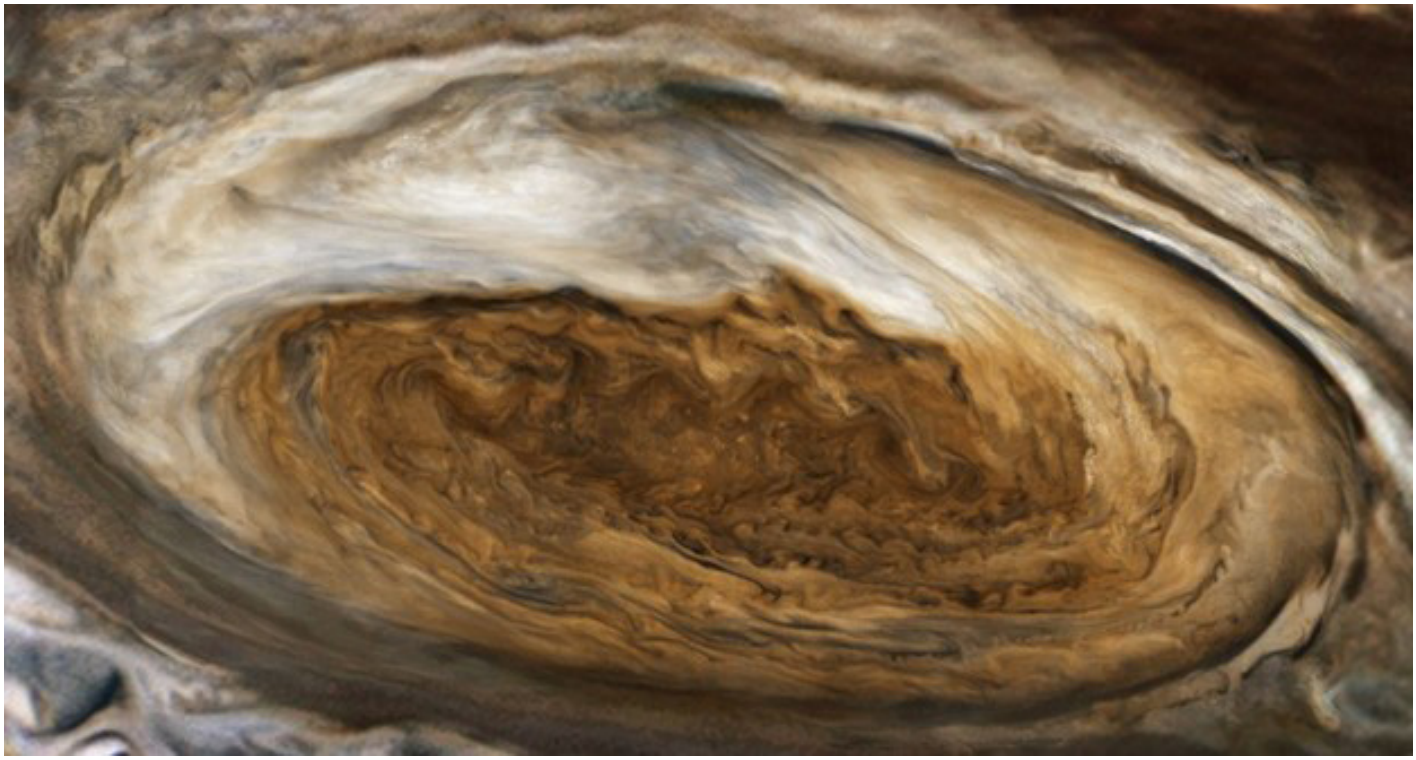

Figure 1 — My favourite image of Jupiter's Great Red Spot, imaged by Voyager I *in 1979. NASA photo.*

stayed in my memory and emotions, watching the comet's impact spots was electrifying; the emotional, pathetic impact on me was unbelievable. These impacts taught us an important lesson. Over the course of cosmic time, Jupiter has been battered by comets and asteroids over and over again, and each time a pathetic or emotional observer might detect a planetary tear coming from the eye of Jupiter.

During this particular winter, on each clear night I watch as Jupiter comes up earlier and earlier and I wave at my old friend that has never failed to greet me on a thousand starlight nights since my teenage years. Its fabulous Great Red Spot is smaller and fainter than it was on that September evening 66 years ago, and it is a lot smaller than the S-L 9 impact spots. But Jupiter never fails to arouse my deepest emotions. Jupiter's pathos is a part of me, and it always will remain a central part of my life. ✶

David H. Levy is arguably one of the most enthusiastic and famous amateur astronomers of our time. Although he has never taken a class in astronomy, he has written more than three dozen books, has written for three astronomy magazines, and has appeared on television programs featured on the Discovery and Science *channels. Among David's accomplishments are 23 comet discoveries, the most famous being Shoemaker-Levy 9 that collided with Jupiter in 1994, a few hundred shared asteroid discoveries, an Emmy for the documentary* Three Minutes to Impact, *five honorary doctorates in science, and a Ph.D. that combines astronomy and English Literature. Currently, he is the editor of the web magazine* Sky's Up!, *has a monthly column, "Skyward," in the local* Vail Voice *newspaper and in other publications. David continues to hunt for comets and asteroids, and he lectures worldwide. David was President of the National Sharing the Sky Foundation, which tries to inspire people young and old to enjoy the night sky.*

RASC Internet Resources

Like us on facebook
www.facebook.com/theRoyalAstronomicalSocietyofCanada

Follow us on X (Twitter) @rasc
twitter.com/rasc

www.rasc.ca
Visit the RASC Website

rasc.ca/rasc-line-communities
Email Discussion Groups

www.rasc.ca/contact
Contact the Society Office

www.rasc.ca/news
RASC eNews

Astronomical Art & Artifact

Icons of Astronomical Heroes: the Inclusion of Women Among the Magic Lantern Portraits

by R.A. Rosenfeld, FRASC
(r.rosenfeld@rasc.ca)

Abstract

In the late Victorian and Edwardian period the Astronomical and Physical Society of Toronto/Toronto Astronomical Society/Royal Astronomical Society of Canada acquired portraits of astronomers as part of its collection of magic lantern slides. Nearly 16% of these were of female astronomers. This figure is surprising, and these artifacts show that there was a desire to include women among its role models. This seems to have been reflected in the proportion of its membership that was female. The bank of imagery of female astronomical role models was not renewed after World War II.

Visages of Note

Role models seem to be essential for many people when shaping the future direction of their lives. Such figures can provide inspiration, or even something as basic as permission to envision entering a field (the latter is particularly important for those from groups underrepresented in a discipline). Not everyone requires a role model, although those who don't may be in the minority. For those who do, identifying a role model is a participatory and ongoing activity (or should be). Role models are discovered in stages by their admirers, each constructing their own version of the hero. How does that work? No two people's conceptions of ibn al-Haytham (ca. 965–post 1040), Isaac Newton (1643–1727), or Irène Joliot-Curie (1897–1956) will be identical, however much they share. Role models can also fall out of favour, as more is learned about their character and work, and as societal values shift.

People like to put faces to their heroes, even when they know actual likenesses are out of reach due to cultural norms, or the hazards of survival. They will make do with plausible but fictitious likenesses because they must. The iconography of scientific heroes has a commonality with religious iconography in such cases; in the complete absence of authentic portrayals, an icon of Saint Catherine of Alexandria (supposedly 4th century CE) won't be any less real than an image of Hypatia of Alexandria (ca. 355–415).[1] Those with faith in either science or religion can argue that images may well contain valid truths about their subjects even when accurate representations from life don't exist.

It is not unknown for professional and amateur scientists to display images of their role models. The Nobel Laureate Pieter Zeeman (1865–1943) found inspiration contemplating the portraits of Ampere, Faraday, Hertz, Onnes, Lorentz, van der Waals, and van't Hoff "on the walls of his office and corridors of his laboratory" (Maas & Lagarde 2024, 45–47). And Albert Einstein famously had a portrait of Issac Newton (and possibly ones of Michael Faraday and James Clark Maxwell) in his study in Berlin (Fölsing 1997, 428).

In the Victorian and Edwardian eras, astronomical societies also choose disciplinary heroes worthy of emulation, whose identities are quietly revealed today in the portraits of astronomers that the institutions acquired in various media. Some of the media could be deceptively humble. Outside the projector, magic lantern slides may seem the least physically imposing of portraits, but when projected, those limitations are exceeded, the likenesses appearing luminously larger than portraits in other media such as oil painting, woodcut, steel engraving, and lithograph. We might expect astronomical societies' choices to conform to the common scientific hagiography of their day. They don't always, and when they don't they can cause surprise, puzzlement, and at best, delight. The collection of the Society that was to become the RASC defies expectations, for it includes many more female astronomers than might be expected.

Genesis and Nature of the Lantern Slide Collection

The Society's collection of magic lantern slides began to be formed in the 1890s. David J. Howell (post-1940), a capable and energetic photographer and projectionist, was the prime mover in developing the collection, with acquisitions through both gift and purchase (Transactions of the Astronomical and Physical Society of Toronto [TPAST] 1891, 54; 1898, 1; 1900, 6). Nearly all the slides were of astronomical phenomena, or of diagrams explaining them (Howell 1892)—depictions of apparatus and installations were added later (Howell 1905, J, 9–10). The first astronomer portraits entered the lantern slide collection in 1892, and both were of Richard A. Proctor (1837–1888), the noted British popularizer of astronomy, whose family developed long-lasting connections to the RASC after his death (Howell 1983, 104).

The next portrait to be added six years later wasn't of Copernicus, or Newton, or Laplace, or John Herschel, as one might expect. It was an image of Anna Draper (1839–1914), one of the outstanding patrons of astrophysics in her day. She was the widow of the pioneering stellar spectroscopist Henry Draper, and herself had considerable experience making and

preparing astronomical apparatus (Jones & Boyd 1971, 213), but her chief claim to notice then, as now, was as the person who intelligently funded the Harvard College Observatory's Henry Draper Memorial. In November 1891, Andrew Elvins remarked at a meeting of the Society that: "Mrs. Draper's work is a noble monument to her husband's memory; with the spectroscope in the hands of Professor Pickering, she has written his name among the stars, where it must remain as long as they endure" (TAPST 1892, 45). Had Victorian propriety allowed it, he could have said more justly that she had written her own name there as well. By the time another six years had passed Anna Draper's portrait wasn't the only one of a woman astronomer in the collection.

Figure 1 — Agnes Mary Clerke, FRAS, magic lantern slide. Reproduced courtesy of the RASC Archives.

Figure 3 — Lady Margaret Huggins, FRAS, magic lantern slide. Reproduced courtesy of the RASC Archives.

Figure 2 — Caroline Herschel, FRAS, magic lantern slide. Reproduced courtesy of the RASC Archives.

Figure 4 — Dr. Dorothea Klumpke, Chevalier de la Légion d'honneur, magic lantern slide. Reproduced courtesy of the RASC Archives.

Before turning to the other portraits of role models, something more should be said of the production and use of magic lantern slides by RASC members. It is clear that there was an art to making effective slides, as there was to using them effectively. D.J. Howell was praised for his skill in both activities. Typical of the reports is the following:

> "Mr. Elvins and Mr. Howell were then called upon to exhibit the Society's lantern slides on the screen, they having kindly made arrangements to do so…There were also several reproductions made by Mr. Howell of star clusters and nebulae, photographs of which had been presented to the Society by Prof. E. C. Pickering of Harvard. The thanks of the meeting were due to Mr. Elvins and Mr. Howell for the very perfect arrangements they had made for showing the slides" (TAPST 1898, 9).

One can get a good sense of the skills involved in making the slides from contemporary handbooks (such as Elmendorf 1895). Even when the labour of coating the glass plates with light-sensitive emulsions was removed by the ready availability of commercially coated slides, the photographers still had to carefully clean the work space, handle the unexposed surfaces carefully, choose and monitor the light source, frame the subject appropriately, focus with care, judge the exposure,

Figure 5 — Annie Russell Maunder, FRAS, magic lantern slide. Reproduced courtesy of the RASC Archives.

Figure 6 — Mary Somerville, FRAS, magic lantern slide. Reproduced courtesy of the RASC Archives.

Figure 7 — Mary Somerville, FRAS, magic lantern slide. Reproduced courtesy of the RASC Archives.

develop the slide using toxic chemicals while controlling the working temperature, colour the image by hand if desired (none of the Society's surviving lantern slides are coloured), and then mount the finished plate. It was a more complicated series of skilled procedures requiring manual dexterity than our processing of electronic images to make digital slides; both require skill, but the pre-digital ones more so.

The technology now seems charmingly antiquated, but around 1900 it was modern, and apparently very effective in skilled hands during presentations.. A hint of the dramatic effects which could be achieved is suggested by recourse to the use of a projectionist's technique for moving between slides to analogically convey the experience of the striking changes effected on the land and skyscapes during a total solar eclipse:

> "Striking, indeed, is the almost instantaneous substitution, as in a dissolving lantern, of one picture for another, the one showing the sky with the blackened Sun like a blot upon it, the other showing the sky suddenly draped in the mantle of Night, upon whose sable bosom glow planet, star and coronal halo, and also roseate jets of incandescent gaseous matter leaping upwards from and falling back upon the Sun" (TAPST 1900, 53).

Apparently C.A. Chant was a skilled user of the technology. As our devices for visual display have changed so much over the century or more since the heyday of magic lantern slides, it is difficult to have any sense of how effective they could be in conveying astronomical spectacle. There is an active community of projectionists engaged in reviving the Victorian techniques, and there may be some among them with an interest in exploring the astronomical material. If so, it may become possible to experience something of what Howell and his colleagues were able to achieve.

A Metric of Societal Values

In 1904 the second catalogue of the RASC's magic lantern slide collection was compiled (Howell 1905). One major change since the first catalogue of 1892 is the growth in the number of portraits of astronomers. From one (male) astronomer represented by 2 slides that year, there were now 40 astronomers, spread across 45 slides (some merited more than 1 depiction!). Seven of those 40 were female. While this isn't gender parity, at 15.9% it's better than might be expected. Stated another way, nearly 16% of the astronomical role models the RASC was willing to project onto a screen for edification were women. This was a period when both the RASC and the British Astronomical Association prided themselves on admitting men and women to full membership, in contrast to some older and more prestigious scientific bodies (Broughton 1994, 45; McKim et al. 2011, 7–10). For the BAA at least, part of the reason for its founding (in 1890, also the year of the RASC's incorporation) was to have an organized group women *could* join, and fully participate in. Some of the prime movers in its inception were prominent woman astronomers, such as Elizabeth Brown (1830–1899, the noted solar observer), Agnes Mary Clerke (1842–1907, the highly respected historian of contemporary astronomy, and also a RASC member), Annie Maunder (1868–1947, the co-discoverer of the Maunder Minimum), and Lady Margaret Huggins (1848–1915, spectroscopist and skilled astrophotographer).

That 15.9% is interesting when compared to the Society's membership numbers. It is in broad accord with the percentage of female membership in the early years that Peter Broughton reported in *Looking Up*: 1893–1914 9%–19%; 1931–1936 16%; 1958 10%; 1968 9%; 1990 8% (Broughton

1994, 45). Peter quite reasonably asked why those numbers were what they were, and what they said about the Society. To the present writer these numbers taken in isolation indicate that it was more societally acceptable to be a female amateur astronomer in the period 1890–1940 than it was afterward, 1950–1990. One could say this is a blow to whig ideas of linear progress ever upwards toward a better tomorrow, but it is more serious than that, as it indicates the RASC was less healthily diverse gender-wise then than it could have been, particularly and counterintuitively during the second half of that century. And what of opportunities for potential LGBTQ members?

The female astronomers in the 1904 catalogue of the RASC's magic lantern slides are: Agnes M. Clerke (slide no. 9; Figure 1), Anna Draper (slide no. 37), Caroline Herschel (slide no. 19, 1750–1848, discoverer of comets, assistant to William Herschel, and a systematic cataloguer of astronomical objects; Figure 2), Margaret Huggins (slide no. 21; Figure 3), Dorothea Klumpke (no. 22, 1861–1942, first woman to earn a Docteur-ès-Sciences at the Université de Paris, and head of the Bureau des mesures at the Observatoire de Paris; Figure 4), Annie Russell Maunder (no. 29; Figure 5), Mary Somerville (slide no. 35, and another portrait not recorded, 1780–1872, the celebrated translator of Laplace's Mécanique Céleste, and an experimenter in her own right; Figures 6 & 7). There has been remarkably little attrition to this part of the collection. Only the slide of Anna Draper is no longer extant. Additionally, the collection now includes a second portrait of Mary Somerville, of unknown provenance (but its physical properties are very similar to the other slides from ca. 1900). What is disturbing is that the Society's selection of portraits of female role models in astronomy was not kept up to date in the period from the late 1920s to the early 1960s. Lantern slides remained a current technology up to the mid-20th century, so where are the portraits of female astronomers from that period? Their absence sadly coincides with the contemporary lower female membership percentages.

One would like to think that the inclusion of images of female role models in astronomy from the late Victorian and Edwardian periods made a difference to some female—and male—RASC members in the period up to World War II. The Society's magic lantern slides are a material evidence of that inclusion. Looking at this material invites comparison—how inclusive are we now? The question is all the more relevant in the age of MAGA barbarity to the south of us (a barbarity that may have more of a presence in Canada than we'd like to admit. ✶

Endnotes

1 Hypatia did not make it into the Society's Victorian and Edwardian pictorial role models of astronomers. Members would likely have been aware of her, through works such as the Rev'd Charles Kingley's polemical fictional treatment (1853), or the more factual and sober account in the 9th edition of the *Encyclopaedia Britannica* (Anon. 1881). Had they decided to add her they would have faced a difficulty. The best known imaginative image of her was Charles William Mitchell's (1854–1903) "Hypatia" of 1885 (Newcastle, Laing Art Galley, TWCMS:B8111), which, while it was viewed with pleasure (perhaps too much pleasure) by an artistically sophisticated public in Great Britain and Western Europe (Anon. 1886), is much less likely to have been found reproducible in a culturally constrained environment like Toronto in the period. The painting can be considered problematic now for its arguably exploitative iconography.

Acknowledgements

This research has made use of NASA's Astrophysics Data System.

[Editor's note: See Blast From the Past upcoming in the June Journal for Agnes Mary Clerke's obituary.]

References

Anon. (1881). HYPATIA. In (Ed.) Baynes, T.S., & Smith, W.R., *Encyclopaedia Britannica; a Dictionary of Arts, Sciences, and General Literature*, 9th edition, vol. XII (p. 596). Edinburgh, Adam and Charles Black

Anon. (1886). Grosvenor Gallery. *The Art Journal*, n.s., 188

Broughton, R.P. (1994). *Looking Up: a History of the Royal Astronomical Society of Canada*. Toronto-Oxford: Dundurn Press

Elmendorf, D.L. (1895). *Lantern Slides: How to Make and Color Them*. New York: E. & H.T. Anthony & Co.

Fölsing, A. (1997). *Albert Einstein, a Biography*. (Tr.) E. Osers. New York-London: Viking

Howell, D.J. (1893). Lantern Slides, the Property of the Society. TAPST for the Year 1892, Including Third Annual Report, Appendix III, 103–104

Howell, D.J. (1905). List of Lantern Slides in the Possession of the Society. *The Royal Astronomical Society of Canada Selected Papers and Proceedings 1904*, Appendix II, 2-10

Jones, B.Z., & Boyd, L.G. (1971). *The Harvard College Observatory: The First Four Directorships, 1839–1919*. Cambridge MA: The Belknap Press

Kingsley, C. (1853). *Hypatia: or, New Foes With an Old Face*, 2 vols. London: John W. Parker and Son

Maas, A. & Lagarde, L. (2024). Nobel Artefacts: Material Heritage of Nobel Prize Laureates in the Netherlands. In (Ed.) Hansson, N. & Maas, A. *Nobel Genius: Prizes, Prestige and Scientific Practice* (pp. 39–63). Leiden: Leiden University Press

McKim et al. (2011). *The British Astronomical Association: the First Fifty Years*, 3rd ed. B.A.A. Memoirs, 42, pt. 1. London: British Astronomical Association

Keep Calm and Orbit On

Interdisciplinarity

By Samantha Lawler, Regina Centre
(samantha.lawler@uregina.ca)

I am on my first sabbatical as a professor (and immensely grateful to have this opportunity!). Once every seven years, professors at many institutions have the opportunity to skip some or all of their normal teaching load and are then encouraged to visit other institutions for collaboration and learning. Among other adventures, I have been very fortunate to spend a few very productive and educational days visiting the University of British Columbia, discussing many aspects of satellite pollution.

If you've read my previous columns[1,2], you'll have noticed that I spend a lot of time thinking about satellite pollution and advocating for better regulation of satellites in orbit. I work with several different groups of mostly astronomers who are all donating huge amounts of time and effort to educate, write, speak, and teach what is happening in orbit, in hopes of mitigating the damage. But sometimes it definitely feels like astronomers are the only ones noticing this environmental disaster unfolding above our heads. My week visiting UBC really proved that wrong!

I heard a talk by a political scientist, Dr. Adam Bower (University of St. Andrews) focusing on the political mechanisms needed to ban antisatellite (sometimes shortened to ASAT) weapons tests. Several countries have conducted these to test and demonstrate offensive capabilities, most recently Russia in late 2021. Every time an ASAT test is conducted, there is a huge injection of debris into Low Earth Orbit (LEO) when the target satellite is exploded by a missile. As the density of active satellites and debris continues to increase in LEO, an injection of debris becomes a higher and higher risk of secondary and tertiary collisions, which could generate more debris, and could even push us into the worst-case scenario of Kessler Syndrome (where the density of objects in LEO becomes so high that a chain reaction of collisions occurs). Kessler Syndrome could destroy many of our existing satellites and limit operations in orbit for decades to centuries. As this talk was coming from a political-science perspective, the point was to discuss how to make a ban on future tests happen at the UN level. Interestingly, the speaker argued that despite the outright hostility that exists between many countries at the moment, protecting the infrastructure in LEO that we all depend on may be enough to bridge these tensions. However, as noted in a discussion with a different political scientist later in the day, this talk did not take into account the United States' plan to place thousands of weapons-capable satellites into LEO in the form of the "Golden Dome" megaconstellation (just when I thought megaconstellations couldn't get any worse than Reflect Orbital…)

Later that same day, I was invited at the last minute to give the introductory portion of the lecture for a large undergraduate course on international law. I spoke for a few minutes about the international law I witnessed play out in real time when I helped several farmers deal with debris from a SpaceX *Crew Dragon* cargo trunk that fell near Ituna, Saskatchewan, in 2024[3]. This was a use case for the 1968 Outer Space Treaty[4] and the 1972 Space Liability Convention[5], which meant that the debris had to be returned to the country of origin (the United States), and that the United States would have been absolutely liable for any damage that occurred. But, those treaties were written in a time when basically only the governments of the US and the USSR were launching objects into orbit, so it's really not at all clear how those rules apply to for-profit corporations and private citizens. SpaceX paid farmers $5,000 per family for "retrieval and storage of spacecraft components," and sent two employees to load the debris into a rented U-Haul truck. International space law in action, apparently! That kind of weird situation is only going to become more and more common as the thousands of satellites in orbit today reenter over the coming years.

The following day I was invited to visit the research lab of Dr. Allan Bertram, who studies chemistry related to aerosols in the stratosphere. A lot of his work right now involves testing for unintended downstream effects of chemicals, like aluminum oxide and titanium oxide, that have been proposed for geoengineering (another thoroughly terrifying topic). The end-of-life plan for every satellite in LEO is to burn it up in Earth's upper atmosphere, and that large mass (Starlink V2 "mini" satellites are about the mass of a Ford F150) doesn't disappear, it gets deposited up there. The metal

Figure 1 — Pieces of a SpaceX Crew Dragon Cargo Trunk that fell on farmland near Ituna, Saskatchewan, in 2024. Barn cat on the far right for scale. Photo taken by the author.

frame, computers, batteries, solar panels, all of it, according to Starlink, turns into vapour and particulates in the upper atmosphere. At least half of a satellite's mass is aluminum, and Dr. Bertram is studying what that aluminum will do when it melts in the atmosphere. The preliminary results are not good; his research group's work supports initial studies that pointed to ozone depletion[6].

And finally, I went to a talk by Dr. Deb Chachra, who is an engineering professor and the author of a book called "How Infrastructure Works"[7], who was speaking to the UBC soil studies research group. Her talk focused on how we build infrastructure to use as little energy as possible to accomplish tasks. This starts with infrastructure as simple as following a footpath rather than tramping through tall grass and bushes, because that saves energy. And that extends all the way up to our modern satellite infrastructure. At one point during the talk, she gave the example of how it now makes more sense energetically to mine aluminum ore in Indonesia, and then ship it to Canada for smelting, because we have abundant hydroelectricity that is cheap and has low emissions. During her talk, I had been multitasking and catching up on a flurry of journalist emails, and I was just about to email photos of SpaceX debris to a journalist for an article about collision risks in orbit. Guess what the satellites are mostly made of? Aluminum! Mined in Indonesia, smelted in Canada, and then sent into orbit, to be deposited as ablated particulates in the atmosphere, or to fall onto the surface of the planet and be discovered by farmers. It was a bit of an overwhelming *EVERYTHING IS CONNECTED* kind of moment.

During my visit to UBC, I was able to connect with people across a huge range of disciplines who are directly or indirectly studying the effects of the commercialization of LEO with megaconstellations, and who are thinking about ways to help with some of the worst problems. As I head off on the next leg of my sabbatical journey, I hope to make even more of these connections, and learn ways to advocate for satellite regulation from many different directions and perspectives. ✶

Endnotes

1 Lawler (2026). Keep Calm and Orbit On: Megaproblems from Megaconstellations. JRASC February 2026.

2 Lawler (2025). Keep Calm and Orbit On: Reflect Orbital is the Worst. JRASC December 2025.

3 Lawler (2024). A New, Deadly Era of Space Junk Is Dawning, and No One Is Ready. Scientific American July 2024.

4 www.unoosa.org/oosa/en/ourwork/spacelaw/treaties/outerspacetreaty.html

5 www.unoosa.org/oosa/en/ourwork/spacelaw/treaties/liability-convention.html

6 Ferreira et al. (2024). Potential Ozone Depletion From Satellite Demise During Atmospheric Reentry in the Era of Mega-Constellations. Geophysical Research Letters 51, 11. doi.

7 Chachra (2025). How Infrastructure Works. Penguin Books ISBN: 9781804995952 org/10.1029/2024GL109280

Sam Lawler is an associate professor of astronomy at the University of Regina. She studies the orbits of small bodies in the outer Solar System, and increasingly studies and advocates for regulation of the thousands of new artificial satellites streaking through her research images, crawling across her huge prairie skies, and crashing onto nearby farmland. She's active on Mastodon@sundogplanets@mastodon.social and BlueSky@sundogplanets.mastodon.social.ap.brid.gy

Great Images

By James Edgar FRASC

Taken by James Edgar with a handheld smart phone on January 26. Lots of crystals in the air that day.

Imager's Corner

Finding Exoplanets from Your Driveway

by Blair MacDonald, Halifax Centre
(b.macdonald@ns.sympatico.ca)

A friend and fellow Halifax RASC Centre member joined me on 2025 December 9, to see if we could observe a transit of HD189733b in front of its parent star. As this was the first attempt to observe the exoplanet transit, it was treated as a bit of an experiment. The first lesson: everything takes longer than expected, so start early. Due to an alignment star being in the trees, it took longer to get the system aligned and the start of the transit was missed by several minutes!

Despite observing from a less-than-ideal urban location, the exoplanet transit was clearly detected, meeting the experiment's primary goal. In addition, using the data collected, other aspects of HD 189733b were explored, such as the existence of an atmosphere.

The Star System

HD189733 is a 7.8 magnitude yellow-orange star in Vulpecula with a transiting exoplanet known as HD189733b, approximately 63 light-years from Earth.

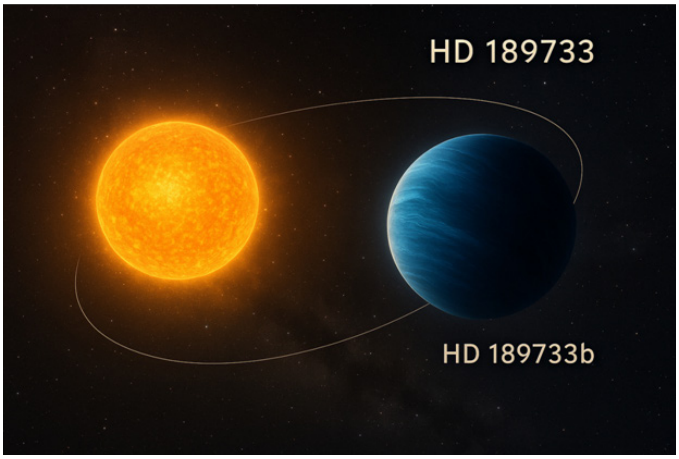

Figure 1 — Graphical representation of the HD189733 system.

HD189733b is a hot Jupiter-type gas giant and orbits approximately 4.6 million km from its star. It completes one orbit every 2.2 days and the light curve dips about 2% at mid-transit. The star is in the centre of the image shown in Figure 2, with M27 to the right. The field is 1.5˚ by 1˚..

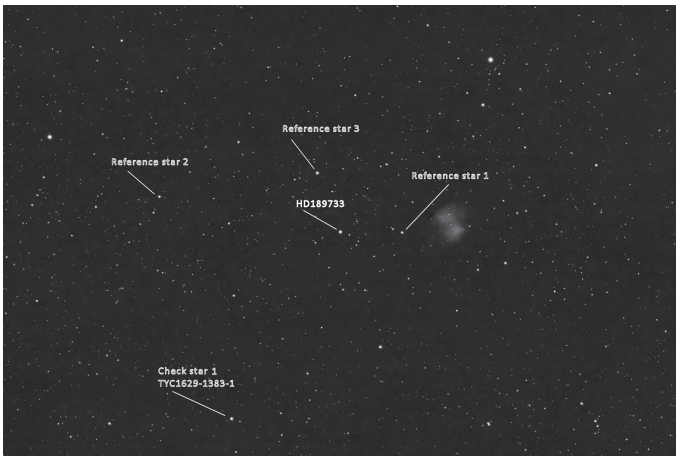

Figure 2 — The field surrounding HD189733, showing the location of the star relative to M27 as well as the locations of the reference stars and a star used to check for systematic errors.

The brightness of the star, and the relatively large mid-transit dip, puts it within the range of the equipment used.

Equipment

The equipment used for the observation consisted of a ZWO ASI2600MC Pro colour camera coupled to a Sky-Watcher Esprit 120 telescope riding on a Celestron CGX-L mount. During the data acquisition, the system was guided by an Orion Star Shoot Autoguider (SSAG) coupled to a 400-mm refractor. Since the equipment usually operates at the end of a driveway, either at home or the cottage, it has been named the Driveway's End Observatory (DEO).

The ZWO camera is a modern CMOS one-shot colour (OSC) camera based on the Sony IMX-571 colour sensor and was cooled to -10 ˚C during data acquisition. It has very low dark current and uses a 16-bit analogue to digital converter (ADC).

Figure 3 — DEO set up at a dark-sky site.

Observing Site

All data was gathered under less-than-ideal conditions from an urban driveway in Bedford, Nova Scotia. Light pollution from streetlights and bright urban Bortle 6 to 7 skies limit the photographic stellar brightness to about magnitude 17.

Figure 4 — Urban observing site where the data was captured. In addition to the lights shown in this picture, Christmas lights interfered. By the end of the observing session the target was setting between the two houses almost at the tree line.

The bright sky causes a lot of photon noise, and an experiment was carried out about four weeks earlier to determine the longest exposure that could be used without saturating any stars in the frame. It was found that a 1.5-second exposure produced an output of about 28000 out of a maximum of 65535 for the target star. Care was taken in selecting the reference stars to avoid any saturation while keeping the signal-to-noise ratio as high as possible.

Data Collection

Using the *Swarthmore College exoplanet transit calculator*, (*Jensen E. L. N. 2013. Tapir: A Web Interface for Transit/Eclipse Observability, Astrophysics Source Code Library ascl:1306.007*) transit times for 2025 December 5, were found with a favourable transit starting just before 6:30 PM AST.

Figure 5 — (Below) Output of the exoplanet transit calculator at https://astro.swarthmore.edu/transits/.

The data was collected, then flats, darks, and flat darks were obtained after the transit was complete. During the transit, HD189733 descended between the two houses visible in Figure 4 ending up at the tree line by the end of the transit. This increasing air mass, the amount of Earth's atmosphere through which the starlight must pass, had an impact on the data quality, reducing the signal-to-noise (SNR) during the observing run as shown in Figure 6.

Data Reduction & Results

In all, 783 images were obtained and each image calibrated with darks, flats, and flat darks. Following de-Bayering, the colour images were split into red, green, and blue monochrome images. The photometry script in *PixInsight* was used to

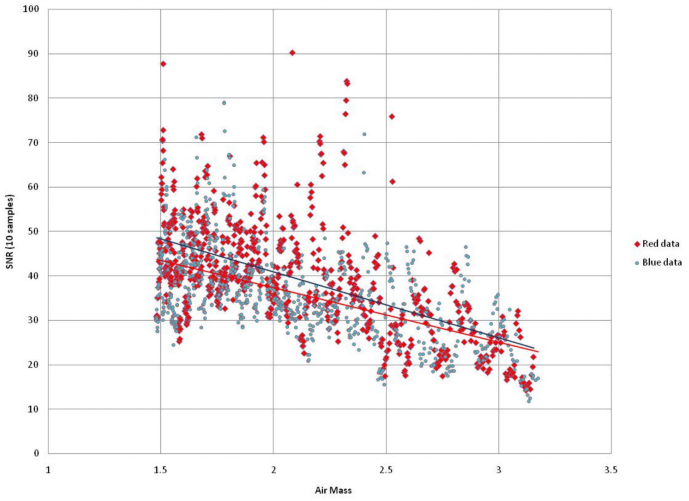

Figure 6 — HD189733 SNR versus air mass during the observation. The lowering SNR impacted the data during the later stages of the transit. The red data is simply the red channel of the OSC camera while the blue data is the blue channel.

Only 1 target matches your constraints (on name, V mag, depth, etc.). Searching for observable transits over 7.0 days...

Upcoming events for the next 5 days and the past 2 days from 12-09-2025; start/end given in timezone UTC.

Night starts/ends at nautical twilight.

Results shown for Other Site latitude = 44.71006, longitude = -63.68678930378416.

Colored text indicates a part of the transit that is during daylight, or a transit at elevation less than the user-specified limits, or that the Moon is relatively full and close to the target.

Click on column headers to sort the table by that column. Click again to reverse the sorting order. To sub-sort, first click one column (e.g. the left-hand one to sort by night), then *shift-click* another column to sort further within the first category. For example, to sort by priority within a given night (when multiple nights are displayed), first click the "Local evening date" header, then shift-click the "Priority" header. The highlighted column shows the current sorting.

The buttons can be used to toggle the visibility of columns, and the column order can be rearranged by clicking and dragging the column header.

Column visibility | Reset column order | Show all columns | Disable tooltips

Search: | Show if visible transit % + baseline % > 0 | V_{max}: | $Depth_{min}$: 0 ppt | Overlap: 0 m. | Other Site

Local evening date	Name	V or Gaia mag	Start—Mid—End	Duration	BJD_{TDB} start-mid-end	Elev. at start, mid, end ±1 hrs	% of transit (baseline) observable, Suggested obs. start, end	Az. at start, mid, end ±1 hrs	HA at start, mid, end ±1 hrs	RA & Dec (J2000)	Period (days)	Depth (ppt)	Comments
Tue. 2025-12-09: Nautical twilight 2025-12-09 21:44 — 2025-12-10 10:30 local time / 2025-12-09 21:44 — 2025-12-10 10:30 UTC													
Tue. 2025-12-09 Nautical twilight 21:44 – 10:30 (UTC)	☐ HD 189733 b Finding charts: Annotated, Aladin, SkyMap; Airmass plot, ACP plan Info: Exoplanet Archive, Simbad, Gaia, TIC	7.7 / Moon 69% @134°	21:22 / 22:22—23:17—00:11 / 01:11 ±0:00	1:49	11019.4302 11019.4681 11019.5060	54° / 44°, 34°, 24° / 14°	100% (82%) 21:44—01:11	244° / 259°, 269°, 279° / 288°	+2.3 / +3.4, +4.3, +5.2 / +6.2	20:00:43.71 +22:42:35.19	2.22	24.0	Ephemeris from Kokori et al. 2023.

Showing 1 to 1 of 1 entries

Script took 1 second for 1 events.

conduct aperture photometry on each image producing red and blue flux tables in comma separated variables (CSV) format. The table contains the timestamp of the image, the V and B magnitudes as read from the Tycho2 catalogue, the position, the catalogue number, and the measured ADC output for each star found in the image.

As there was very little information on the red magnitude of the stars used in the data reduction, the R magnitude was estimated from the V and B values using.

$$R = V - 0.587(B - V) - 0.011$$

This comes from estimating the star colour, and thus temperature, from the B–V colour index. A simple web search will turn up a host of mathematical formulae, all in the same form with different constants, and the formula used was chosen as it best fit the limited red data available on several stars in the image field. It should be noted that the accuracy of this empirical formula drops off as B–V becomes greater than 1.2.

Initial checks were carried out to validate the data and to look for any indication of the transit. The raw data, measured in ADC counts (simply the value of the ADC from 0 to 65535) from the camera, represent the values captured directly by the camera and extracted using the *PixInsight* photometry script. For those interested in more correct units, the camera gain was 0.25 e/ADU, its quantum efficiency is about 0.8 and each exposure was 1.5 seconds. The collected data clearly shows the effects of atmospheric extinction, as the air mass was steadily climbing throughout observation, causing the collected starlight to decrease in intensity during the data acquisition as shown in Figure 7.

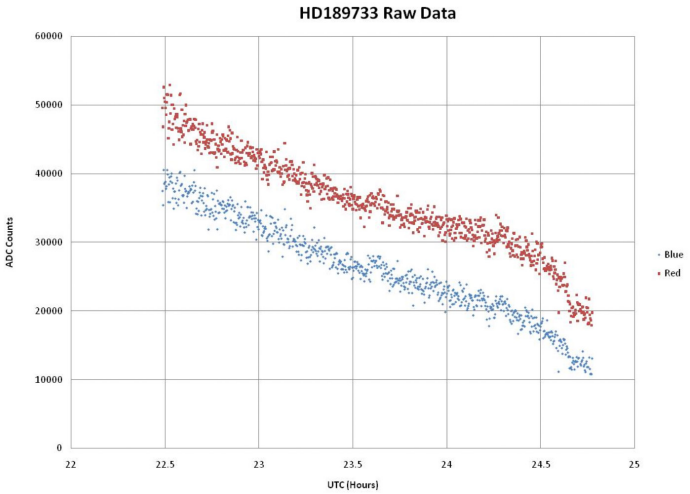

Figure 7 — Raw data from the target star collected during the observation. The downward slope is caused by atmospheric extinction.

These effects of atmospheric extinction could be corrected by applying the appropriate first order extinction corrections to the data; however, as differential photometry was used, the first order effects of loss due to extinction are cancelled out when the ADC value of the target star is divided by the ADC value of the reference star. The plot shown in Figure 8 shows the ADC counts received from the first reference star; note that it also shows a slope due to extinction effects.

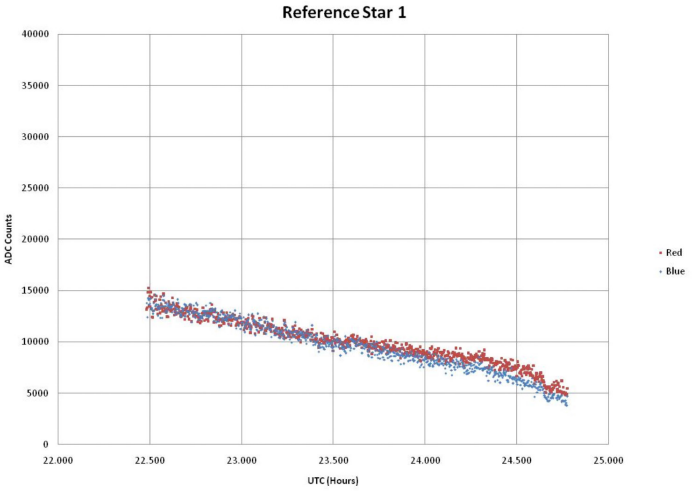

Figure 8 — Raw data from the first reference star collected during the observation. The downward slope is similar to that seen in Figure 7.

The target star (S_t) differential ADC values are calculated from

$$\Delta S_t = \frac{S_t}{S_{ref}} \qquad \text{(Eq1)}$$

Where: S_t is the measured brightness (ADC value) of the target star

S_{ref} is the measured brightness (ADC value) of the reference star

Plotting ΔS_t against time shows that, by using the differential ADC value, most of the atmospheric extinction effects are removed as they cancel in the division.

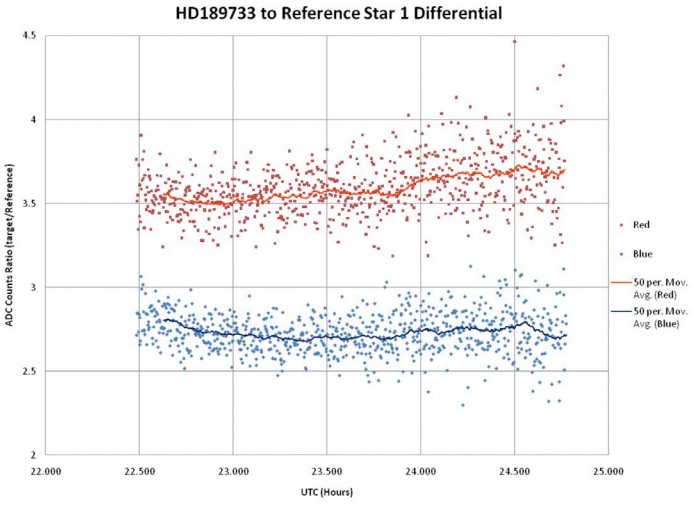

Figure 9 — Differential data easily showing the transit in the red channel.

The moving average of the red channel differential data shows the transit ending around 00:20 UTC. (The hour count was allowed to exceed 24 for purposes of the plotting program.) The data also shows that the start of the transit was missed by a few minutes. The moving average filter, used to smooth the data in Figure 9, is less than optimal as it puts an *n* sample delay in the output, where *n* is the number of samples used in the moving average. The data was re-smoothed using an adaptive symmetric nearest neighbour linear least-squares fit algorithm that gives better smoothing with minimal delay. In addition, three estimates of the brightness, each using different reference stars, were averaged to reduce the noise in the data, resulting in the plot shown in Figure 10.

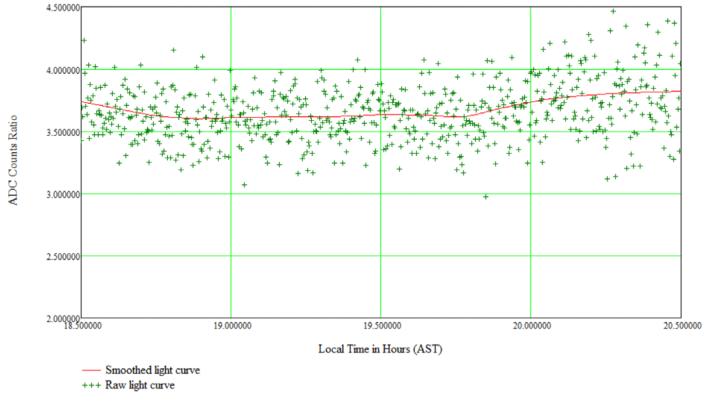

Figure 10 — Averaged data with an adaptive smoothing filter makes the transit clearly visible.

This approach is clearly superior to the simple moving average and is used for all smoothed data plots unless otherwise noted. With the data verified, and knowing that it contains the transit, the rest of the data reduction was carried out.

Atmospheric extinction affects blue stars more than red stars, as noted in *The Cepheid impostor HD 18391 and its anonymous parent cluster* by *D.G. Turner, V.V. Kovtyukh, D.J. Majaess, D.J. Lane, and K.E. Moncrieff* published in *Astronomical Notes* in 2009. There are also differences caused by where the starlight falls within the bandpass of the colour filter. These effects are not corrected using differential techniques and need to be removed from the data. The second-order extinction coefficients ks_b and ks_{br}, were measured using the technique outlined in the *Workbook for Astronomical Photoelectric Photometry (ISBN 0-9628592-1-4)* and used to complete the correction for atmospheric extinction. Tracking a red and a blue star throughout the observing session and plotting the observed colour index against the colour index times the air mass allowed the calculation of the required coefficients to remove extinction effects. Note that the colour index coefficient is ks_{br}, not k_{bv}, as the colour filters were not standard UBV filters. The filters were, in fact, the Bayer RGB filters of the ZWO OSC camera. Because of this, and because it was not necessary for the purpose of obtaining evidence of the transit, no effort was put toward transforming the data to a standard system, short of removing the extinction effects. The approximate combined QE and filter response of the ZWO camera is shown in Figure 11. Although not an exact match for proper photometric filters, it is not too far off.

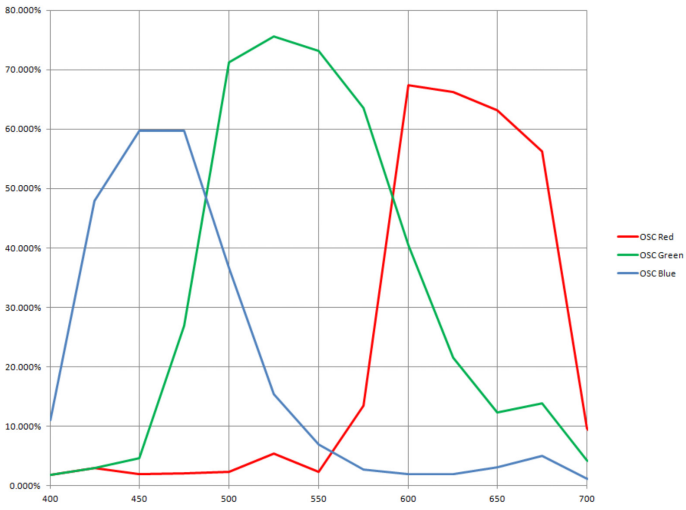

Figure 11 — ZWO camera colour filter response. This plot takes the quantum efficiency and the optical window of the camera into account.

After the coefficients were determined, the magnitude of the target star was calculated using

$$S_{tmag} = S_{ref\_mag} - 2.5 \cdot \log\left(\frac{S_t}{S_{ref}}\right) - ks \cdot \Delta(b - r) \cdot X \qquad \text{(Eq2)}$$

Where: S_t is the measured brightness of the target star

S_{ref} is the measured brightness of the reference star

S_{ref_mag} is the magnitude of the reference star from the *Tycho2* catalogue

ks is the second order extinction coefficient for the colour channel

$\Delta(b-r)$ is the difference in colour index of the target and reference stars

X is the air mass

Three separate magnitudes were calculated using three different reference stars (Figure 2).

Next, the three target magnitudes were averaged to reduce the noise in the data using

$$S_{tavg} = -2.5\log\left(\frac{\frac{S_{t1}}{10^{-2.5}} + \frac{S_{t2}}{10^{-2.5}} + \frac{S_{t3}}{10^{-2.5}}}{3}\right) \qquad \text{(Eq3)}$$

Where: S_{t1}, S_{t2}, and S_{t3} are the target magnitude estimates made using each reference star and Eq2.

The above calculations were done for the red and blue colour channels and represent the corrected instrumental magnitude

as measured above the Earth's atmosphere. Finally, the data was converted back to a linear brightness and both the red and blue channels normalized to their respective maximums, then the plot of the transit was produced.

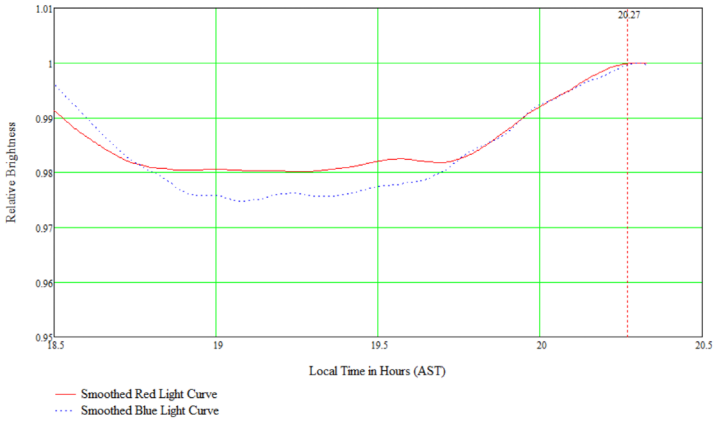

Figure 12 — Red and blue normalized light curves for HD189733 after correction for atmospheric extinction. The end of the transit is marked by the dashed red vertical line.

The data plotted in Figure 12 agrees well with measurements published by Gardner-Watkins et al. - *A Six Year, Low-resolution, Multibroadband Transit Photometry Study of HD 189733b* published in *The Astronomical Journal, 165*:5 (18pp), January 2023.

Colour	Gardner-Watkins	DEO Data
Red depth	0.025	0.020
Blue depth	0.028	0.024
Δ(Blue- Red)	0.003	0.004

Table 1 - DEO data compared to Gardner-Watkins Study

The authors would like to thank Dr. David Turner (RASC Halifax) for suggesting that corrections for atmospheric extinction be applied to the data. This substantially improved the agreement with the Gardner-Watkins results.

If a planet has an atmosphere, Rayleigh scattering due to particulates in the clear upper layers attenuate blue light more than red. This is one of the key detectable indicators that an exoplanet has an atmosphere. Since the camera used is a one-shot colour unit, red and blue light are captured simultaneously. This opens up an interesting possibility of using very broadband spectroscopy for planetary atmosphere detection. Examining the plots of Figure 12 shows this technique can be useful, as there is clear evidence that blue light has been attenuated more than red, indicating that HD189733b does indeed have an atmosphere.

As a final check on the data, the same exercise was carried out on the check star shown in Figure 2 to see if it also showed any sign of the transit. If it did then there may have been a problem with the reference stars chosen, calling the transit detection into question. Figure 13 shows the check star light curve has a residual variation that does not match that of HD189733.

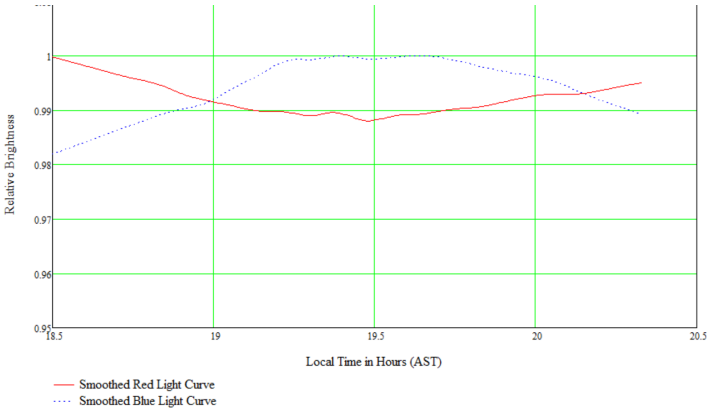

Figure 13 — Normalized light curves for the check star.

Using the end of transit (EOT) time, shown in Figure 12 and the barycentric Julian EOT time from Figure 5, it is possible to estimate the distance from Earth to the Sun on the date of the observation.

Figure 14 shows how the problem is set up.

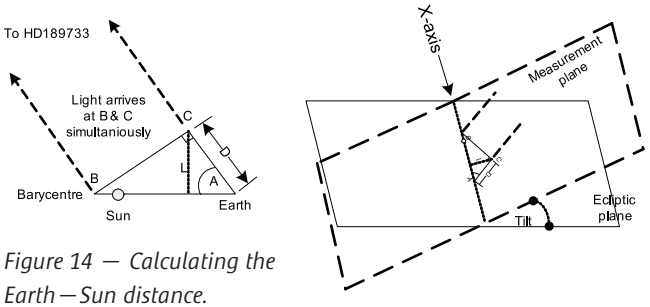

Figure 14 — Calculating the Earth—Sun distance.

The general idea is that the angle A and distance D can be used with some simple trigonometry to calculate the Earth to barycentre distance

$$D_{\text{Earth-barycentre}} = D/\cos(A) \qquad \text{(Eq4)}$$

Since the barycentre lay beyond the Sun, as seen from Earth during December, the Sun to barycentre distance can be subtracted to give the Earth Sun distance. A", the angle between the Sun and HD189733 as seen from the Earth, is measured along the equatorial plane, not the plane in which the distance D is measured. This angle is 43.42° (*courtesy of the ECU planetarium program by the late Dr. David J. Lane*) and must first be projected on the ecliptic plane using

$$A_{\text{Tilted Plane}} = \operatorname{atan}\left(\frac{\tan(\theta_{\text{Reference Plane}})}{\cos(\text{tilt})}\right) \qquad \text{(Eq5)}$$

where theta is the angle measured on the reference plane and

tilt is the angle between the tilted and reference planes. The tilt of the ecliptic relative to the equatorial plane is 23.4393° yielding an angle A′=45.886°. Next, the plane of the distance measurement is defined with its X-axis being the Earth-Sun line on the ecliptic and tilted around the Earth-Sun line by the ecliptic latitude of HD189733 which is 42.175°. This plane contains the Sun, the Earth, the barycentre, and HD189733 and is the plane along which the transit timing is measured as it contains the direct light path from the star to the Earth. Figure 14 shows this arrangement, but the angle A′ now needs to be projected from the ecliptic to this tilted measurement plane, again using Eq5, yielding a final angle A of 54.302°. The distance, D, is calculated from the EOT time predicted at the barycentre, from Figure 5, and the measured EOT time as read from Figure 12. Taking the difference of these two times and multiplying by the speed of light in a vacuum yields the distance D = 89,637,944.94 km. Applying equation 4 to this using the projected angle gives the Earth to barycentre distance of 153,618,081 km. Finally the barycentre to Sun distance of 820,000 km is subtracted, as the barycentre was behind the Sun from the Earth's perspective, giving an Earth-Sun distance of 152,798,081 km. The actual Earth-Sun distance was found using the solar distance calculator (https://dqydj.com/solar-distance-calculator/) to be 147,338,091 km, an error of just 3.7%.

Conclusions

An experiment was conducted to determine if it was possible to detect the transit of an exoplanet with a small telescope and a commercially available amateur CMOS camera from a very light polluted urban environment. Not only is it possible, but the data is of high enough quality to gain insight into the exoplanetary system. The transit timing measurement allows the estimation of the Earth-Sun distance to a surprising accuracy of better than 4%. The measurement seems to be resistant to noise in the data even though the EOT time happens when the measurement SNR is at its lowest. Indeed, the biggest source of error is likely the reading of the EOT time from Figure 12.

The detection of an exoplanet, the detection of an exoplanet atmosphere and a measurement of the Earth Sun separation, not bad for a five-inch telescope under urban skies! ✶

Blair MacDonald is a retired electrical technologist. He's been an RASC member for 35 years and has been interested in astrophotography and image processing for about 30 years.

Mostly Variable Stars

Who Discovered Variable Stars?

by Hilding Neilson
(hneilson@mun.ca)

Who discovered that stars are variable? My introductory astronomy textbook will highlight David Fabricius in 1595 as having observed variability in the star Omicron Ceti, or Mira, and will also note that he died soon after. We are told that no other variable stars were discovered until 1784 when John Goodricke found that Delta Cephei is variable. Afterward, more and more variable stars were discovered. Of course, we should note that the supernova in 1054 was observed by people from around the world, but there is not one single discoverer attributed to that explosive variable. There have been some notes about earlier observations of variable stars, such as the variability of Algol, which was noted in the Egyptian-Cairo Calendar (1271–1163 BCE) (Jetsu and Porceddu 2015). But, even so, why are we sure that Fabricius was the first to discover variable stars?

Hamacher (2018) reported on historical observations of variable red giant stars by Aboriginal Australians (Indigenous Australians), in particular Betelgeuse, Antares, and Aldebaran. It was widely known that Aboriginal Australians across the continent have rich and detailed astronomy traditions (see for example Clarke 2014, Norris 2015). In that work, the author shares the oral sky knowledge of Kokatha communities from South Australia who share stories about the hunter Nyeeruna (in what astronomers call Orion) who chases the Yugarilya sisters (Pleiades) to make them his wives. The sisters are protected by their eldest sister, Kambugudha, who taunts and kicks dust at Nyeeruna. Nyeeruna threatens them with his fire club that contains magic (Betelgeuse). When Kambugudha lifts her left foot (Aldebaran) that is also fire magic. She kicks dust at Nyeeruna, embarrassing him and dissipating some of the magic in his club.

Over time, the magic returns to the club (i.e. Betelgeuse brightens), Nyeeruna tries again, but Kambugudha calls Babba, the father Dingo, to attack Nyeeruna, who is humiliated again and the club fades. Hamacher (2018) notes that similar stories are told across the Great Victoria Desert and in central Australia.

In the second story, Hamacher (2018) shares a Ngarrindjeri story where they tell of a person becoming a star that varies in brightness over different times. Hamacher (2018) shows that, based on the story and the details, it must be a reference to the star Antares. This shows that the Australian stories definitely refer to the variability of the red giant and supergiant stars that was not recognized by professional astronomers. That is unfortunate since Aboriginal Australians have been living on those lands since time immemorial (or about 65,000

years based on archaeological evidence) and have a deep oral tradition that carries observations and data to today.

While I personally don't find it surprising that Indigenous peoples observed stellar variability, it apparently required "confirmation." Schaefer (2018) published a follow-up article, where he asks if "untrained peoples can discover the variability" of stars and then compares the variability of the three stars reported by Hamacher (2018) with the brightness of stars near them to show that the variability is "easily detected by inexperienced observers." Schaefer (2018) clearly concludes that Aboriginal Australians could and did discover variability in those stars. However, it is unclear why it was necessary for him to have to conclude this when we could just believe the oral traditions. The only reason I can see is that there is a tendency to dismiss Indigenous Knowledges in western science and, especially, astronomy. But, today, it should not be controversial in any way that Indigenous people observed and noted the variability of stars since we have watched the Great Dimming of Betelgeuse that would be readily apparent to any observers who spent enough time observing the star.

From this, one thing that did stand out was the point in Hamacher (2018) that the stories he reports are the only known descriptions of pulsating variable stars in "any Indigenous oral tradition." I was both surprised and unsurprised by that statement. It was unsurprising because of the dismissiveness that western scientists have traditionally held (Aikenhead & Michell, 2010), but also surprising because many, if not all, Indigenous cultures have distinctive observing practises of the sky since time immemorial. In Canada, we have learned and shared some of the Indigenous sky stories, such as the story of Muin and the Seven Bird Hunters during the International Year of Astronomy in 2009 (Bartlett et al. 2009), the teachings by Elder Wilfred Buck (Buck) and the writings in this *Journal* by Frank Dempsey (2008, 2009a, 2009b) just to mention a few. However, what is in the public domain mostly just scratches the surface. I will note that I have heard a few stories that seem to reference variability in red giant and red supergiants stars, but they are not my stories, so it is not for me to repeat them. But, McDonald reported stories from Inuit communities of weather monitoring by watching the flickering of the stars near the horizon, and similar stories are reported by Cannon (2025) for Dene, and others. McDonald also reported Inuit stories about sunspot observations.

These stories and knowledges demonstrate that Indigenous peoples are trained astronomers. Furthermore, oral traditions span thousands of years, meaning Indigenous astronomies are the most extreme of time-domain astronomy. These knowledges are science, culture, and more.

I started by asking about who discovered variable stars? I think it is safe to say that there is no one discoverer who should be given credit, but then maybe we can ask about how we give credit for other discoveries. For instance, many of us work with and teach the Hertzsprung-Russell Diagram, but Ejnar Hertzsprung published the plot first (Hertzsprung, 1911), a few years before it was published by Henry Russell Norris (Norris, 1914). But, Hertzsprung published the work in Danish so Norris got credit because his version was more accessible. We have all heard about how Dr. Jocelyn Bell Burnell did not win the Nobel Prize for the discovery of pulsars while her Ph.D. supervisor did (Parachini, 2021). We can cite Edwin Hubble of the Hubble sequence, Hubble law, and more. But much of his work would not have been possible without the discovery of the Leavitt Law (Cepheid Period-Luminosity Relation), yet we did not call the discovery the Leavitt Law until it was proposed by Wendy Freedman less than 20 years ago (Freedman, 2008).

These are just three examples of named discoveries and what these three examples have in common is power. The people who won the awards and had their names added to discoveries were in positions of power and authority while those who didn't mostly missed out. And that is a result of sexism, nationalism, and, of course, colonialism. ✶

References

Aikenhead, G. & Michell, H. 2010, *Bridging Cultures: Indigenous and Scientific Ways of Knowing Nature*, Pearson

Buck, W., 2018, *Tipiskawi Kisik: Night Sky Star Stories*, Manitoba First Nations Educations Resource Centre Inc.

Cannon, C., 2025, *In the Footsteps of the Traveller*, University of Manitoba Press

Dempsey, F., 2008, *JRASC, 102*, 59

Dempsey, F., 2009a, *JRASC, 103*, 65

Dempsey, F., 2009b, *JRASC, 103*, 233

Freedman, W., 2008, in *Celebrating 100 Years of the Leavitt Cepheid Period-Luminosity Relation.*

Hamacher, D.W., 2018, *AuJAn, 29*, 89. doi:10.1111/taja.12257

Harris, P., Marshall, L., Marshall, M., & Bartlett, C. 2017, *Muin and the Seven Bird Hunters*, Nimbus Publishing

Hertzsprung, E., 1911, *POPot, 63*

MacDonald, J. 1998, *The Arctic Sky: Inuit Astronomy, Star Lore and Legend*, Royal Ontario Museum

Norris, H.R., 1914, *PA, 22*, 331

Parachini, J., 2021, *Listening to the Stars: Jocelyn Bell Burnell Discovers Pulsars*, Albert Whitman & Company

Schaefer B.E., 2018, *JAHH, 21*, 7. doi:10.48550/arXiv.1808.01862

Hilding Neilson, Ph.D., is an astrophysicist and professor in the Department of Physics & Physical Oceanography at Memorial University of Newfoundland & Labrador in St. John's Newfoundland, where his research focuses on stellar and exoplanet physics and the stories we can learn from stars and planets. He is also Mi'kmaw from Ktaqmkuk and works to integrate Indigenous knowledge in astrophysics research and how we relate to outer space exploitation and the future of large astronomical observatories. Dr. Neilson has been featured on numerous outlets, including the CBC, The Globe and Mail*,* The Guardian*, and more. He has also published over 50 research articles.*

John Percy's Universe

Deneb and the Like

John R. Percy, FRASC
(john.percy@utoronto.ca)

Most readers know Deneb, the alpha star in Cygnus, and one of the three stars that make up the Summer Triangle. It passes directly overhead as seen from Southern Ontario. The name comes from the Arabic word for "tail" (of the swan). Similar names have been given to several other stars marking the tail of other celestial animals. But how much do you know about Deneb? How much do professional astronomers know about it? Not as much as you might think.

This column was motivated by the recent work of my astronomer friend Joyce Guzik (Los Alamos National Laboratory, Los Alamos, New Mexico). Like me, her research interests are in variable stars. Also like me, she promotes and encourages the work of skilled amateur astronomers, especially through the American Association of Variable Star Observers (AAVSO). In recent years, Guzik has organized the scientific papers sessions at the annual AAVSO conferences and edited the conference proceedings. I have been intrigued by her research on Deneb and related stars, as presented at these conferences.

From spectroscopy, we know that Deneb has a spectral type of A2 Ia, meaning that it is a very luminous supergiant of moderate temperature. The A2 is part of the stellar temperature sequence OBAFGKM; Deneb's "surface" temperature is about 8,700 K. There is also a stellar luminosity sequence: Ia, Ib, II, III, IV, and V, in order of decreasing luminosity. (Altair and Vega, the other two stars in the Summer Triangle, are also A-type stars, but are luminosity class V—the most common "main sequence" kind.) I refer you to the "Spectroscopy of Stars" section in the RASC *Observers Handbook* for more information.

Type Ia supergiants are very rare, but their great luminosity makes it more likely that they will be found among the brightest stars. Deneb is young (11.6 My) and massive (15–20 times the mass of the Sun), and began its life as a hot, bright main-sequence star. Its past and future evolution is not clear, however, including whether it will become a red supergiant in future, or has already been one.

To start with, the distance to Deneb is uncertain. Different yardsticks give different results. From its membership in the Cygnus OB7 stellar association, its distance is 2620 light-years, giving it a luminosity of 200,000 times that of the Sun. Its revised *HIPPARCOS* parallax gives a distance of 1410 ± 196 light-years, and a luminosity of 55,000 times that of the Sun. That's a big difference—nearly a factor of four.

Deneb has been known as a photometric variable for almost a century; see Abt (1957) for a classic paper. Its average period is 11.7 days, but the cycle length, amplitude, and light-curve shape are quite variable from cycle to cycle. The cause of the 11.7-day variability is presumed to be pulsation. The star does not fall in the famous Cepheid instability strip in the Hertzsprung-Russell graph of luminosity versus temperature. It may be related to hotter classes of pulsating stars, of which there are several.

The consensus is that the variability of the amplitude is due to "beating" between closely spaced periods of different pulsation modes that are excited in the star. The light curve of Deneb often shows evidence of shorter-period modes, superimposed on the 11.7-day cycles. Incidentally: my students and I have been studying pulsating red giants for many years (Percy 2025b). Such stars also have variable amplitudes, and we have recently shown that beating is the likely cause of amplitude variability in most of these stars (Percy and Pago 2025).

Understanding non-regularity in variable stars requires long datasets if there is to be any chance of understanding the cause. Guzik and her collaborators have recently set out to study a possible regularity to the irregularity: larger-amplitude variations seem to appear, then damp out after several cycles, then resume after about 70 days (Guzik et al. 2023). For this study, they needed continuous accurate observations for many months. They found these in several places.

AAVSO *Photoelectric Photometry* (PEP). AAVSO observers have been making photoelectric observations for almost half a century. Such observations are challenging for bright variables, because traditional PEP requires one or more constant comparison stars, close to the variable star in position and brightness, and this is usually not possible for very bright variables like Deneb. But it can be done. Figure 1 shows a typical Johnson V PEP light curve for Deneb. The observations are from the AAVSO International Database.

The Solar Mass Ejection Imager (SMEI; 2003–2011). This spacecraft was designed to measure solar coronal mass ejections, but it also repeatedly observed almost every star brighter than V = 6. Guzik et al. (2024 and 2025) show *SMEI* light curves of Deneb that are up to 8.6 years long. In principle, these observations would be excellent for studying the long-term behaviour of Deneb and the like, but the *SMEI* data require extensive processing and corrections, which are uncertain at the low level of variability of this star.

The Transiting Exoplanet Survey Satellite (TESS). This satellite, launched in 2018, studies exoplanets by measuring the very small decrease in brightness of their star as they pass in front of it. You have probably heard of *TESS*; it has revolutionized

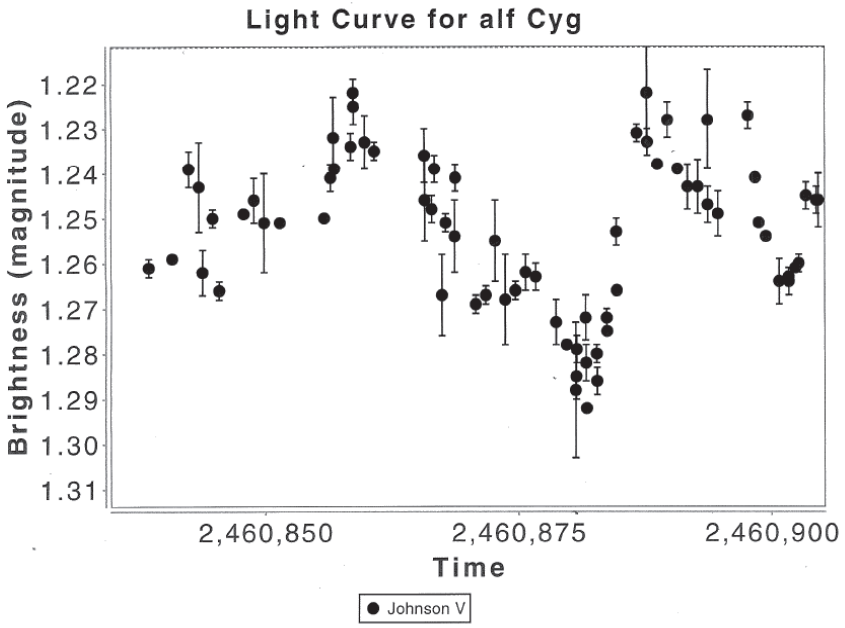

Figure 1. A light curve—Johnson V versus Julian Date—for Deneb. The error bars are a measure of the uncertainty of the magnitudes. The observations were made through the AAVSO Photoelectric Program. Although the average period is about 12 days, the cycle lengths (and amplitudes) can be quite variable, as this graph shows. Source: AAVSO.

the study of planets around other stars. *TESS* monitors a huge fraction of the sky, typically for about 27 days in each zone of the sky, then it moves on to other zones. Guzik et al. (2026) have examined 27-day light curves of 75 Alpha Cyg variables as a prelude to a more detailed study of these stars.

BRITE Constellation. I have recently written about this "constellation" of car-battery-sized nanosatellites that can obtain long-term light curves of bright variables (Percy 2025a). *BRITE* was conceived by my colleague Slavek Rucinski in collaboration with Kieran Carroll and Rob Zee, developed in Toronto, and eventually became a Canada-Austria-Poland collaboration. Guzik et al. (2025) show a typical light curve of Deneb obtained with *BRITE*. Catherine Lovekin (Mount Allison University) is the Canadian expert on Alpha Cygni variables, and is also a key member of the Canadian *BRITE* team.

Guzik et al.'s results, so far, suggest that the intervals between resumptions of larger-amplitude pulsation are most commonly 100 to 125 days, rather than 70 days, though the resumptions occasionally skip intervals (Guzik et al. 2025).

There are over a hundred Alpha Cyg variables in the AAVSO Variable Star Index (VSX); many of them are also in the *General Catalogue of Variable Stars*—the official catalogue. Guzik et al. (2024) describe preliminary observations of some of these. They include Rigel (Beta Ori), Saiph (Kappa Ori), Alnilam (Epsilon Ori), Aludra (Eta CMa), and 6 Cas. The brightest is Rigel—even brighter than Deneb. Although the authors hesitate to quote periods, because of the complicated variability and the limited data, the periods appear to be a few days, with complex light curves and small and variable amplitudes—much like Deneb. As mentioned, many Alpha Cyg variables are now being monitored by *TESS*, but the datasets are only 27 days long, which can be limiting for such complex variable stars. AAVSO PEP observations can help.

So next time you look at Deneb—or any other bright star—ask yourself: I wonder what this star is really like, physically, and how astronomers know. And how can I help—by being a "citizen scientist" and observing variable stars, for instance? ✶

Acknowledgements

I thank Joyce Guzik for re-introducing me to these stars, and for sending a preprint of Guzik et al. (2026).

References

Note: Guzik et al. (2023, 2024, 2025) can be accessed on arXiv at https://arxiv.org/archive/physics by inserting the nine-digit ID given at the end of the reference.

Abt, H.A. (1957), "The variability of supergiants", *ApJ., 126*, 138.

Guzik, J.A., Abt, H.A., Jackiewicz, J., and Kloppenborg, B. (2023), "Abrupt periodic pulsation resumptions in Deneb," *Proceedings of the AAVSO 112th Annual Meeting; arXiv: 2410.23936.*

Guzik, J.A., Kloppenborg, B,. and Jackiewicz, J. (2024), "Deneb and the Alpha Cygni variables," *Proceedings of the 2024 Society for Astronomical Sciences (SAS) Symposium; arXiv: 2410.23985*

Guzik, J.A., Kloppenborg, B., Richardson, N., Jackiewicz, J., Morrison, N., Calderwood, T., and Pigulski, A. (2025), "Abrupt pulsation resumptions in Deneb: an update," *Proceedings of the 113th Annual Meeting of the AAVSO,* arXiv: *2503.20058.*

Guzik, J.A., Whitley, C., Moore, N., Marshall, M., and Jackiewicz, J. (2026), "Alpha Cygni variables as seen from the Transiting Exoplanet Survey Satellite," *Proceedings of the AAVSO 114th Annual Meeting.*

Percy, J.R. (2025a), "A suitcase and six car batteries," *JRASC, 119*, 48.

Percy, J.R. (2025b), "Cool stars are really cool!", *JRASC, 119*, 241.

Percy, J.R. and Pago, A.F. (2025), "A study of amplitude variability in a sample of pulsating red giants," *Journal of the AAVSO, 53*, 150.

John Percy FRASC is Professor Emeritus, Astronomy & Astrophysics, University of Toronto, and a former President (1978–80) and Honorary President (2013–17) of the RASC.

Dish on the Cosmos

Cloud 9: A Stellar Name for a Not-So-Stellar Object

by Pamela Freeman
(pamela.freeman@ucalgary.ca)

The *Hubble Space Telescope* has put its eyes on the first potential RELHIC from the Universe's early days. A RELHIC is a REionization Limited HI Cloud, a mini dark-matter halo that contains starless gas. It is, as some have dubbed it, a "failed galaxy." Since its gas is unprocessed by star formation, it remains pristine. RELHICs are an intriguing class of objects that had only been theorized before.

RELHICs are a consequence of the ΛCDM model—the Greek capital letter Λ, which relates to dark energy, and CDM, for Cold Dark Matter, model. This model describes the composition of dark energy, dark matter, and baryonic matter that evolved from the Big Bang to the web of galaxies we see today. So far, it is successful at explaining the large-scale structure in the Universe and in the Cosmic Microwave Background.

In this understanding of the cosmos, dark-matter halos act as the host for galaxy formation, but not all halos will form galaxies. There should be low-mass dark-matter halos that remain starless; galaxies will only form in halos bigger than some critical mass (a mass that changes over cosmic time). Below this critical mass, some small halos won't be able to retain their gas at all. Nearer to the critical mass, some halos find a balance: the gas will be reionized by the ultraviolet background, which prevents it from settling and forming galactic structure, yet there's enough matter for some ionized particles to recombine, forming a neutral hydrogen core. This is a RELHIC. These starless halos are a novel way to study galaxy formation and dark matter, and to understand our model of the Universe at these relatively smaller scales.

This candidate RELHIC was first spotted by the Five-hundred-meter Aperture Spherical radio Telescope (FAST) in China. Initially, FAST was pointed toward the spiral galaxy M94 (the Cat's Eye Galaxy) in the northern constellation Canes Venatici (Latin for "hunting dogs," and often depicted as the dogs of Boötes) to map out the structure and motion of neutral hydrogen contained in this galaxy. Neutral hydrogen, denoted as HI, emits a signature emission at 1420 MHz or 21 cm, a wavelength long enough to pierce through the intervening dust and gas that could otherwise obscure the structure of a galactic or extragalactic source. In these radio observations, presented in Zhou et al. (2023), they also mapped out the region surrounding M94 to look for satellites or faint structures associated with it. They spotted numerous HI features: a filament, seven clouds relatively nearby, and one isolated cloud a little further away. The team dubbed each HI feature a Cloud, sequentially from 1 onward. The one that caught the most attention was Cloud 9, an object not quite like other HI clouds that have been observed. (A note from the European Space Agency press release: the phrase Cloud 9 has no significant cultural meaning for the Chinese, but it happens to work quite well in this context.)

Cloud 9, the isolated feature, sparked interest with its curious location, size, and lack of an optical counterpart—the area was compared to observations from the Dark Energy Spectroscopic Instrument Legacy Imaging Survey (DESI LS), which provided some constraint on the stellar content that could be contained within this HI cloud. Through the radio observations, they calculated that the total amount of matter in the cloud, as determined by the motion of the object, far exceeds the amount of ordinary baryonic matter observed. To quote the authors, the amount of dark matter "absolutely dominates" over that of ordinary matter.

From these observations alone, Cloud 9 was not necessarily a RELHIC. It became a leading theory supported by its round shape, small HI core, and narrow distribution of gas velocities. In other words, it did not look like a rotating galaxy as we know it. The other leading explanation for Cloud 9 was that it is a dark, gas-dominated, dwarf galaxy, similar to the faint galaxies surrounding the Milky Way, and that the DESI observations were not deep enough to capture its weak starlight.

The tantalizing prospect that Cloud 9 was a RELHIC was picked up by a team of modellers, who found the FAST observations were consistent with theoretical constructions of RELHICs (Benítez-Llambay and Navarro 2023; including Julio F. Navarro of the University of Victoria). This only further supported the need for more observations into the true nature of Cloud 9. With follow-up observations by the Green Bank Telescope (GBT) and the Very Large Array (VLA), both in the USA, the groundwork was laid for Hubble in the radio band.

The GBT's 100-m dish imaged Cloud 9 at a coarser resolution than FAST, as its smaller dish has a larger beam. This proved useful for capturing the extent of the signal in the FAST detection and confirming the presence of Cloud 9 (Karunakaran and Spekkens 2024; including Ananthan Karunakaran of the University of Toronto and Kristine Spekkens of the Royal Military College of Canada and Queen's University). Intriguingly, the GBT data showed a broader and more asymmetric spectral line profile than that of FAST, implying that there was more complicated structure present in the cloud.

The VLA, an array of 27 25-m dishes, captured finer resolution than the GBT or FAST. This close study of Cloud 9 (Benítez-Llambay et al. 2024, including Julio F. Navarro) detected the HI signal yet with another different spectral

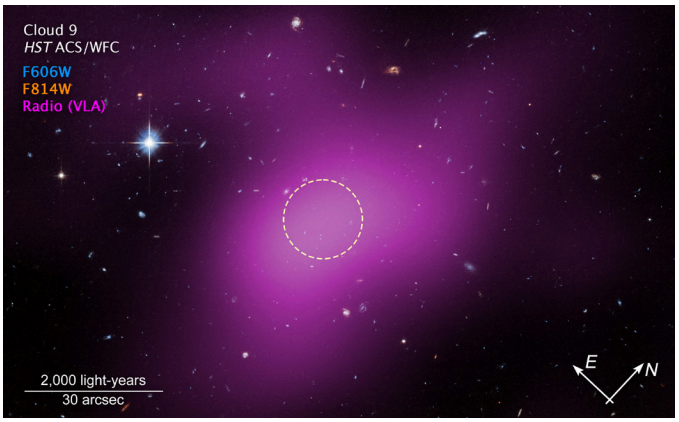

Figure 1 — The Very Large Array (VLA) and ***Hubble Space Telescope*** *(HST) data of Cloud 9, a starless dark-matter halo near the spiral galaxy M94. The image is about 10,000 light-years wide. The magenta shows neutral hydrogen gas observed in radio wavelengths by the VLA, with the peak circled by yellow dashes. The cyan and orange show data from two HST filters, F606W and F814W, respectively. From the HST, only background galaxies are seen, with no stars within the gas of Cloud 9. Credit: NASA, ESA, VLA, Gagandeep Anand (STScI), Alejandro Benítez-Llambay (University of Milano-Bicocca); Image Processing: Joseph DePasquale (STScI)*

line profile and with a complex spatial distribution. The mismatched line shape is of little concern, as the spatial scales from all three telescopes would capture different parts of the system, potentially at different velocities and contributing to a different profile. The distribution of gas implies the cloud is nonrotating and asymmetric—it is in balance but has been perturbed by something. They also recalculated the total mass held within the halo—a mere million solar masses of hydrogen gas to five billion solar masses of dark matter—and found it to be strikingly close to the critical mass of halos that form galaxies. Overall, from this suite of radio observations, Cloud 9 is consistent with our understanding of a RELHIC.

These studies also considered the possibility that Cloud 9 was in no way associated with M94. It could have been a random object that appeared close to M94 based on its projection in the sky. A comparison of their recessional velocities—how fast they are moving away from us due to the expansion of the Universe—showed similar values and lent support to them being at similar distances. The perturbation of Cloud 9 in the VLA data could also be an indication of interaction with M94.

After three sets of radio observations, it was time to leave the radio regime and look for a stellar counterpart to the HI gas. A deeper optical view of the potential stellar content in Cloud 9 was needed, and the *Hubble Space Telescope*'s Advanced Camera for Surveys was an ideal instrument to provide that.

The limit of stellar content presented by DESI is similar to the faint dwarf galaxies near our own Milky Way. Specifically, Benítez-Llambay et al. (2024) compared Cloud 9 to Leo T, a galaxy sitting about 420 kpc away from the Milky Way, one of the faintest members of the Local Group of galaxies. If Leo T was instead at the distance of Cloud 9, it would be incredibly difficult to spot it in a DESI image. The radio observations are not enough alone to distinguish Leo T from Cloud 9—mock VLA observations of Leo T show similar features.

In the new Hubble observations (Anand et al. 2025; including Julio F. Navarro), the limit of stellar content in Cloud 9 dropped from around 100,000 solar masses to near 3000 solar masses. A Leo T analogue would clearly be seen in this image, and given the amount of HI gas within Cloud 9, the ratio of gas to stars is unlike that typically seen for dwarf galaxies. Hubble has steered Cloud 9 directly into the RELHIC camp, making it the best example so far of a potential galaxy that didn't make the cutoff.

To understand Cloud 9 further, astronomers must stretch into other frequency bands. The JWST can complement Hubble in determining the limits of stellar content in Cloud 9. Other telescopes that can capture red Hα emission (another transition of atomic hydrogen) will examine the effect of the UV background, the source of reionization in RELHICs.

As for other potential RELHICs, astronomers don't have to rely on serendipitous detections. Astronomers are hunting for them intentionally through a few different means: they may appear in emission in large scale HI surveys of the sky, in absorption against background light from distant galaxies, as they distort gravitationally lensed images of distant galaxies. Cloud 9 is likely to not be the only RELHIC for astronomers to become excited about. For what it has now signified, Cloud 9 is a stellar name for a not so stellar object.

This is one of the many radio-related press releases from the American Astronomical Society's winter meeting, which happens annually in the first week of January. Head to the NRAO's public website (https://public.nrao.edu/news/) to see other results from the VLA and ALMA that kick-started the year in (US-focused) radio astronomy! ✶

References

Anand, G.S., Benítez-Llambay, A., Beaton, R. et al. 2025, *ApJL, 993*, L55, https://doi.org/10.3847/2041-8213/ae1584

Benítez-Llambay, A. and Navarro, J.F. 2023, *ApJ, 956*, 1, https://doi.org/10.3847/1538-4357/acf767

Benítez-Llambay, A., Dutta, R., Fumagalli, M., and Navarro, J.F. 2024, *ApJ, 973*, 61, https://doi.org/10.3847/1538-4357/ad65d9

Karunakaran, A. and Spekkens, K. 2024, Res. Notes *AAS, 8*, 24, https://doi.org/10.3847/2515-5172/ad1ee6

Zhou, R., Zhu, M., Yang, Y., et al. 2023, *ApJ, 952*, 130, https://doi.org/10.3847/1538-4357/acdcf5

Pamela Freeman recently finished her Ph.D. in astrophysics at the University of Calgary. Specifically, she studies the chemical make-up of star-forming clouds with radio telescopes. Generally, she loves to observe anything and everything about nature.

Obituary

Jack Newton 1942–2025

by Chris Gainor FRASC, Victoria Centre

Jack Newton, who was one of the highest profile amateur astronomers of his time and a leading member of three RASC Centres, has passed away at age 83.

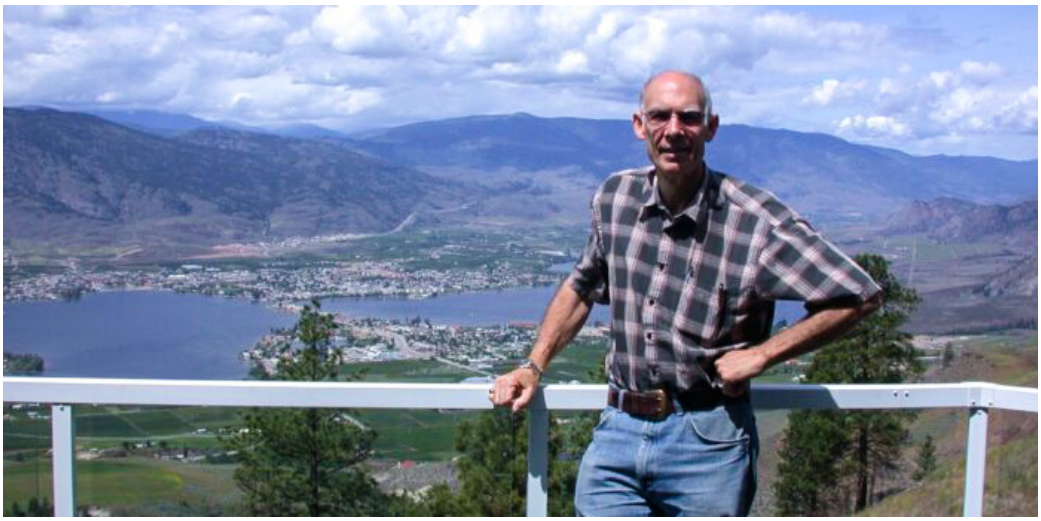

Newton gained fame for his skills as an astrophotographer in the heyday of colour photographic film and helped lead the transformation to digital astrophotography. His photographs appeared in many publications and often graced their covers. He also was known for his research work, seeking out supernovae and making other discoveries. He authored six books on amateur astronomy and astrophotography.

Newton, along with his wife Alice, was well-known for the observatories he built in his homes. He achieved all this while holding down a full-time job managing Marks and Spencer stores around Canada.

In retirement, Jack and Alice Newton operated their Observatory B&B on Anarchist Mountain near Osoyoos, B.C., from 2000 to 2023. They were among the founders of Arizona Star Village in Portal, Arizona. Guests at the B&B picked up astronomical skills and enjoyed the photos that Newton took year-round in B.C. and Arizona.

John "Jack" Borden Newton was born in Winnipeg on 1942 August 13, and his fascination with astronomy began when he was age 8 or 9. As the space age dawned in 1958, Jack joined the RASC Winnipeg Centre and quickly became involved in the Moonwatch program that was set up to track U.S. *Vanguard* satellites.

In Winnipeg, Newton began his astrophotography work and built his first domed observatory at his home. He served as Centre president in 1970–1972 but was transferred to Toronto the following year. During his six years in Toronto, Newton served as Centre president in 1975–1976. His astrophotography gained wide notice during that time, and he was honoured with the Queen's Silver Jubilee Medal in 1977 and the RASC Ken Chilton Prize in 1979.

When he was transferred to Victoria, Newton served as Centre president in 1980–81 and 1990–91. His and Alice's home in Sooke, complete with a fully outfitted observatory, became a popular place for Victoria Centre members and astronomers from farther afield. Asteroid 30840 Jackalice was named in their honour, and Jack won the RASC Chant medal in 1989. The Victoria Centre named its service award the Newton Ball Award after Jack Newton and fellow member George Ball, with whom he collaborated on astrophotography.

As an astrophotographer, Newton popularized "cold camera" techniques and, in 1991, became the first amateur astronomer to create full-colour CCD images of deep-sky objects—capturing the Ring and Dumbbell Nebulae in a way previously achieved only by professional astronomers. His photos appeared in *Astronomy*, *Sky & Telescope*, *SkyNews*, *National Geographic*, and *Life* magazines. His articles appeared in this *Journal* and elsewhere; he was a sought-after speaker at many RASC meetings.

As a member of the Puckett Observatory World Supernova Search Team, Newton was credited with more than 200 supernova discoveries. He also served as a director of the Astronomical Society of the Pacific, and helped launch Project Astro, which provides teachers with astronomical course content.

Jack Newton passed away on 2025 November 11, in Oliver, B.C. He is survived by Alice, his children, Suzanne and Rob, and four grandchildren.

"Jack Newton proved that with passion, curiosity, and a tireless spirit, a self-taught amateur astronomer could make a professional impact," a statement from his family said. "He was a mentor and a tireless advocate for preserving the dark skies he so loved. His light, captured in countless images and ignited in the minds of those he taught, will continue to shine brightly."

Photo credit: Alice Newton.

Astrocryptic

by Curt Nason (nasonc@nbnet.nb.ca)

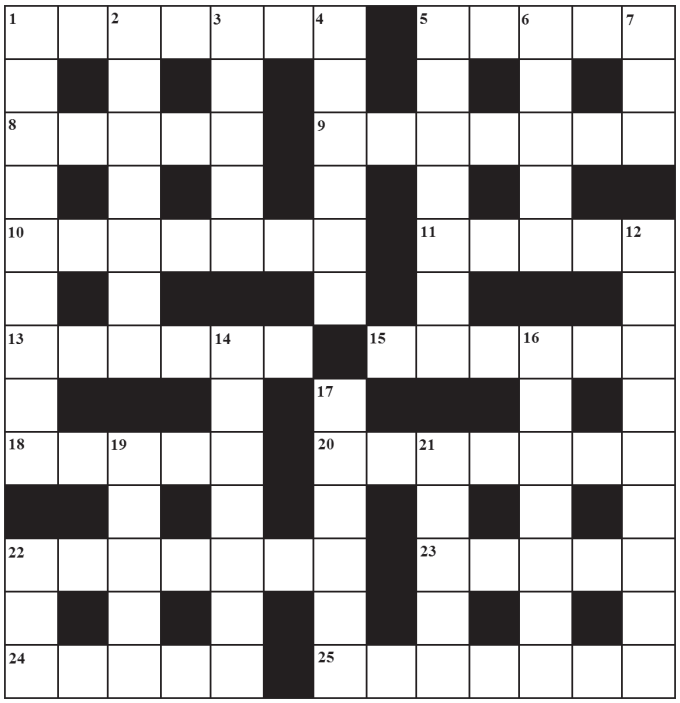

ACROSS

1. Rave about being in the Hubble at a full Moon (7)
5. Send money back for a rig to limit length of exposure (5)
8. High energy telescope was focused on variable O star (5)
9. I retain it to keep moving (7)
10. Ride around an island of the sparkling river (7)
11. A star seen back in Pope Benedict's time (5)
13. Break the LAN connection once shared by bull and charioteer (6)
15. Proverbially, the world's yours in this nebula (6)
18. Northern pointer he followed after his friend went back (5)
20. A crab using AI to make coffee (7)
22. One brace broke, with nothing to stop the dish from collapsing (7)
23. Diana turns around Galle's ring (5)
24. Nebulous burning issue below the belt (5)
24. High clouds turning blue before a confining nor'easter (7)

DOWN

1. Strumpet declared a dark patch below the belt, so I hear (9)
2. Yarkovsky was one who sounded in a hurry (7)
3. Additional lead-in to terrestrial visitor (5)
4. I drift around near winter solstice to see it in binos (6)
5. Time to honour Mars and Tyr (7)
6. I gained much weight on his eclipse cycle (5)
7. Poor seeing with air rising through the inlet (3)
12. A dark patch initially seen near Tarazed (8,1)
14. How some view Boötes, windy or not (3,4)
16. Galileo's Callisto in trial over minor matters (7)
17. Big city thug glowers cloudily above a spout (6)
19. His comet spawned Andromedids and one in Lugosi (5)
21. Winter star hopping in a stellar nebula (5)
22. Popular alien came up from Florida (3)

Answers to previous puzzle

Across: **1** CELESTRON (anag); **6** ERG (hid); **8** NEUTRON (neu(t)ron); **9** DIANA (2 def); **10** ANSAE (2 def); **11** HARRIOT (rev+riot); **12** REMOTE (anag); **14** MATHER (M+anag); **18** REGATTA (anag); **20** NOVAS (rev); **22** BENNU (be+anag); **23** KATHRYN (anag); **24** NEA (e.g.); **25** BOB'S KNOBS (2 def)

Down: **1** CENTAUR (2 def); **2** LOUIS (2 def); **3** SERPENT (anag); **4** RONCHI (anag); **5** NADIR (anag); **6** EDASICH (anag); **7** GIANT (anag); **13** MAGENTA (anag); **15** ALNITAK (Al+Ni+tak); **16** RISINGS (2 def); **17** MARKAB (M(ark)ab); **18** RUBIN (ru(b)in); **19** THUMB (2 def); **21** VIRGO (v+i+r+g+o)

Great Images

By Trevor Chandler

Trevor Chandler "During a visit to a small observatory in B.C.'s Okanagan Valley, I was informed that the ISS would be passing over. An intervalometer was used to capture the star trails. Sixty one-minute exposures."

Journal

Highly detailed image of the Moon by Omar Alnaji of Mississauga, Ontario. He writes "This image shows a detailed surface of the Moon, which was in its waning-gibbous phase at the time, and the craters can be seen near the sunlit border. This was the first (successful) stacked image that I have done of the Moon's surface. I found the different techniques used to sharpen and align this image to be very intriguing, as it was slightly different from the techniques used for planetary photography. It also makes me wonder how much more detail I can capture as I learn astrophotography while using different equipment.